

*The Polymorphs and Solvates of Phenylbutazone  
and their Phase Transition Behaviour*

Thesis submitted in fulfilment of the requirements for a  
Master of Philosophy degree

By

Jonathan J. Targett

London, England

2009

University College London  
Chemistry Department  
Christopher Ingold Laboratories  
20 Gordon Street  
London WC1H 0AJ

## Dedication

*To Lindsay and to my parents*

*“...seit sich der Wert des Geldes wie Gas verflüchtigt: die neuen Reichen haben plötzlich ihr Herz entdeckt für gotische Madonnen und Inkunabeln und alte Stiche und Bilder;”*

Excerpt from: *The Invisible Collection* in *Meisternovellen* by Stefan Zweig

## Acknowledgements

The author acknowledges the following staff and faculty members of University College London without whose guidance, little experimental work could have been carried out:

Dr A. Aliev - Nuclear Magnetic Resonance Spectroscopy, (NMR).

Dr J.K. Cockcroft - Single Crystal Diffractometry (SCXRD)<sup>1</sup>, Powder X-ray Diffraction (PXRD), Synchrotron Powder X-ray Diffraction<sup>2</sup>.

Dr. S. Firth - Differential Scanning Calorimetry (DSC), Thermogravimetric Analysis, (TGA).

M. Vickers - Powder X-ray Diffraction (PXRD), Synchrotron Powder X-ray Diffraction<sup>2</sup>, Infrared Spectrometry (IR).

I express my thanks to Professor Paul Barnes for sage counsel, and to the inhabitants of Room 320 in the Ingold building for their, generally, useful suggestions, when I was stuck. The Science Reading Rooms of the British Library provided access to some of the reference material cited in this investigation. Certain illustrations used in this text have been obtained from literature sources, and have been reproduced with kind permission of their publishers.

Funding for this work was provided by the Engineering and Physical Sciences Research Council of the United Kingdom.

### A Note on Referencing

Literature references are cited at the relevant point in the text rather than in a grouped literature review. Once a particular literature reference has been introduced in the text, it has not necessarily been cited again.

---

<sup>1</sup> SCXRD experiments were carried out jointly by the author with this contributor.

<sup>2</sup> Synchrotron PXRD data was collected by this contributor on behalf of the author.

## **Declaration**

This declaration confirms that the text has been prepared solely by the undersigned, and that it has not been submitted previously towards the conferral of a degree at another institution. In the reference section, acknowledgement is given to publications, from which content has been excerpted for use in this document.

Jonathan Targett

Date Submitted

## Abstract

In this study, which was conducted between March 2007 and December 2008, the crystal structure of the alpha polymorph of phenylbutazone has been determined by single crystal X-ray diffractometry. The present findings support those of Singh & Vijayan (1977) and Paradies (1987). Efforts to grow single crystals of the beta and delta polymorphs of phenylbutazone did not locate specimens of adequate quality for structure determination. Nonetheless it was possible to isolate high purity powder samples of these two forms. The powder diffraction pattern of the delta polymorph was measured with improved accuracy at the Diamond synchrotron, and reveals a number of peak overlaps in previously published diffraction patterns of this crystal form. The improved diffraction data have enabled the crystal system of the delta form to be identified as orthorhombic, and space-group selection has been narrowed down to Pnn2 or Pnnm.

Four new solvated forms of phenylbutazone have been identified. The crystal structures of two of these new solvates have been determined by single crystal diffractometry. Both have space-group  $C2/c$ , and may be considered isostructural with five formerly identified solvates, whose structures were published by Hosokawa *et al.* in 2004.

Previously phenylbutazone has been found to change polymorphic forms at above-ambient temperatures. This behaviour has been examined both in a differential scanning calorimeter and on a powder X-ray diffractometer equipped with isothermal sample heating, where the transition of the alpha and beta polymorphs to the delta polymorph was observed. Thermodynamic methods of predicting the transition temperatures of polymorphs are discussed, particularly those derived from dissolution data. In the case of phenylbutazone, a substantial amount of dissolution data has been collected elsewhere, and these data are used to generate computational predictions of the polymorphic transition temperatures for comparative purposes.

## Table of Contents

<i>1</i>	<i>Molecular Polymorphism</i> .....	12
1.1	Introduction.....	12
1.2	Designation of Polymorphs.....	14
1.3	Phenylbutazone .....	15
1.3.1	Background .....	15
1.3.2	Crystal Forms - Summary of Literature Findings .....	17
1.3.3	Making the Different Crystal Forms .....	25
<i>2</i>	<i>Analytical Techniques Employed</i> .....	27
2.1	Distinguishing between Polymorphs & Solvates .....	27
2.2	Description of Individual Analytical Techniques .....	31
2.2.1	Visual Melting Point Determination .....	31
2.2.2	Powder X-ray Diffraction, (PXR)D) .....	31
2.2.3	Single Crystal X-ray Diffraction, (SCXR)D).....	35
2.2.4	<sup>1</sup> H Nuclear Magnetic Resonance Spectroscopy, (NMR) .....	36
2.2.5	Differential Scanning Calorimetry, (DSC) & Thermogravimetric Analysis, (TGA)....	37
2.2.6	Infrared Spectrometry, (IR).....	37
<i>3</i>	<i>Structure Determination of Polymorphs and Solvates</i> .....	38
3.1	Indexing of Powder Diffraction Data.....	38
3.1.1	Peak Input Selection for PXR)D) Indexing .....	43
3.2	Indexing of Phenylbutazone Crystal Forms .....	45
3.2.1	Polymorphs .....	46
3.2.2	Solvates .....	58
3.3	Structure Determination from PXR)D) Data .....	61
3.4	Collection of Single Crystal Diffraction Data.....	64
3.4.1	Growing Suitable Crystals .....	64
3.5	Structure Determination from Single Crystal Diffraction Data .....	68
3.5.1	Refinement of SCXR)D) Solutions – Theoretical Background.....	70
3.5.2	Summary of SCXR)D) Structure Refinements.....	77
3.6	Structural Models.....	83
3.6.1	Alpha Polymorph .....	83
3.6.2	Propylene Carbonate & Methyl-tert.-butylether Solvates.....	85
<i>4</i>	<i>Polymorphic Outcome of Solvent Crystallization</i> .....	92
4.1	Preferential Solubility Model.....	92

4.2	Dissolution .....	94
4.2.1	Ideal Solution Theory.....	94
4.2.2	Non-Ideal Solution Theory .....	99
4.2.3	Solubility of Phenylbutazone .....	103
4.3	Role of Solvent .....	107
4.4	Targeted Crystallization of Polymorphs .....	110
4.4.1	Theoretical Background.....	111
4.4.2	Observed Crystallization Behaviour of Phenylbutazone .....	114
4.4.3	Preparation of Pure Phenylbutazone Polymorphs.....	115
5	<i>Transitions of Polymorphs and Solvates.....</i>	<i>118</i>
5.1	Predicting Transitions .....	118
5.2	Measurement of Transitions.....	124
5.2.1	Results for Polymorphs .....	125
5.2.2	Results for Solvates.....	127
5.3	Kinetic Considerations.....	133
5.4	Transitions of Phenylbutazone during Constant Gradient Heating.....	141
5.4.1	Polymorphs .....	141
5.4.2	Solvates .....	145
5.5	Discussion of Results .....	146
5.5.1	Polymorphs .....	146
5.5.2	Solvates .....	150
	<i>Conclusions.....</i>	<i>151</i>
	<i>Appendix 1 – Reference PXRD Patterns of Phenylbutazone’s Polymorphs .....</i>	<i>161</i>
	<i>Appendix 2 – DSC/TGA Scans of Phenylbutazone’s Polymorphs .....</i>	<i>166</i>
	<i>Appendix 3 – IR Spectra of Phenylbutazone’s Polymorphs.....</i>	<i>169</i>
	<i>Appendix 4 – <sup>1</sup>H NMR Spectrum of Phenylbutazone in CDCl<sub>3</sub> .....</i>	<i>170</i>
	<i>Appendix 5 – Treatment of Background Counts .....</i>	<i>172</i>
	<i>List of Abbreviations.....</i>	<i>176</i>

## Table of Figures

Figure 1 – Phenylbutazone.....	15
Figure 2 - Major Peak Comparison of Delta Form .....	19
Figure 3 - Major Peak Comparison of Alpha Form.....	20
Figure 4 - Major Peak Comparison of Beta Form.....	20
Figure 5 - PXRD Patterns of Two New Solvates with Space Group C2/c.....	24
Figure 6 - PXRD Patterns of New Solvates with Cyclic Ketone Solvents .....	25
Figure 7 - Identification Decision Tree .....	30
Figure 8 - Comparison of MTBE Solvate PXRD Pattern with Major Beta Peak Positions.....	32
Figure 9 - Beam Delivery at Station I11 .....	34
Figure 10 - Generalized Parallelepiped Representation of the Unit Cell .....	38
Figure 11 - $H,K,L$ Indexing Example - Planes of a Cubic Lattice.....	38
Figure 12 - Example of a Reciprocal Lattice .....	40
Figure 13 – Example of Improved Resolution from Summation of Repeated PXRD Scans .....	44
Figure 14 - Phenylbutazone Delta Form in Space-group Pnn2 (or Pnnm) .....	53
Figure 15 - Phenylbutazone Delta Form in Space-group Pba2 (or Pbam) .....	53
Figure 16 - Terminal Residuals from Rietveld Refinements of Delta Form PXRD Pattern .....	56
Figure 17 - Structural Model of Solvate with Tetrahydrofuran of Hosokawa <i>et al.</i> .....	60
Figure 18 - Comparison of THF Solvate Calculated Pattern & 150K Pattern .....	61
Figure 19 - Phenylbutazone Polymorph Specimens .....	64
Figure 20 - Alpha Form Crystal under Polarized & Non-polarized Light .....	65
Figure 21 – Alpha Form Crystal Selection for SCXRD .....	65
Figure 22 - Alpha Single Crystal after Heating .....	66
Figure 23 - Single Crystals that Yielded Structure Solutions on the SCXRD Goniometer.....	67
Figure 24 - Checklist for Structure Solution .....	68
Figure 25 - Example Section of 2D Fourier Map of Alpha Form created in Jana2004 .....	71



Figure 26 - Visualization of the Ewald Sphere .....	76
Figure 27 - Refinement Analysis of Structural Models – Alpha Form .....	80
Figure 28 - Refinement Analysis of Structural Models - MTBE Solvate .....	81
Figure 29 - Refinement Analysis of Structural Models – Propylene Carbonate Solvate.....	82
Figure 30 - Alpha Form Asymmetric Unit - Singh & Vijayan, 1978 .....	83
Figure 31 - Asymmetric Unit of Alpha Form .....	84
Figure 32 - Unit Cell of Alpha Form.....	84
Figure 33 - Comparison of Calculated & Observed PXRD Patterns of Alpha Form.....	85
Figure 34 - Unrefined Model of Solvate of Propylene Carbonate – solved by SIR2004 .....	86
Figure 35 - Asymmetric Unit of Methyl-tertiary-butylether Solvate .....	87
Figure 36 - Unit Cell of Methyl-tertiary-butylether Solvate.....	87
Figure 37 - Asymmetric Unit of Propylene Carbonate Solvate .....	88
Figure 38 - Unit Cell of Propylene Carbonate Solvate .....	88
Figure 39 - Observed & Calculated PXRD Patterns of MTBE Solvate.....	89
Figure 40 - Observed & Calculated PXRD Patterns of Propylene Carbonate Solvate .....	90
Figure 42 - Ideal Solubility of Phenylbutazone Polymorphs vs. Temperature.....	103
Figure 43 - Ideal and Non-Ideal Solubilities of Phenylbutazone .....	104
Figure 44 - Solubility of Polymorphs in Phosphate Buffer Solution; Kaneniwa <i>et al.</i> ....	105
Figure 45 - Free Energy Change vs. Temperature for Alpha-Delta and Beta-Delta Transitions .....	120
Figure 46 - Solubility & Predicted Transition Temp. Vs Measurement Temp. ....	122
Figure 47 - PXRD Patterns of Alpha Form at Stepped Temperatures.....	126
Figure 48 - PXRD Patterns of Beta Form at Stepped Temperatures.....	127
Figure 49 - Decomposition of Tetrahydrofuran Solvate over Time .....	128
Figure 50 - Decomposition of Methyl-tertiary-butylether Solvate over Time.....	129
Figure 51 - PXRD Patterns of Propylene Carbonate Solvate before & after Heating .....	130
Figure 52 - PXRD Patterns of MTBE Solvate before & after Heating .....	131
Figure 53 - PXRD Patterns of Tetrahydrofuran Solvate up to Transition to Delta Form.....	132

Figure 54 - PXRD Patterns of Cyclohexanone Solvate up to Melting Temperature.....	132
Figure 55 - 2D Nucleation and Growth Model.....	139
Figure 56 - Alpha Form Transition & Melting Endotherm by DSC .....	142
Figure 57 - Conversion Curve of Alpha-Delta Transition Endotherm .....	142
Figure 58 - Plot of Kinetic Expression of Alpha-Delta Conversion after Freeman Carroll.....	143
Figure 59 - Beta Form Transition & Melting Endotherm by DSC .....	144
Figure 60 - DSC Scan of Tetrahydrofuran Solvate .....	145
Figure 61 - DSC Scan of Cyclohexanone Solvate .....	146
Figure 62 - Beta Transition & Melting - Müller .....	149
Figure 63 - Background Count Distribution of PXRD Patterns - Flat Plate Diffractometer .....	174

## List of Tables

Table 1 - Identification of Phenylbutazone Polymorphs by Citation .....	18
Table 2 - NMR Chemical Shifts for Phenylbutazone and a Selection of its Solvates .....	23
Table 3 - Unit Cell Dimension Comparison of the Alpha Form .....	46
Table 4 - Selected Unit Cell Solutions of Beta Form .....	49
Table 5 - Probable Unit Cell Dimensions of Delta Form.....	50
Table 6 - Fulfilment of General Reflection Conditions for Delta in Pnn2 & Pnnm.....	54
Table 7 - Fulfilment of General Reflection Conditions for Delta in Pba2 & Pbam .....	54
Table 8 - Automatic Refinement of Delta PXRD Data in EXPO2004 .....	55
Table 9 - Tentative Unit Cell Dimensions of Cyclohexanone Solvate .....	59
Table 10 - Phenylbutazone Alpha SCXRD Measurement Resolution.....	76
Table 11 - Unit Cells of Solvates Determined by SCXRD .....	77
Table 12 - Refinement Statistics of Solved Phenylbutazone Structures.....	79
Table 13 - Overview of 7 Isostructural Solvates of Phenylbutazone .....	91
Table 14 - Crystallization Results of Solvent Screening of Phenylbutazone .....	109
Table 15 - Polymorphic Crystallization Outcomes – Datta & Grant, 2005.....	114
Table 16 - Crystallization Outcomes of Stirred Methanol/Water Solution Experiments .....	117
Table 17 - Temperatures of Transition of Phenylbutazone’s Polymorphs .....	147
Table 18 - Enthalpies of Melting & Transition of Phenylbutazone’s Polymorphs .....	148

# 1 Molecular Polymorphism

## 1.1 *Introduction*

Scientists and non-scientists alike are instinctively aware of the ability of the substances that they encounter to take up a variety of different crystal packing arrangements. This phenomenon, which is known as allotropism among elements of the periodic table, is readily apparent to the layman familiar with the manifold forms of the element carbon: graphite is one allotrope of carbon, while diamond is another. The fact that these two substances, which differ only in their packing arrangement, exhibit such strikingly different physical properties, underscores the importance of an understanding of crystal structure, and raises the prospect of valuable discoveries, where new crystal forms possessing useful properties can be identified and isolated.

In molecular compounds the existence of multiple crystal packing arrangements is termed polymorphism. The reader is referred to the extensive literature on the subject for a comprehensive set of definitions, [1-3]. In those instances where a stable crystal form contains solvent bound-up in a regular arrangement in the crystal lattice, the crystal form is designated as a solvate or solvated form. This phenomenon is sometimes referred to as pseudo-polymorphism.

An understanding of the conditions under which a substance changes from one crystal form to another is of importance in ensuring that the material is produced and delivered in the desired form, and may also have value in the design of manufacturing techniques.

Although wide divergences in physical properties such as those between graphite and diamond are rarely encountered among different polymorphs, less pronounced differences are commonplace, resulting primarily from differences in the lattice energies of the individual

crystal structures. These divergences often give rise to differences in the density and dissolution rates of individual crystal forms. Despite the potentially adverse consequences for formulators resulting from differences in crystal packing arrangements, formal specifications for polymorphic form are seldom encountered outside the pharmaceutical industry.

Study of polymorphism has established roots, and is carried out systematically in certain industries. The pharmaceutical industry is required to screen the various polymorphic forms of its ingredients, [4, 5], both to maintain uniform processing during manufacture, and to ensure predictable dissolution and bioavailability of solid dosage forms in vivo. Nonetheless a number of instances have occurred, in which the existence of a new crystal form has emerged only during the later stages of product development, [6].

Many APIs, including phenylbutazone, lack water-solubility, and must therefore be specially formulated and/or chemically modified in order to be administered. Among the techniques to achieve this objective are, [7];

- Micronization
- Preparation of salts of the API
- Use of surfactants
- Compounding with water-soluble carriers; e.g. cyclodextrin, liposomes or dendrimers

Selection of more soluble polymorphic forms may also be helpful. During formulation and subsequent manufacturing, the difference in solubility of particular polymorphs needs to be taken into account, along with the many other factors that affect solubility; for example, the compression force used to manufacture tableted forms of pharmaceutical preparations.

Routine quality control tests, such as powder X-ray diffraction, readily show up changes in the polymorphic form of end products and intermediates subsequent to specific manufacturing processes, however the determination of the full crystal structure, a proof of what underlies the quality control procedure, remains in many cases an elusive goal.

With a view to simplifying the workflow of drug development groups, in particular, much theoretical effort has been expended to develop computational methods capable of predicting how individual molecules are likely to pack, solely by using thermodynamic and geometric measurements. These models have been put to the test in series of blind tests organized by the Cambridge Crystallographic Data Centre. The model developed at UCL by Professor S. Price's group, [8], searches for packing arrangements that are predicted to have low lattice energies. Although notable successes have been achieved in predicting stable polymorphs computationally, this approach tends to generate a larger number of putative polymorphic forms than are actually found to exist, [9, 10].

Nevertheless prediction techniques such as these have the potential to augment purely crystallographic methods of achieving the challenging objective of determining the crystal structure of ever larger molecules purely from their powder X-ray diffraction patterns, [11].

## **1.2 *Designation of Polymorphs***

Several investigators refrain from assigning names to identified crystal forms, referring instead to a form number. This less specific designation circumvents the pitfall of assigning a transferable nomenclature to a species, whose nature is not necessarily fully apparent; for instance a crystal form that is not a polymorph but, in fact, a solvated form. A methodology for distinguishing between solvated and non-solvated forms is described in Section 2.1.

Bernstein points out that no formal rules exist for the labelling of polymorphs; Greek letters,

Roman letters and Roman numerals are the most frequently encountered designations. In this investigation Greek letters have been adopted to identify polymorphs of the molecule under study, mainly because substantial previous investigation has led to the emergence of a reasonably robust nomenclature based upon the Greek alphabet. In the case of solvates, the crystal form is identified as a solvate of the target molecule with a particular solvent. This does not address the possibility that there may be more than one solvate of a particular molecule with the solvent in question, an issue that is discussed further in the context of structural identification of phenylbutazone's solvates.

### 1.3 *Phenylbutazone*

#### 1.3.1 Background

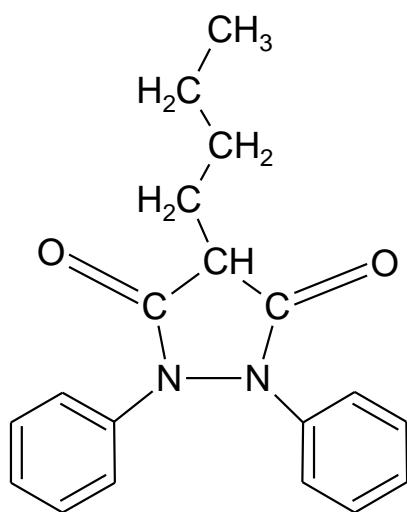


**Figure 1 – Phenylbutazone**

Phenylbutazone, (1,2-diphenyl-4-n-butyl-3,5-pyrazolidinedione), is an active pharmaceutical ingredient, API, which is used primarily in non-steroidal, anti-inflammatory preparations to relieve pain associated with arthritis and other chronic musculoskeletal conditions. It also possesses antipyretic and analgesic effects, [12, 13].

The first commercial dosage form was launched in 1952 by the Swiss firm, Geigy, under the trade-name Butazolidin<sup>®</sup>. Bulk synthesis was carried out using malonic acid ester, [14], as starting ingredient. In humans the drug has since been found to be toxic to bone marrow, and it is therefore no longer administered in several countries. However it still finds application in veterinary preparations, particularly in those for horses.

The compound is known to form solvates, [13, 15], readily in a range of common crystallization solvents. Furthermore, phenylbutazone exists in at least three polymorphic forms, which can be obtained by conventional, evaporative solvent crystallization [16-19], as well as at least one other which has been prepared both by grinding, [20] and spray-drying, [21-23]. A further two polymorphs have been reported to exist. Literature findings are summarized in the following section; (Table 1).

Transitions of solid phenylbutazone crystal forms to other forms have been widely reported, and there is consensus that the form known as the delta form is the polymorph which is formed upon heating of the other polymorphic forms, [18, 24, 25]. Descriptions of the nature of these transitions are less consistent. Certain researchers have suggested that melting of the polymorph undergoing transition takes place followed by recrystallization in the delta form.

There are no reports of reversibility of the transitions; once the alpha or beta form sample has changed to the delta polymorph, recooling does not result in a retransition from the delta form to other polymorphs.

Upon melting and subsequent refreezing, phenylbutazone is observed to form a wax-like mass, which exhibits little or no crystallinity. Conversely phenylbutazone is observed to crystallize readily from organic solution, under most conventional crystallization conditions, into highly-ordered polymorphic forms with little or no amorphous content.



Although readily soluble in a wide range of organic solvents, phenylbutazone is barely soluble in water. Dissolution in aqueous buffer solutions is possible, and the solubility of the compound has been comprehensively studied across a range of common processing temperatures in phosphate buffer solutions, [17-19, 26-28]. Furthermore phenylbutazone is among a relatively small number of pharmaceutically active ingredients whose solubility parameter has been studied in detail, [29], enabling its solubility to be predicted in a wide range of common solvents according to the methodology developed by Hildebrand, Prausnitz and Scott, [30-33].

The tendency of phenylbutazone's polymorphs to display varying rates of dissolution is examined in depth by Tuladhar *et al.*, [19, 28, 34], Kaneniwa *et al.*, [26] and Al-Meshal, [35]. Stella *et al.*, [36, 37] attribute this behaviour to non-instantaneous protonation and deprotonation of phenylbutazone, and identify the sole hydrogen atom on the central 5-membered ring as the proton that is donated. Phenylbutazone is therefore designated a carbon acid, and its pKa has been determined to lie between 4.50-4.70.

### **1.3.2 Crystal Forms - Summary of Literature Findings**

Data on the polymorphic form that results upon crystallization of phenylbutazone from a particular solvent under atmospheric conditions have been published by a number of groups of researchers, in the context of uncovering new polymorphic and solvated forms. Grinding and spray drying studies have brought to light additional crystal forms. The existence of between 3 & 6 polymorphs has been claimed, however a complete crystal structure of only one of these forms has been deposited in the Cambridge Structural Database, CSD, [38]; this structure corresponds to the polymorph commonly referred to as the alpha form. Several solvate structures have also been deposited on the CSD.

A second structure of the alpha form has also been published, [39], however a literature search revealed no structure solutions of the remaining polymorphs, including the commonly encountered polymorphs referred to as the delta and beta forms. The previous structure solutions of the alpha form and all solvate structure solutions were achieved by single crystal X-ray diffraction, SCXRD. The polymorphs identified by individual research groups are shown in the following table. In many of the earlier papers, alternative designations had been used for the polymorph in question; these designations have been superseded by the widely-adopted Greek letter nomenclature, which is shown in the column headings. The availability of structure solutions is mentioned. In most cases, the primary means of identification of polymorphic form is PXRD, and this has been indicated.

**Table 1 - Identification of Phenylbutazone Polymorphs by Citation**

Group	Form $\alpha$	Form $\beta$	Form $\delta$	Other Polymorphs	Solvates
Matsunaga <i>et al.</i> , 1976	“Form II” PXRD	“Form III” PXRD	“Form I” PXRD		
Ibrahim <i>et al.</i> , 1977		“Form III” PXRD	“Form IV” PXRD		“Form I”(iso-butanol) & “Form 2”(cyclohexane)
Singh & Vijayan, 1977	CS				
Chauvet & Masse, 1978, [40]	“Form II”† DSC	“Form III” DSC	“Form I” DSC		
Müller, 1978	PXRD	PXRD	PXRD	Gamma	iso-butanol, cyclohexane
Tuladhar, 1982	“Form D” DSC	“Form C” DSC	“Form A” DSC	Form E, Form B (possibly $\gamma$ )	
Matsuda <i>et al.</i> , 1982	PXRD	PXRD	PXRD	Epsilon <sup>sp</sup>	
Matsumoto <i>et al.</i> , 1988	PXRD	PXRD	PXRD	Zeta <sup>gr</sup> , Epsilon <sup>gr</sup>	
Paradies, 1987	CS				
Hosokawa <i>et al.</i> , 1994					Chloroform, Tetrahydrofuran <sup>CS</sup> , 1,4-Dioxane <sup>CS</sup> , Benzene <sup>CS</sup> , Cyclohexane <sup>CS</sup> , Tetrachloromethane <sup>CS</sup>

PXRD = identified by PXRD, DSC = identified by DSC, CS = crystal structure solution by SCXRD,

sp = formed by spray-drying, gr = formed by grinding,

†the two DSC peaks correspond to form alpha, however Matsuda *et al.* query the identity of this crystal form

The methods used to identify polymorphs and solvates are described in detail in Chapter 2. In common with most of the cited literature references, powder X-ray diffraction was the primary technique used to distinguish between crystal forms during this investigation. The PXRD patterns of the various polymorphs mentioned in the literature were compiled, and stick diagrams were prepared for subsequent polymorph and solvate identification.

### 1.3.2.1 Polymorphs

Reference PXRD patterns of the polymorphs alpha, beta and delta were collected both in-house and on beam-line I11 of Diamond Light Source at Didcot, Oxfordshire. For the purposes of comparison, peak intensities were recalculated on a scale of zero to one, scaled in relation to the intensity of the maximum peak after subtraction of background counts; (Appendix 5). Good agreement was found between the patterns of the alpha, beta and delta forms collected during this investigation and PXRD patterns obtained from the literature; see following figures.

**Figure 2 - Major Peak Comparison of Delta Form**

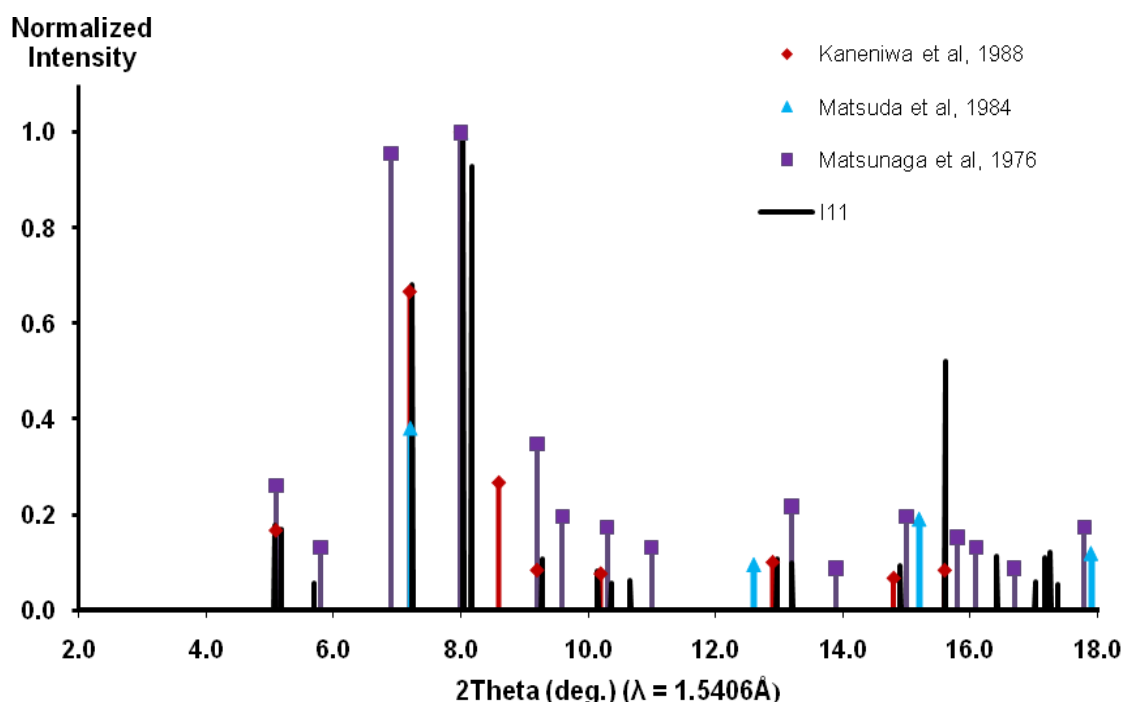


Figure 3 - Major Peak Comparison of Alpha Form

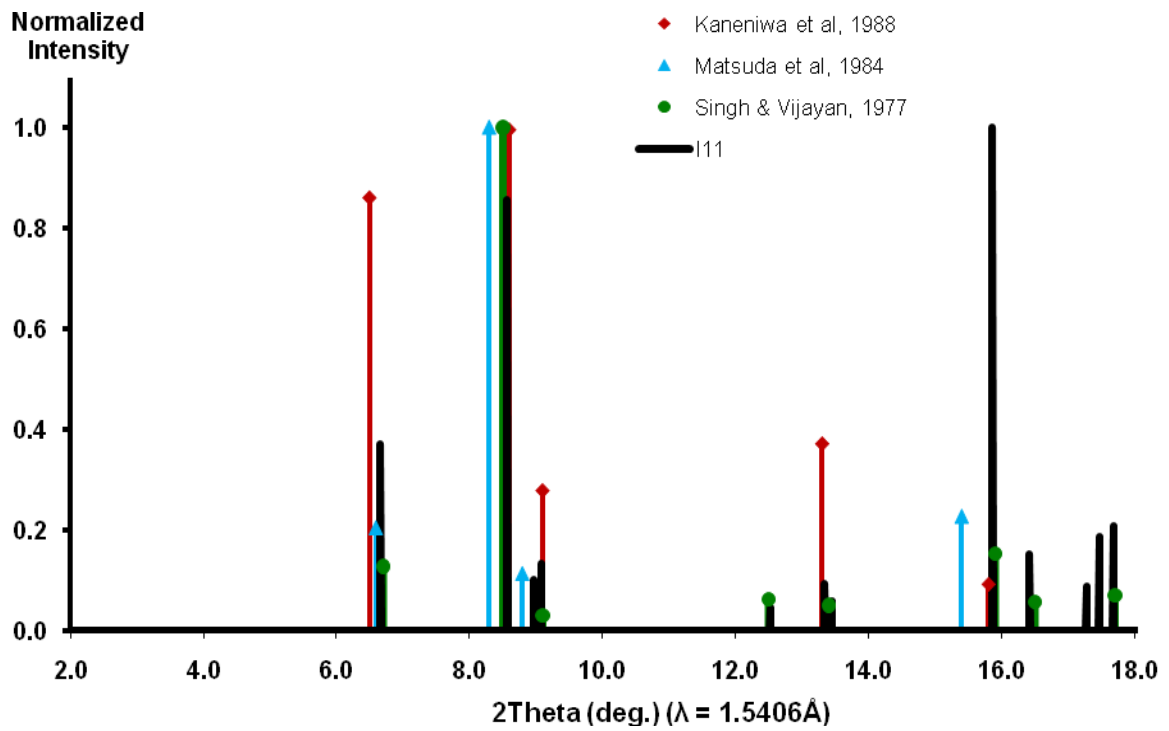
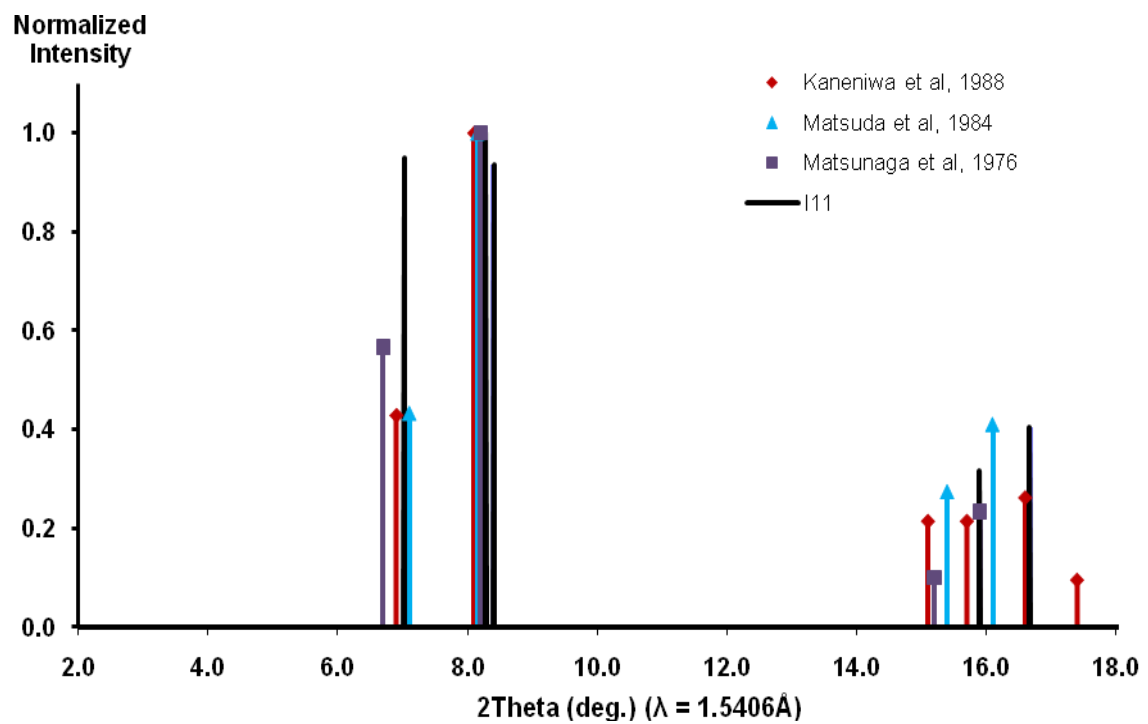


Figure 4 - Major Peak Comparison of Beta Form



Besides the three widely identified polymorphs, alpha, beta & delta, form names have been proposed for a number of other putative polymorphs. The most notable of these was obtained by a research team in Kobe, Japan, [23] using a spray-drying technique in which the new polymorph was produced concomitantly with the beta and delta forms. Matsuda *et al.* used the designation epsilon,  $\epsilon$ , to refer to this new form. First mention of this form is made in a paper from this group dating from 1980, [21].

In 1988 a Japanese group at Showa University in Tokyo, [20], revealed that prolonged grinding of phenylbutazone could also bring about the formation of form epsilon. In addition the same paper by Matsumoto *et al.* reported that the grinding procedure first gave rise to an intermediate form, to which they assigned the designation zeta,  $\zeta$ ; the existence of this form has not been confirmed by other research groups subsequently.

Solely on the basis of thermal analysis data, Müller also proposes the existence of a new form, which he designates gamma,  $\gamma$ . From crystallizations employing solely the solvent n-heptane, Tuladhar presents analytical data for 5 distinct crystal forms including the polymorphs alpha, beta and delta. Basing his conclusions primarily on DSC results, he identifies one of the two new forms as the polymorph designated form gamma.

Efforts to reproduce the novel crystal forms encountered by Tuladhar using n-heptane were not successful. Storage of an n-heptane solution of phenylbutazone for a number of weeks was observed to give rise to an amorphate. However, fresh solutions crystallized to give samples of known polymorphs; frequently in concomitant mixtures. The polymorphs most frequently obtained when using n-heptane were alpha/delta mixtures, but the beta form was also found to be present in certain mixtures prepared at above-ambient temperature.

### 1.3.2.2 Solvates

The crystal structures of phenylbutazone's solvates have been investigated more successfully than those of its polymorphs. Structures of six solvates with the solvents listed below have been deposited into the Cambridge Structural Database by Hosokawa *et al*, [13]. The structures of the solvates with the first five of the solvents in this list have been determined by SCXRD and found to be monoclinic with space-group C2/c; (Table 13):

- benzene
- cyclohexane
- 1,4-dioxane
- tetrahydrofuran
- tetrachloromethane
- chloroform<sup>3</sup>

In addition there are literature reports of the formation of a solvate with iso-butanol, [16]. During a solvent screening carried as part of this investigation, four further solvates have been identified. These were formed with:

- cyclohexanone
- cyclopentanone
- methyl-tertiary-butylether
- propylene carbonate

In order to confirm the presence of solvent in the new crystal forms, nuclear magnetic resonance spectra; (Section 2.2.4), were collected for each of the four new solvates. A

---

<sup>3</sup> Only unit cell dimensions and space-group have been determined for this solvate.

comparison of peak multiples and strengths between NMR spectra of pure phenylbutazone and those of certain of its solvates is shown in the following table.

An indication of the strength of the central peak, (s = strong, m = medium, w = weak), is given beside each peak multiple.

**Table 2 - NMR Chemical Shifts for Phenylbutazone and a Selection of its Solvates**

Group	Reference Chemical Shift (ppm)	Pure Phenylbutazone		Tetrahydrofuran Solvate		Methyl-tert-butylether Solvate		Cyclopentanone Solvate		Cyclohexanone Solvate		Propylene Carbonate Solvate		
<b>1</b>	CH3	0.90	Triplet	s	Triplet	s	Quartet	m	Triplet	s	Quartet	s	Triplet	s
<b>2</b>	CH2	1.36	Quartet	w	Quartet	w	Quartet	w	Quartet	m	Quartet	m	Triplet	w
<b>3</b>	CH2	1.48	Quartet <sup>n</sup>	w	Quartet	w	Quartet <sup>n</sup>	w	Triplet	m	Triplet	m	Quartet <sup>n</sup>	s
<b>4</b>	CH2	2.08	Quartet <sup>n</sup>	w	Quartet <sup>n</sup>	w	Quartet <sup>n</sup>	w	Quartet <sup>n</sup>	m	Quartet <sup>n</sup>	m	Quartet <sup>n</sup>	w
<b>5</b>	CH	3.38	Quartet <sup>n</sup>	w	Triplet	m	Triplet	w	Quartet <sup>n</sup>	m	Quartet <sup>n</sup>	m	Triplet	w
<b>6</b>	Phenyl, para	7.17	Quartet <sup>n</sup>	m	Quartet <sup>n</sup>	m	Quartet <sup>n</sup>	w	Quartet <sup>n</sup>	m	Quartet <sup>n</sup>	m	Quartet <sup>n</sup>	w
<b>7</b>	Phenyl, meta & ortho	7.31	Quartet <sup>n</sup>	s	Quartet <sup>n</sup>	s	Quartet <sup>n</sup>	s	Quartet <sup>n</sup>	s	Quartet <sup>n</sup>	s	Quartet <sup>n</sup>	m

<sup>n</sup> denotes that the number of recorded peaks was higher than a quartet

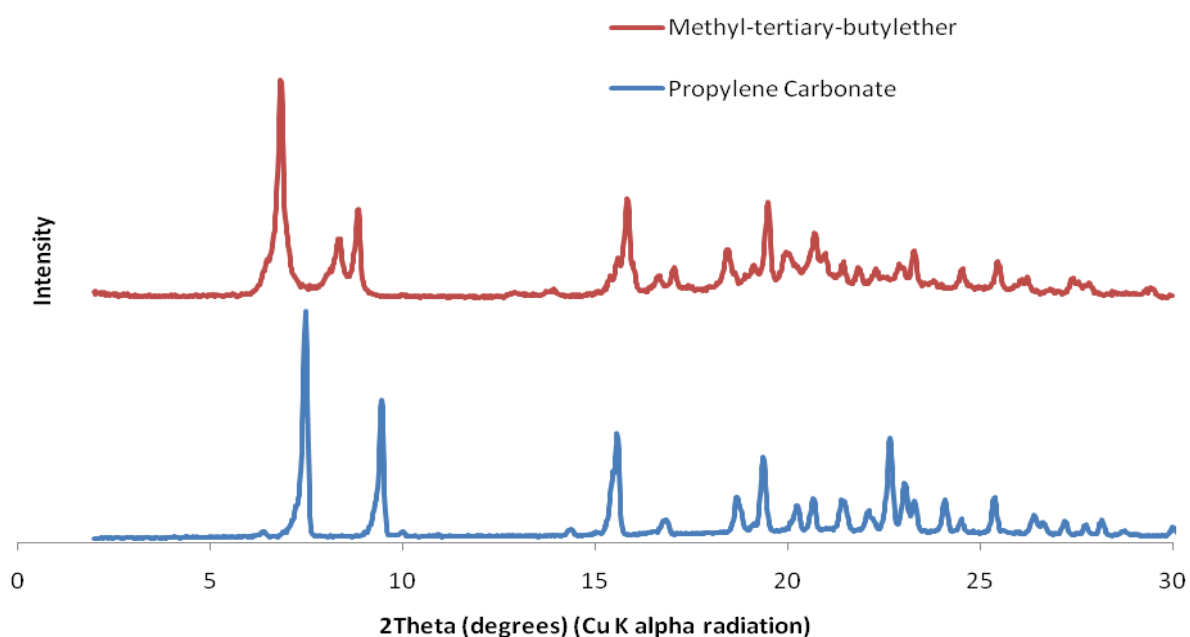
Although groupings of as many as nine peaks are observed, for reasons of clarity, multiplets of four or more peaks are designated as quartets. Chemical shift positions for the various phenylbutazone moieties in the reference spectrum are in close agreement with those appearing in spectra of the various solvated forms. Consistency of relative peak intensities is generally good also.

The size of the peak multiple for a particular moiety is observed to vary somewhat between individual crystal forms. For position 5, which has been identified as phenylbutazone's proton donating group, a markedly lower number of peaks are present in the samples of the

solvates with tetrahydrofuran, methyl-tert.-butylether and propylene carbonate; only a triplet is observed in each case. For position 3, the converse is observed; the cyclic-ketone solvate spectra exhibit a smaller multiplet than the remaining solvates.

The structures of the four new solvates were investigated by PXRD and SCXRD. Structure solutions of the solvates with methyl-tertiary-butylether and propylene carbonate were determined successfully; (Section 3.2.2), and were found to be monoclinic with space-group C2/c in common with five solvates examined by Hosokawa *et al.*. PXRD patterns of the four new solvates are shown in the following figures.

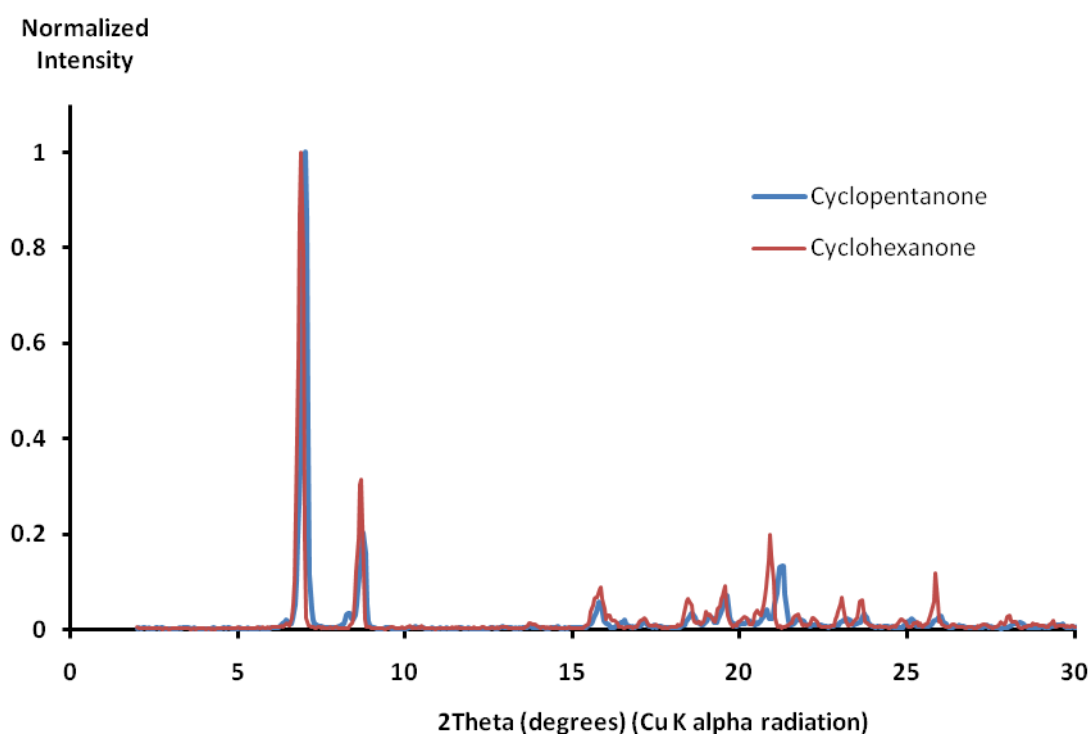
**Figure 5 - PXRD Patterns of Two New Solvates with Space Group C2/c**



The PXRD patterns of the solvates with the two cyclic-ketones share near identical major PXRD peak positions, suggesting that these two solvates have essentially identical crystal structures. Their PXRD patterns are also very similar to that of the solvate with propylene carbonate shown above.



Figure 6 - PXRD Patterns of New Solvates with Cyclic Ketone Solvents<sup>4</sup>



In the course of the present investigation, several samples of the solvate with tetrahydrofuran were prepared. Good reproducibility of the PXRD pattern was observed between different batches prepared in-house, however this PXRD pattern does not resemble that of Hosokawa *et al.*. Further investigation of this solvate was carried out, and the results are presented in Section 3.2.2.2.

### 1.3.3 Making the Different Crystal Forms

The preparation of the solvates of phenylbutazone did not entail special crystallization procedures. The alpha and delta polymorphs are readily obtained by conventional solvent crystallization techniques, also. Concomitant mixtures of these two polymorphs often occur. Results of evaporative crystallizations in a range of solvents are displayed in Table 14, where

---

<sup>4</sup> Patterns have been normalized to the same maximum intensity.

experiments intended to yield pure samples of the alpha, beta and delta forms have been summarized also.

It proved straightforward to produce pure batches of the alpha form by solvent recrystallization using either the delta or beta form as starting material. However production of pure delta form from solution was not reproducible. Pure delta form was obtained reliably by isothermal heating of the solid alpha and beta forms below the melting temperature of the delta form, but above their respective transition temperatures; (Chapter 5).

The beta form is obtained reproducibly as a precipitate by the addition of water, in which phenylbutazone is insoluble, to solutions in a number of organic solvents; the use of water miscible solvents such as methanol and ethanol is most frequently described. The precipitate, which is formed exothermically, often contains amounts of other polymorphs, most notably the delta form. Rapid stirring of the precipitation mixture has been found to assist the formation of a high proportion of the beta form, and investigation of the influence of the water:solvent ratio is also discussed in Section 4.4.3.3. It has been possible to isolate pure beta form crystals at the edge of crystallization samples formed by evaporation from organic solvent without the use of water. In addition the beta form is encountered in concomitant mixtures with the other polymorphs after evaporative crystallization in single solvents, particularly when this crystallization occurs at above-ambient temperatures.

The zeta and epsilon forms reported in the literature are produced by extended grinding, presumably through the use of an automated mill. They were not encountered during the course of solvent evaporations with single solvents or binary solvent mixtures. Existence of the gamma polymorph could not be confirmed either.

## 2 Analytical Techniques Employed

In this investigation the principal method used to identify the crystal form present has been powder X-ray diffraction. Borka and Haleblian, [41] , conclude that, “*X-ray diffraction methods on single crystals or powdered samples almost never fail due to their outstanding ability of detecting differences in crystal structures*”, whereas they consider infrared spectrometry merely as, “*a sensitive, but not necessarily infallible method in identifying polymorphs*”. PXRD patterns are typically included in patent filings of drug molecules in the United Kingdom.

Reference infrared spectra of the alpha, beta and delta polymorphs of phenylbutazone were collected, and are included as an appendix, however this technique was not relied upon for day to day polymorph identification.

Differential scanning calorimetry finds regular use in the pharmaceutical industry to identify polymorphic forms, [42-45], particularly those of less crystalline substances such as waxes. In the case of phenylbutazone, which undergoes transitions in polymorphic form that are invisible to the naked eye, DSC is a very revealing technique. Nonetheless DSC was not employed as a primary means of polymorph identification.

### 2.1 *Distinguishing between Polymorphs & Solvates*

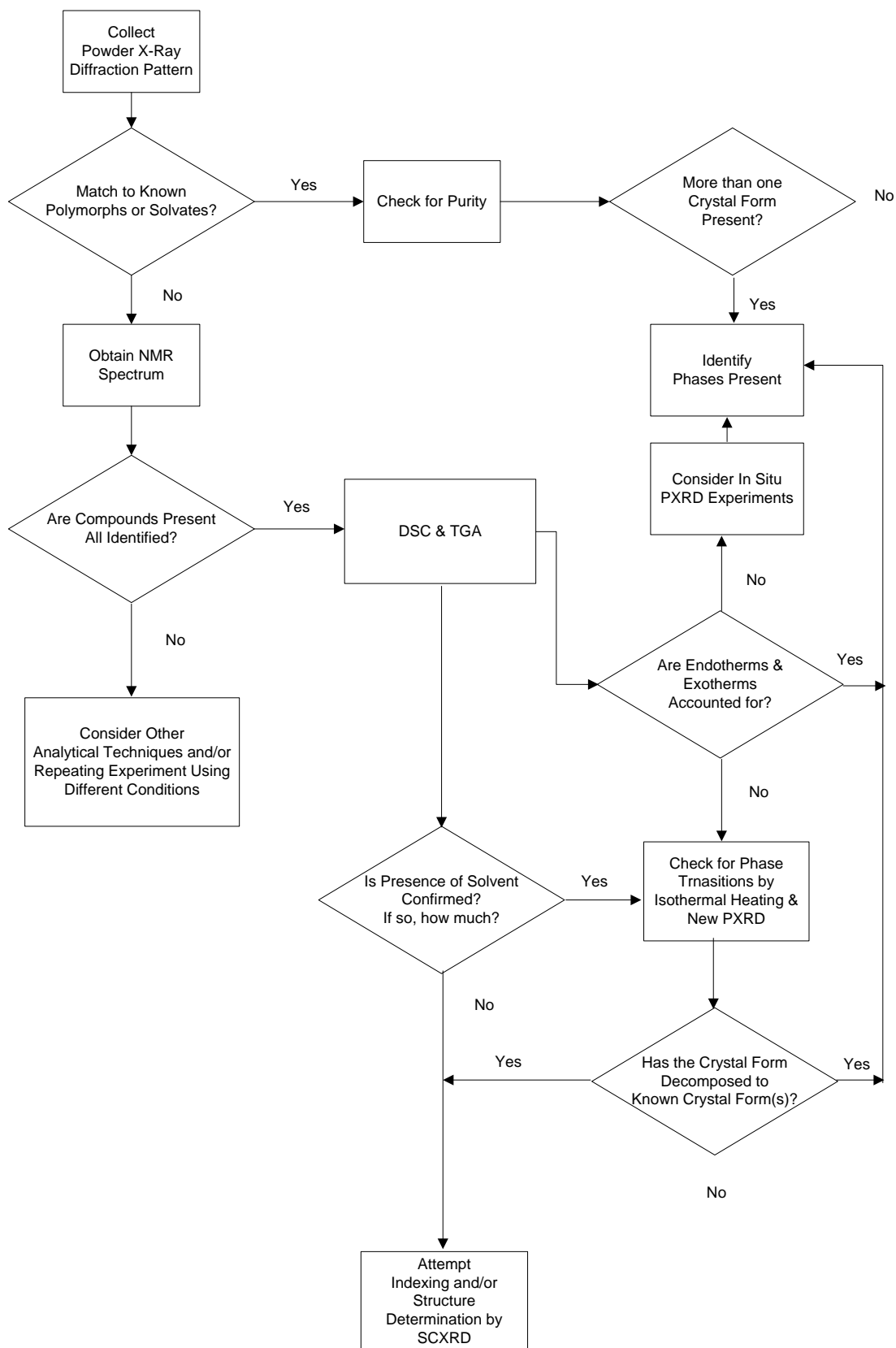
Powder X-ray diffraction served as the primary means, by which to identify solvated crystal forms as well as polymorphs. Upon obtaining a PXRD pattern whose peak positions did not correspond to those of known or putative polymorphs, confirmation of the presence of a solvated form was carried out by the methods described overleaf:

- a.  **$^1\text{H}$  Nuclear Magnetic Resonance Spectroscopy** provides chemical shifts and peak intensity ratios that are characteristic of the substances present in a sample. The presence and identity of a given solvent is clearly identifiable, where reference spectra are available, or  $^1\text{H}$  chemical shift data have been collected for the solvent in question.  $^1\text{H}$  Nuclear Magnetic Resonance spectroscopy also provides a crosscheck for the presence of side products in mixtures, where there is the likelihood of chemical reaction.
- b. **Thermogravimetric Analysis** shows up weight loss associated with desolvation, and provides corroboration of a hypothesis that a crystal form is solvated. In addition it provides insight into the manner, in which solvent is released from a known solvate. TGA may also be used for quantitative estimation of the ratio of solvent to solute, important information for crystal structure determination. However this technique is prone to error in cases where not all solvent is integrally bound-up in the crystal lattice; for example:
- solvates of high-boiling solvents, which retain surface solvent at ambient temperatures to give “wet” powder samples
  - solvates of volatile solvents, in which the solvent molecules are able to escape from all or part of the lattice prior to thermal decomposition of the crystal
- c. **Isothermal Heating** of a sample in an oven at a temperature slightly below its melting point, followed by a further PXRD scan, shows up the presence of solid-state transitions between polymorphs; (Chapter 5). Many solvated forms also exhibit a crystal form change upon heating; the most common transition is solvent expulsion leading to formation of a known polymorph.

- d. **Single Crystal Diffractometry** can confirm the presence of solvent molecules in crystal structures, assuming that the solvent molecules are readily distinguishable on the electron density map. Positive identification may be hampered by a tendency of solvent molecules to take up positions in the crystal lattice that are not entirely regular; a phenomenon often referred to as disorder.

The following decision tree summarises the chain of testing steps, which was used in this investigation to arrive at a conclusion about the nature of an unknown crystal form:

**Figure 7 - Identification Decision Tree**



## **2.2 Description of Individual Analytical Techniques**

### **2.2.1 Visual Melting Point Determination**

Heating of samples in glass capillaries was carried out in an electrically heated melting point apparatus equipped with a mercury thermometer. Samples were warmed gradually at a temperature gradient of under 5K/minute, until a change from the solid to the liquid state could be confirmed by visual inspection of the sample within the capillary.

### **2.2.2 Powder X-ray Diffraction, (PXRD)**

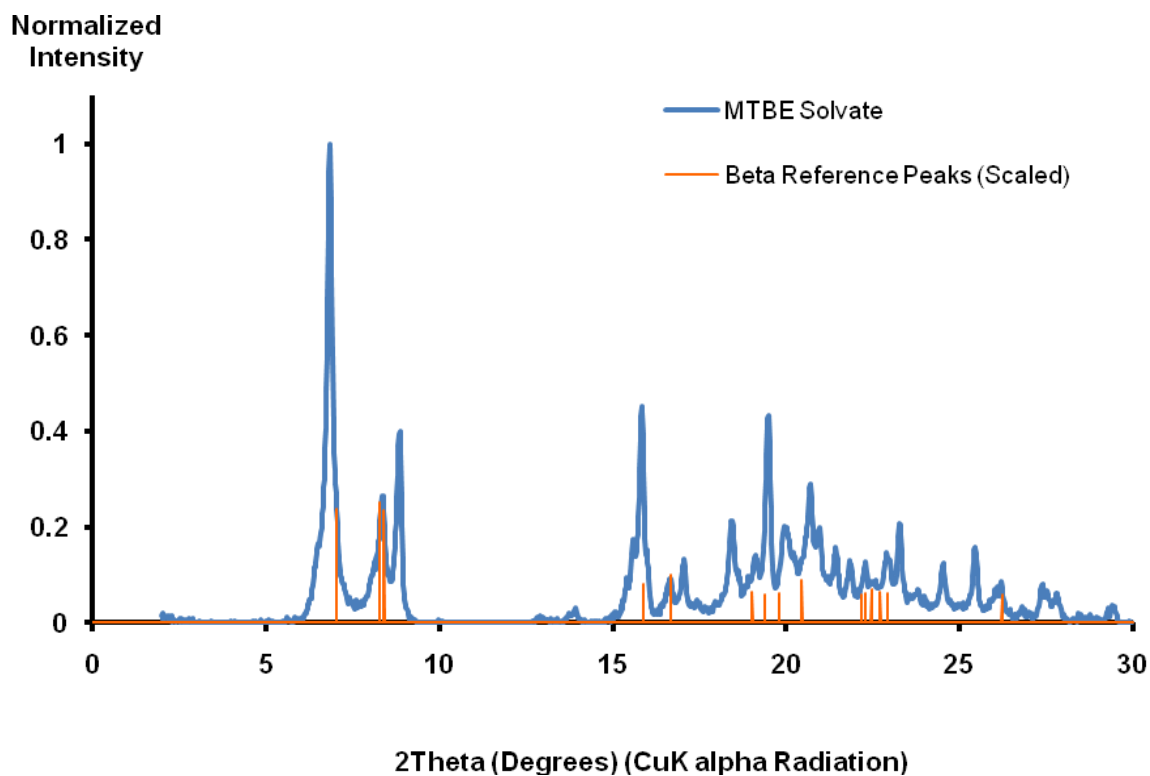
Sample particle sizes were reduced by careful grinding using pestle and mortar, and sieved in order to reduce texture and to help avoid preferred orientation. Unless otherwise specified, data were collected in conditions of ambient temperature and pressure.

In all cases raw data consisting of 2theta, intensity and error measurements were exported into Microsoft Excel<sup>®</sup>, in which various data processing tasks could be accomplished; e.g. phase identification, background count analysis and selection of peaks for unit cell indexing. Where necessary, rebinning of datasets into different 2theta step sizes was carried out either directly in Excel<sup>®</sup>, or in Matlab<sup>®</sup>, from where rebinned data were re-exported into Excel<sup>®</sup>.

Comparison charts, showing scaled reference peak positions, were used extensively to identify the polymorphs present in crystallization batches. In most cases they were capable of dispelling ambiguity, but not always. For example, the newly identified solvate of phenylbutazone with methyl-tertiary-butylether has a peak at  $2\theta = 8.3^\circ$  (CuK $_{\alpha}$  radiation). This peak position happens to be nearly identical to that of the largest peak in the diffraction pattern of the beta form;  $2\theta = 8.28^\circ$  (CuK $_{\alpha}$  radiation).

Scaling of the reference peaks is inconclusive in this case; the breadth of the largest peak at  $2\theta = 6.9^\circ$  does not preclude the possibility that some beta form is present.

**Figure 8 - Comparison of MTBE Solvate PXRD Pattern with Major Beta Peak Positions<sup>5</sup>**



In-house diffraction experiments were carried out on two diffractometers; one with flat plate geometry, the other with transmission geometry. Off-site access was obtained to Station I11 at the Diamond Light Source, which is equipped with a high-speed, powder diffractometer.

The capabilities of these instruments are outlined in the following sub-sections.

---

<sup>5</sup> Average background count has been subtracted before scaling.



### **2.2.2.1 Flat Plate Diffractometer, Siemens D500**

The following operating conditions were maintained throughout; transformer voltage 30kV and X-ray tube output current of 40mA, to generate radiation from a  $\text{CuK}_\alpha$  X-ray tube. Diffraction patterns collected on this instrument typically display low, linear background counts. The device is periodically calibrated with a quartz test sample to correct for 2theta zero drift. This diffractometer was employed for routine polymorph identification.

### **2.2.2.2 Transmission Geometry Diffractometer, Stoe Stadi<sup>®</sup>-P**

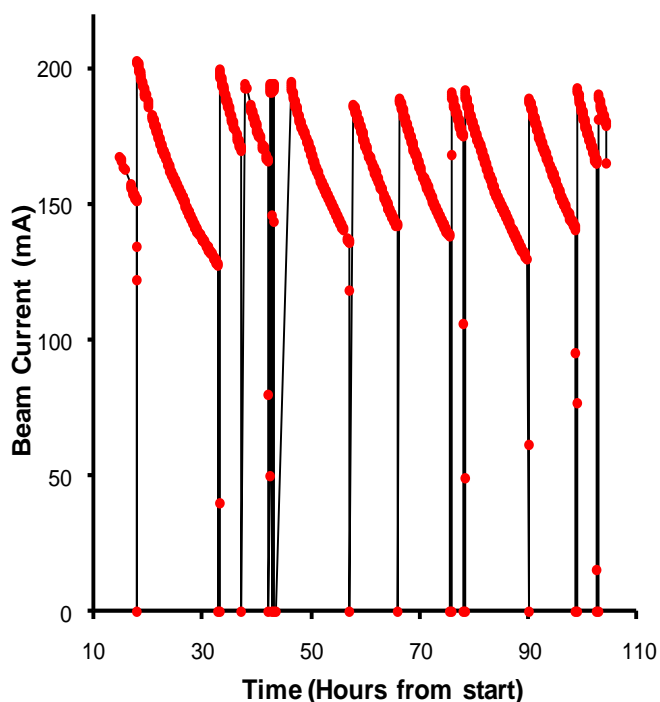
A transformer voltage of 30kV and X-ray tube output current of 40mA were maintained throughout.  $\text{CuK}_\alpha$  and  $\text{CoK}_\alpha$  X-ray tubes were employed.

This instrument may be used with a stationary, wide-angle detector capable of collecting a 2theta range of  $40^\circ$  in a single data collection period of as little as 5 minutes. For more detailed scans, a moving detector is used; this steps around the desired 2theta arc, pausing to collect X-ray counts over discrete time intervals.

The moving detector used on the Stoe Stadi<sup>®</sup>-P diffractometer has more than one channel; i.e. data counts are collected at more than one 2theta position simultaneously. In four channel detection, a typical operating mode, the final count reading comprises the sum of the readings at four different step positions, as recorded by each of the four channels individually.

This instrument is also equipped with a liquid nitrogen jet that incorporates a heating element and thermostatic control, enabling the sample to be cooled or heated isothermally across a temperature range of 100-500K.

### 2.2.2.3 Multimode Diffractometer, Station I11, Diamond Light Source



This apparatus utilizes a monochromatic synchrotron beam,  $\lambda = 0.8269\text{\AA}$ , whose intensity varies over time; (see figure opposite). Much lower counting times are needed to reach desired count levels, when compared with the in-house diffractometers described earlier.

**Figure 9 - Beam Delivery at Station I11**

The diffractometer, [46], uses a moving detector, and can collect a dataset across a  $2\theta$  range of  $180^\circ$  with step intervals of  $0.01^\circ$  in less than an hour. It is able to operate in flat-plate or transmission geometry modes. In this instance, data were collected exclusively in transmission mode, and samples were contained in capillaries. In contrast to the Stoe Stadi-P, the radiation beam is directed at the sample using parallel beam optics.

The data from each of the detectors were corrected for relative  $2\theta$  position, relative efficiency, and for synchrotron beam decay, before being merged into a single diffraction dataset. This equipment reveals peak overlaps in diffraction patterns collected on conventional diffractometers, greatly facilitating determination of the unit cell and space-group of a particular crystal form; (Section 3.1).

### 2.2.3 Single Crystal X-ray Diffraction, (SCXRD)

X-ray diffraction data of single crystals were collected on a Bruker four circle diffractometer equipped with a Smart Apex<sup>®</sup> area detector consisting of a charge-coupled device. The X-ray radiation employed in this diffractometer is MoK<sub>α</sub> ( $\lambda = 0.7103\text{\AA}$ ). Control of all instrument parameters is exercised by the Bruker Saint<sup>®</sup> software package, which also performs data reduction. This suite incorporates XPrep and XShell modules for structure solution, as well as a version of Shelx for solution refinement; the suite is referred to collectively as Shelxtl<sup>®</sup>. All single crystal datasets were collected at 150K. This temperature is maintained by a liquid nitrogen flow, which is controlled by means of a Windows<sup>®</sup> PC with an appropriate software interface. Data collection takes place in two distinct steps:

- An orientation matrix consisting of about 60 frames is collected, from which automatic unit cell determination is attempted; total duration, 0.5-2 hours.
- A full dataset consisting of approximately 1800 frames is collected; total duration, 7-15 hours.

The results of the unit cell determination step were used to reach a decision, whether to proceed with the collection of a full dataset. In general, the absence of a reasonable set of unit cell dimensions from the first step militated against collection of a full dataset. It was far from unusual to test half a dozen crystals in the first step, before encountering a specimen whose results augured well enough to proceed to the second step.

The diffractometer's preset angle selections were employed in both steps.

## 2.2.4 <sup>1</sup>H Nuclear Magnetic Resonance Spectroscopy, (NMR)

Only <sup>1</sup>H NMR spectra were collected. Samples were dissolved in CDCl<sub>3</sub>, and examined in a Bruker, Avance500<sup>®</sup> spectrometer. Calibration is performed using solvent residual peaks; 7.26ppm for CDCl<sub>3</sub>. Data processing is carried out using Bruker Xwin<sup>®</sup> NMR software.

A reference spectrum was prepared for pure phenylbutazone, and is displayed in Appendix 4. The presence of multiplet peak positions is indicated by shading of groups of peaks. These reference data were used to match chemical shift positions in subsequent spectra; for example those collected from samples of phenylbutazone's solvates. In many cases solvent components and residues could be identified using literature data, [47]. In those cases where literature chemical shift data were not located, a reference spectrum was prepared for the solvent under investigation.

The relative positions of the hydrogen atoms on the alkyl chain and the phenyl groups may be deduced from the chemical shifts of the various functional groups contained in similar molecules that are present in literature listings; e.g. in spectra of common solvents. For phenylbutazone the chemical shifts of the phenyl group hydrogen atoms are in the vicinity of 7ppm, whereas the alkyl hydrogen atoms are in the region of 0.8 to 3.5ppm.

NMR spectrum analyses of phenylbutazone are available from literature sources, [7, 48]. The in-house reference spectrum is in good agreement with the analysis of Tanaka *et al.* with only one exception; the peak at 1.57ppm. This most likely indicates the presence of a trace of water, whose chemical shift in CDCl<sub>3</sub> is measured at 1.56 ppm by Gottlieb *et al.*. The outlying peak at 7.25ppm is very probably that of the solvent residual. The chemical shifts are marked according to the moiety to which they pertain, and given a magnitude (strong, medium, weak, trace) according to the size of the central peak in the multiplet, [49].

### **2.2.5 Differential Scanning Calorimetry, (DSC) & Thermogravimetric Analysis, (TGA)**

A Netzsch Jupiter<sup>®</sup> combined DSC & TGA was used. In most cases, both thermogravimetric and calorimetric measurements were carried out simultaneously. This equipment is able to carry out consecutive isothermal heating and constant-gradient temperature increase steps. Reference DSC scans of the alpha, beta and delta polymorphs are shown in Appendix 2.

Thermogravimetric Analysis was used, in certain instances, when the presence of a solvate was suspected. The TGA is equipped with a precision balance inside the furnace, enabling high-accuracy measurement of weight changes during heating cycles. Weight loss during the TGA scan is an indicator of the presence of solvent; the heating of pure phenylbutazone was not accompanied by weight loss; i.e. no tendency towards sublimation was confirmed during heating in the solid phase, and no discernable weight loss through vapourisation occurred after melting. Some drift in scale readings was encountered in TGA measurements, and zero correction runs with no sample in the pan were carried out in order to confirm that drift was the result of buoyancy effects.

### **2.2.6 Infrared Spectrometry, (IR)**

Infrared spectra were collected across a wavenumber range of 400-4000 $\text{cm}^{-1}$  at a resolution of 4  $\text{cm}^{-1}$ , using a Shimadzu FTIR-8700, Fourier Transform Spectrometer. KBr sample disks were prepared using a Specac press, capable of applying a pressure equivalent to a weight of 15 tons on the sample mixture. Data processing was carried out with Shimadzu's *Hyper*<sup>®</sup> I.R. personal computer software package, which is based on *Spectacle*<sup>®</sup> by LabControl GmbH. Reference IR spectra of the alpha, beta and delta forms of phenylbutazone are shown in Appendix 3.

### 3 Structure Determination of Polymorphs and Solvates

#### 3.1 Indexing of Powder Diffraction Data

Indexing of powder diffraction patterns seeks to match observed interplanar distances,  $d_{hkl}$ , with the appropriate reflection plane,  $h,k,l$ , in simultaneous solution sets that fit the observed data with as high a figure of merit, FOM, as possible in order to determine the most probable unit cell dimensions for a crystal form. Peak intensity information is generally not required.

Figure 10 - Generalized Parallelepiped Representation of the Unit Cell<sup>6</sup>

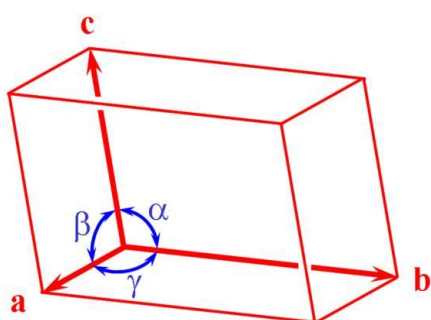
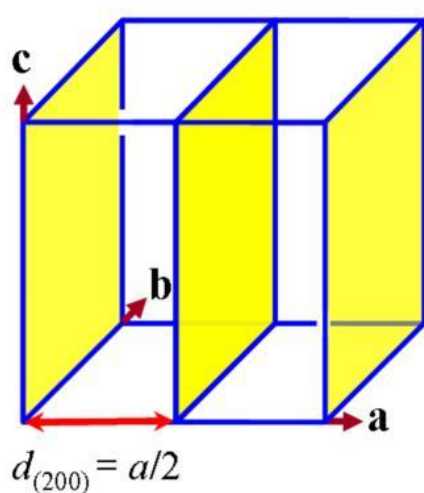


Figure 11 -  $H,K,L$  Indexing Example - Planes of a Cubic Lattice<sup>7</sup>



<sup>6</sup> Reproduced from Pecharsky & Zavalij, *Fundamentals of Powder Diffraction*, 2005, Springer, New York, p6.

<sup>7</sup> Reproduced from Pecharsky & Zavalij, *Fundamentals of Powder Diffraction*, 2005, Springer, New York, p47.

The geometrical relationships between observed d-spacings and their associated plane indices are provided in a variety of different text books on crystallography, [50, 51]. For triclinic, monoclinic and orthorhombic unit cells, the crystal systems encountered during this investigation, these relationships are shown below:

**Equation 1 - Triclinic d-Spacing**

$$\frac{1}{d_{hkl}^2} = \frac{\left[ \frac{h^2}{a^2 \sin^2 \alpha} + \frac{2kl}{bc} (\cos \beta \cos \gamma - \cos \alpha) + \frac{k^2}{b^2 \sin^2 \beta} + \frac{2hl}{ac} (\cos \alpha \cos \gamma - \cos \beta) + \frac{l^2}{c^2 \sin^2 \gamma} + \frac{2hk}{ab} \cos \alpha \cos \beta - \cos \gamma \right]}{(1 - \cos^2 \alpha - \cos^2 \beta - \cos^2 \gamma + 2 \cos \alpha \cos \beta \cos \gamma)}$$

**Equation 2 - Monoclinic d-Spacing, (*angle  $\beta$  unique*)**

$$\frac{1}{d_{hkl}^2} = \frac{h^2}{a^2 \sin^2 \beta} + \frac{k^2}{b^2} + \frac{l^2}{c^2 \sin^2 \beta} + \frac{2hl \cos \beta}{ac \sin^2 \beta}$$

**Equation 3 - Orthorhombic d-Spacing**

$$\frac{1}{d_{hkl}^2} = \frac{h^2}{a^2} + \frac{k^2}{b^2} + \frac{l^2}{c^2}$$

Where:

$h$  = Index number of plane along x-axis

$k$  = Index number of plane along y-axis

$l$  = Index number of plane along z-axis

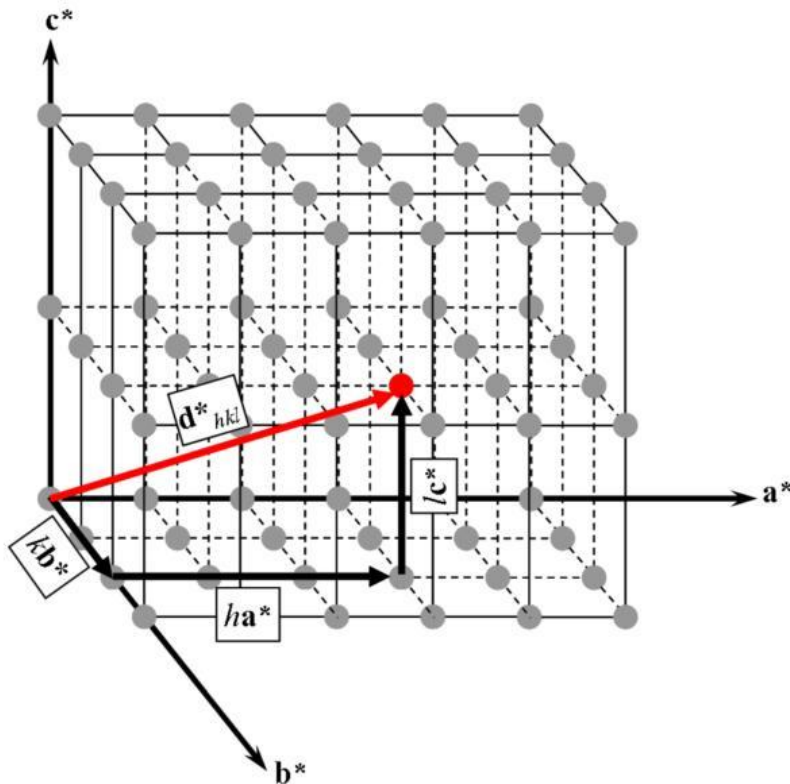
$d$  = Perpendicular distance between a plane with index,  $hkl$ , and the origin.

$a$ ,  $b$  and  $c$  represent lengths of dimensions of the unit cell;

$\alpha$ ,  $\beta$ , and  $\gamma$  represent the angles between the cell lengths  $a$ ,  $b$  and  $c$ ;

In most cases the equality for which simultaneous solutions are sought is expressed in terms of reciprocal lattice points, the points which correspond to individual planes, when the planes of the crystal structure in direct space are projected into reciprocal space.

**Figure 12 - Example of a Reciprocal Lattice<sup>8</sup>**



The reciprocal unit cell dimensions, which are denoted by an asterisk, have vector properties and are derived from the direct space unit cell dimensions as follows:  $a^* = 1/a$ ,  $b^* = 1/b$ ,  $c^* = 1/c$ , and  $d^* = 1/d$ . The distance,  $d^*$ , from the origin to a reciprocal lattice point,  $h,k,l$ , is given vectorially by:

**Equation 4 - General Expression for Reciprocal Lattice d-Spacing**

$$d^*_{hkl} = ha^* + kb^* + lc^*$$

<sup>8</sup> Reproduced from Pecharsky & Zavalij, *Fundamentals of Powder Diffraction*, 2005, Springer, New York, p167.



The quantity,  $d_{hkl}^*$ , may equally well be expressed in scalar terms analogously to the three equations for the direct space interplanar distance shown earlier. Typically the symbol  $Q$  is used to denote the value of  $d_{hkl}^{*2}$ :

**Equation 5 - Triclinic Reciprocal Lattice d-Spacing**

$$Q = d_{hkl}^{*2} = (ha^*)^2 + (kb^*)^2 + (lc^*)^2 + 2hka^*b^* \cos \gamma^* + 2hla^*c^* \cos \beta^* + 2klb^*c^* \cos \alpha^*$$

**Equation 6 - Monoclinic Reciprocal Lattice d-Spacing, (*angle  $\beta$  unique*)**

$$Q = d_{hkl}^{*2} = (ha^*)^2 + (kb^*)^2 + (lc^*)^2 + 2hla^*c^* \cos \beta^*$$

**Equation 7 - Orthorhombic Reciprocal Lattice d-Spacing**

$$Q = d_{hkl}^{*2} = (ha^*)^2 + (kb^*)^2 + (lc^*)^2$$

Indexing was carried out on a Windows<sup>®</sup> personal computer using software designed exclusively for this purpose. A recent survey of powder X-ray diffraction techniques by The Royal Society of Chemistry, [52], catalogues crystallographic software packages designed for unit cell indexing. An overview of the differences in the methods by which these indexing programs search for unit cell parameters is provided in the IUCr's 2002 monograph on structure determination from PXRD data, [53].

The software employed in this investigation was the collection of indexing programs contained in the Crysfire suite, which is available from the website of the Collaborative Computational Project 14, [54].

The following programs included in this suite were used to search for unit cell solutions from PXRD peak sets:

- ITO
- TREOR
- KOHL
- LZON
- DICVOL
- FJZN

Q-matching to observed peaks forms the basis for the search algorithms in ITO, TREOR, DICVOL and in the more recent indexing program, KOHL, [55, 56].

For all the programs included in Crysfire, common figure of merit values are reported in a summary output of solutions. For each solution the first reported statistic is the number of peak positions or “lines” that were included in the simultaneous solution set.

The maximum value, 20 lines indexed, indicates that a match between 20 calculated and observed index lines was found within the prescribed tolerance for the 2theta values (or d-spacings).

Most programs in Crysfire caution against the adoption of solutions in which fewer than 17-18 lines have been successfully matched to a set of index values for a particular unit cell solution.

The bases of the most common FOMs are as follows:

**Equation 8 - de Wolff Figure of Merit,  $M_{20}$**

$$M_{20} = \frac{Q_{20}}{2\langle Q \rangle N_{20}}$$

Where:

$Q_{20}$  =  $Q$  value of 20<sup>th</sup> observed and indexed line

$N_{20}$  = Number of calculated reflections up to the  $d$  value corresponding to  $Q_{20}$

$\langle Q \rangle$  = Average discrepancy between observed and calculated  $Q$  values for these 20 lines

**Equation 9 - Smith and Snyder Figure of Merit,  $F_N$**

$$F_N = \frac{1}{\langle |\Delta 2\theta| \rangle} \frac{N}{N(\theta_g)}$$

Where:

$\theta_g$  = Limit value of  $2\theta$  for individual search

$\langle |\Delta 2\theta| \rangle$  = Average value of the modulus of differences between observed and calculated  $2\theta$

$N(\theta_g)$  = Number of different calculated  $Q$  values up to  $\theta_g$

$N$  = Number of observed lines below  $\theta_g$

The higher the values of the FOMs, the closer the match between individual observed and calculated values of  $2\theta$  (or  $d$ -spacing). For  $M_{20}$  values of 10 or higher constitute a good match, whereas for  $F_N$  values of 20-60 indicate a solution with a high confidence level.

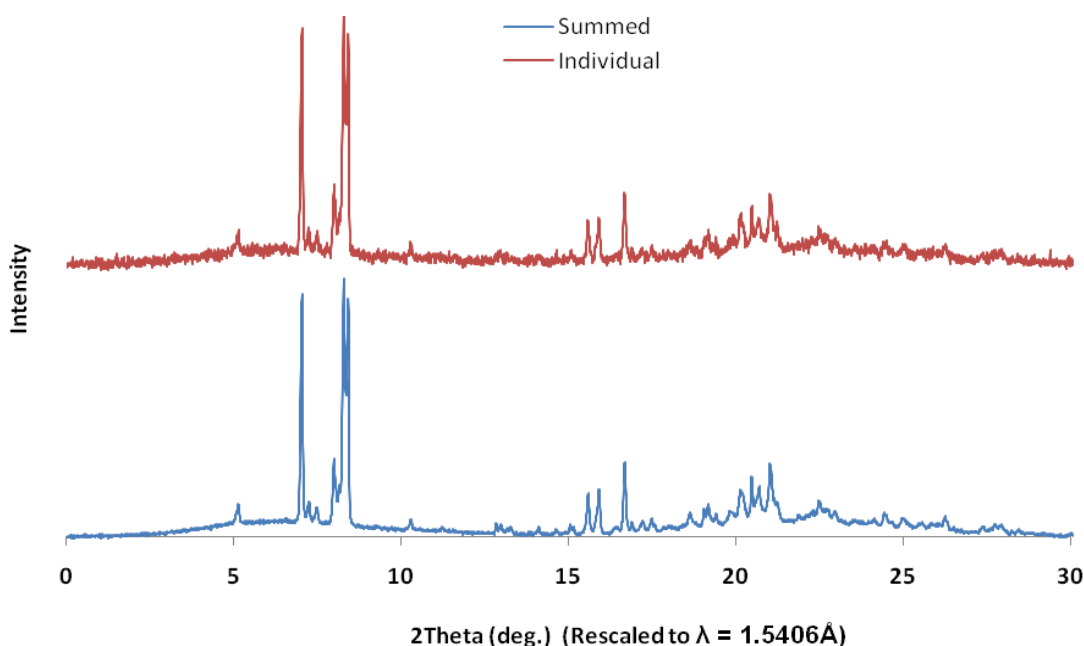
### 3.1.1 Peak Input Selection for PXRD Indexing

The importance of high quality PXRD data for accurate unit cell determination is stressed by many texts on crystallography. Synchrotron PXRD data generally offer very clear peak information, and are ideal for indexing purposes. Another method to improve peak selection is through the use of composite patterns comprised of several patterns of the same sample, in which count numbers at each  $2\theta$  step are added to give a cumulative pattern.

Composite patterns allow the effects of background counts to be averaged across several datasets. If the assumption can be made that background fluctuations occur randomly above or below a mean number of background counts for an individual diffraction dataset, then addition of multiple diffraction datasets for the same sample results in an averaging out of background fluctuations. This leads to a flatter overall background, enabling small diffraction peaks to be resolved from background noise with greater confidence. Analysis of background count information and discussion of its statistical treatment is provided in Appendix 5.

The following patterns show an individual plot of one PXRD pattern and a composite plot of several PXRD patterns of the same sample of phenylbutazone collected at Station I11 of the Diamond synchrotron facility.

**Figure 13 – Example of Improved Resolution from Summation of Repeated PXRD Scans**



When carrying out pattern summation, care was taken to be sure that underlying peak positions of the individual patterns did not show marked deviations which, upon superimposition of additional patterns, would obscure the underlying peak information.

### ***3.2 Indexing of Phenylbutazone Crystal Forms***

When examining sets of possible unit cell dimensions, solutions from higher symmetry crystal systems were favoured, assuming that their figures of merit reached acceptable values, and provided that the suggested unit cell dimensions did not exceed sensible limits. Higher symmetry than an orthorhombic lattice, [57], was not anticipated, however. Knowledge of the unit cell volume of the alpha form of phenylbutazone was one indicator of likely unit cell dimensions of other crystal forms, but the possibility of discovering additional symmetries in unit cells of double or quadruple the size was borne in mind.

In general, it proved difficult to arrive at firm conclusions about unit cell solutions of phenylbutazone crystal forms from Crysfire output alone. Unlike the unit cell determination example shown by Ladd and Palmer, [50], there were very few instances in which two separate programs in the suite arrived at the same solution, making the identification of a single set of unit cell dimensions difficult, unless a priori structural information was to hand.

Crysfire's output has been formatted to integrate with Chekcell, a program that validates individual solutions, and which runs a comprehensive set of space-group tests in order to arrive at suggestions of the likeliest unit cells and space-groups for a given powder pattern. Chekcell also includes search routines for sub-cells and super-cells of an individual unit cell solution, and permits trials of different space-group selections on each unit cell solution proposed. This program was used extensively to help narrow down the selection of probable unit cell dimensions.

In order to test the robustness of solution sets, the Crysfire programs were also run iteratively on slightly modified sets of peak inputs with the objective of identifying solutions that withstood specific minor peak omissions.

Partly owing to the inconclusive nature of the indexing results, manual checks of individual unit cell solutions were carried out. General listings of index positions with no observed extinction conditions were calculated using a spreadsheet prepared for this purpose.

Access was also obtained to the Fortran program, Dragon, [58], which not only calculates index positions for a given unit cell in a particular crystal system, but which also applies extinction conditions for individual space-groups. Dragon output data can readily be exported into spreadsheets, where a simple, graphical check of the validity of proposed indexing solutions can be carried out.

The results of unit cell determination of individual polymorphs and solvates of phenylbutazone are described in the following sub-sections.

### 3.2.1 Polymorphs

#### 3.2.1.1 Alpha

**Table 3 - Unit Cell Dimension Comparison of the Alpha Form<sup>9</sup>**

Cell Dimension Group	Space Group	a (Å)	b (Å)	c (Å)	$\alpha$ (°)	$\beta$ (°)	$\gamma$ (°)	Volume (Å <sup>3</sup> )
Singh & Vijayan, 1977 (Single Crystal 2300 Reflections)	P2 <sub>1</sub> /c	21.695 (±0.004)	5.823 (±0.002)	27.881 (±0.004)	90	108.06 (±0.10)	90	3348.57
Paradies, 1987 (Single Crystal - 296K 4977 Reflections)	P2 <sub>1</sub> /c	21.701 (±0.009)	5.822 (±0.002)	27.866 (±0.009)	90	108.06 (N/A)	90	3347.20
Targett & Cockcroft, 2008 (Single Crystal - 150K 7765 Reflections)	P2 <sub>1</sub> /c	21.415 (±0.004)	5.729 (±0.001)	27.782 (±0.005)	90	108.068 (±0.003)	90	3240.40
Targett & Cockcroft, 2008 (PXRD – 298K – 20 lines, FOM 30.9)	P2 <sub>1</sub> /c	21.719	5.826	27.882	90	108.066	90	3354.05

<sup>9</sup> In the case of single crystal diffraction results, the estimated error is also provided in parentheses.

The preceding table summarizes the unit cell dimensions of the alpha form, including the solutions of Singh & Vijayan and Paradies; these results were obtained from single crystal X-ray diffraction experiments. In this investigation the alpha form's unit cell was determined first by single crystal diffraction as outlined in the next section. Subsequently a very similar solution was obtained from the synchrotron powder diffraction data collected at Diamond using the indexing program, KOHL. The slightly larger size of the unit cell calculated from PXRD data is most likely attributable to the higher temperature at which the data were collected.

Refinement of the unit cell was carried out on the single crystal dataset; (Section 3.5.2). The synchrotron PXRD pattern revealed peak overlaps present in the literature PXRD patterns collected on standard X-ray diffraction equipment; (Figure 2). Both the synchrotron PXRD pattern and a listing of index positions are shown in Appendix 1.

### **3.2.1.2 Beta**

The unit cell dimensions of the beta form have not been reported in the literature. In this investigation, beta form powder diffraction patterns displayed larger variations in peak positions than those encountered in PXRD datasets of the alpha and delta forms.

It seems reasonable to infer that the beta form is the least ordered crystal structure among the three commonly encountered forms. This conclusion is supported by comparison of the baselines of the various polymorphs; the beta form pattern has a less uniform baseline than the other two polymorphs.

A reference PXRD pattern of the beta form was collected at Diamond, however this revealed the presence of a small proportion of the delta polymorph. Delta peaks were extracted from the data, before compilation of input peaks for unit cell determination using Crysfire.

Indexing was further complicated by a difference in the low angle peak positions in PXRD patterns collected in-house and those collected at Diamond Light Source. In-house data consistently indicated the presence of a very small peak at  $2\theta = 4.15^\circ$ . However this peak was absent from the synchrotron PXRD patterns and from literature patterns of the beta form. Indexing was carried out both with and without the peak at  $2\theta = 4.15^\circ$  included.

With the peak at  $2\theta = 4.15^\circ$  included, Crysfire yielded unit cell solutions that were either triclinic (space-group  $P\bar{1}$  or  $P\bar{1}$ ) or monoclinic (space-group  $P2_1$ ); the former outnumbering the latter by a factor of about 5. Unit cell sizes lay between<sup>10</sup> 1800-4400Å<sup>3</sup> for the triclinic solutions and between 4000-6000Å<sup>3</sup> for the monoclinic solutions.

Without the peak at  $2\theta = 4.15^\circ$ , only one monoclinic solution was found; unit cell size of 4000Å<sup>3</sup>. A near identical monoclinic solution could also be found when the  $2\theta = 4.15^\circ$  peak was included, however only 16 out of 20 observed peak positions are matched in this solution; the  $2\theta = 4.15^\circ$  peak was not among the matched peaks.

Leaving aside the issue of inclusion or exclusion of the  $2\theta = 4.15^\circ$  peak, it became apparent that even very slight variations in the peak inputs led to changes in the dimensions of triclinic solution sets. Furthermore only one solution among over 40 alternatives was encountered, on which two programs agreed.

In view of these difficulties, indexing solutions of the beta form are presented with only low confidence. The most probable solutions are shown in the table that follows:

---

<sup>10</sup> Excludes one outlying triclinic solution at 7930Å<sup>3</sup>.



**Table 4 - Selected Unit Cell Solutions of Beta Form**

Cell Dimension System & Space-group	a (Å)	b (Å)	c (Å)	$\alpha$ (°)	$\beta$ (°)	$\gamma$ (°)	Volume (Å <sup>3</sup> )
*Triclinic, P1 Lines Indexed 20, FOM 10	13.8	15.3	11.7	113	86	116	2030
*Triclinic, P1 Lines Indexed 20, FOM 10	12.5	13.7	12.1	111	105	95	1836
Triclinic, Lines Indexed 19, FOM 8	6.9	12.8	22.2	81	77	91	1887
Monoclinic, P2 <sub>1</sub> /c Lines Indexed 16, FOM 8	14.1	23.5	13.6	90	117	90	4000- 4040 <sup>†</sup>

<sup>†</sup>Several variations of this solution were found, differing by less than 0.2Å in dimension

\* Excludes peak at  $2\theta = 4.15^\circ$

### 3.2.1.3 Delta

Similarly to the beta form, a search of the literature did not yield any indications of the unit cell dimensions of the delta form of phenylbutazone. Synchrotron PXRD data of the pure delta form were obtained at Diamond; (Appendix 1).

Although not entirely conclusive, the results of Crysfire indexing of the delta form pattern may be presented with much higher confidence. The KOHL output was again the most illuminating. It indicates that the unit cell is probably orthorhombic with two long dimensions of approximately 34Å each and a shorter third dimension of between 5-10Å. However no fewer than 9 variations of this solution were located, differing only in their shortest cell dimension; (20 lines indexed, FOM ~ 20). Initially the smallest cell volume in this family that Kohl located was 8588Å<sup>3</sup> which corresponds to  $c = 7.22\text{Å}$ . Upon varying the choice of input peaks, the solution with  $c = 11.505\text{Å}$  established itself as the most likely, however performing a sub-cell search on this solution in Chekcell revealed a favourable solution with dimension,  $c = 5.753\text{Å}$ , half the size of the most robust cell solution, and sharing

approximately the same short dimension as the alpha form. Reassuringly the same solution of  $6837\text{\AA}^3$ , possessing a short dimension of  $5.75\text{\AA}$ , could also be determined separately using the indexing program ITO.

**Table 5 - Probable Unit Cell Dimensions of Delta Form**

Cell Dimension System & Index Stats.	Z Factor	a ( $\text{\AA}$ )	b ( $\text{\AA}$ )	c ( $\text{\AA}$ )	$\alpha$ ( $^\circ$ )	$\beta$ ( $^\circ$ )	$\gamma$ ( $^\circ$ )	Volume ( $\text{\AA}^3$ )
Orthorhombic 20 lines indexed, FOM 20.4	32	34.825	34.135	11.505	90	90	90	13677
Orthorhombic 20 lines indexed, FOM - subcell	16	34.816	34.147	5.751	90	90	90	6837

Identification of the space-group symmetry was carried out using the automatic space-group determination facility in Expo2004, which reports the fit to a particular space-group with its own figure of merit calculation, [59].

For the unit cell solution with Z value of 32, the highest figure of merit recorded by Expo was 0.20; this was achieved in the space-group  $P2_12_12_1$ . Four further space-group alternatives were determined to have FOM values between 0.02-0.06. For the unit cell solution with Z value of 16, fifteen different space-groups had figures of merit between 0.01-0.10; the highest amounted to 0.08.

As is discussed later on, more reflection conditions are observed than the three general conditions of space-group  $P2_12_12_1$ ;  $h00 = 2n$ ,  $0k0 = 2n$ ,  $00l = 2n$ . Primarily for this reason, the subcell option is favoured, and subsequent analysis is based upon the assumption that  $Z = 16$  is the correct value. This leads to a calculated density of  $1.20\text{g/cm}^3$  compared to a value of  $1.26\text{g/cm}^3$  for the alpha form.

A listing of the most probable space-groups for the unit cell size  $6837\text{\AA}^3$  was obtained from Expo. In depth space-group testing was then carried out in the following manner:

- a) First a space-group was assumed, and this assumption was used to generate a listing of index positions observing the relevant reflection conditions. A plot of theoretical index positions vs. the observed peak positions was then prepared. Plots for the space-groups Pnn2 and Pba2 are shown later in this section.
  
- b) After the list of likely space-groups had been narrowed down by visual index position matching, the reflection conditions were examined in Excel<sup>®</sup> in order to identify systematic absences, [60, 61]. Searches were conducted for:
  - General Absences – hkl – indicating a centred lattice
  - Zonal Absences – 0kl, h0l and/or hk0 – indicating the presence of a glide plane(s)
  - Row Absences – h00, 0k0, 00l – indicating the presence of a screw axis(es)
  
- c) Lastly individual Rietveld refinements of the structural model were conducted for each of the shortlisted space-groups. The residual factors resulting from each space-group trial give numerical output, with which to compare the match to the observed data for each assumed space-group. The definitions of the two residual outputs from the refinement are provided overleaf, [50, 62].

**Equation 10 – Definition of Profile R-factor,  $R_p$**

$$R_p = \frac{\sum_j |y_{obs,j} - y_{calc,j}|}{\sum_j y_{obs,j}}$$

**Equation 11 - Definition of Weighted Profile R-factor,  $R_{wp}$**

$$R_{wp} = \frac{\sum_j w_j (y_{obs,j} - y_{calc,j})^2}{\sum_j w_j (y_{obs,j})^2}$$

Where:

$y_{obs,j}$  = Observed count number at point,  $j$

$y_{calc,j}$  = Calculated count number at point,  $j$

$w_j$  = Weighting factor of point,  $j$

The International Tables for Crystallography Volume A list a total of six minimal non-isomorphic supergroups to space-group 34, Hermann Mauguin symbol Pnn2, suggested by Expo. All these alternatives were checked using DRAGON. Among these, one space-group, Pnnm shares not only the same index positions; (Appendix 1), but also the same reflection conditions. This space-group cannot be discounted solely by using information from the powder diffraction data.

Also checked were the space-groups Pba2 and Pbam. These share identical index positions with one another and, between  $d = 24.4\text{-}5.7\text{\AA}$ , with space-group Pnn2 also, but their index positions diverge slightly from those of space-group Pnn2 at d-spacings below  $5.7\text{\AA}$ .

The related space-group Pban fits the data less well; the two small observed peaks at  $2\theta = 5.69^\circ$  and  $5.76^\circ$  are absent from the theoretical index positions. All the quoted  $2\theta$  values have been rescaled for  $\text{CuK}\alpha$  radiation of wavelength  $1.5406\text{\AA}$ .

**Figure 14 - Phenylbutazone Delta Form in Space-group Pnn2 (or Pnnm)**

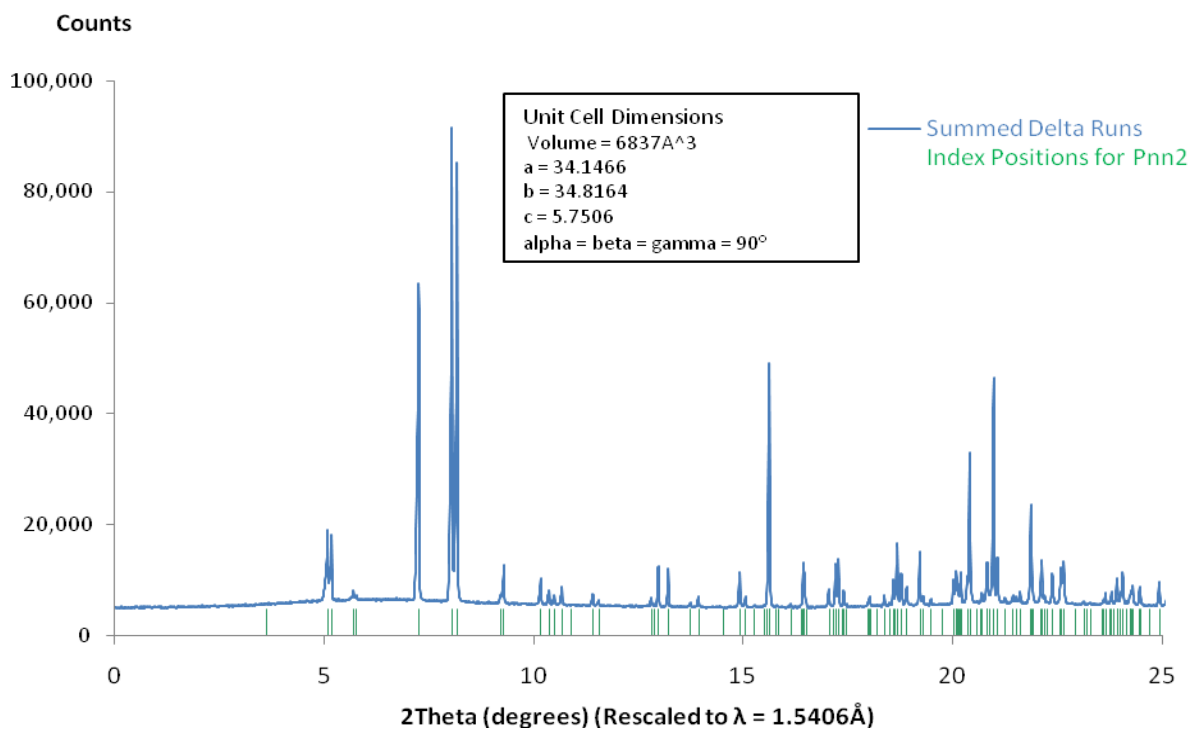
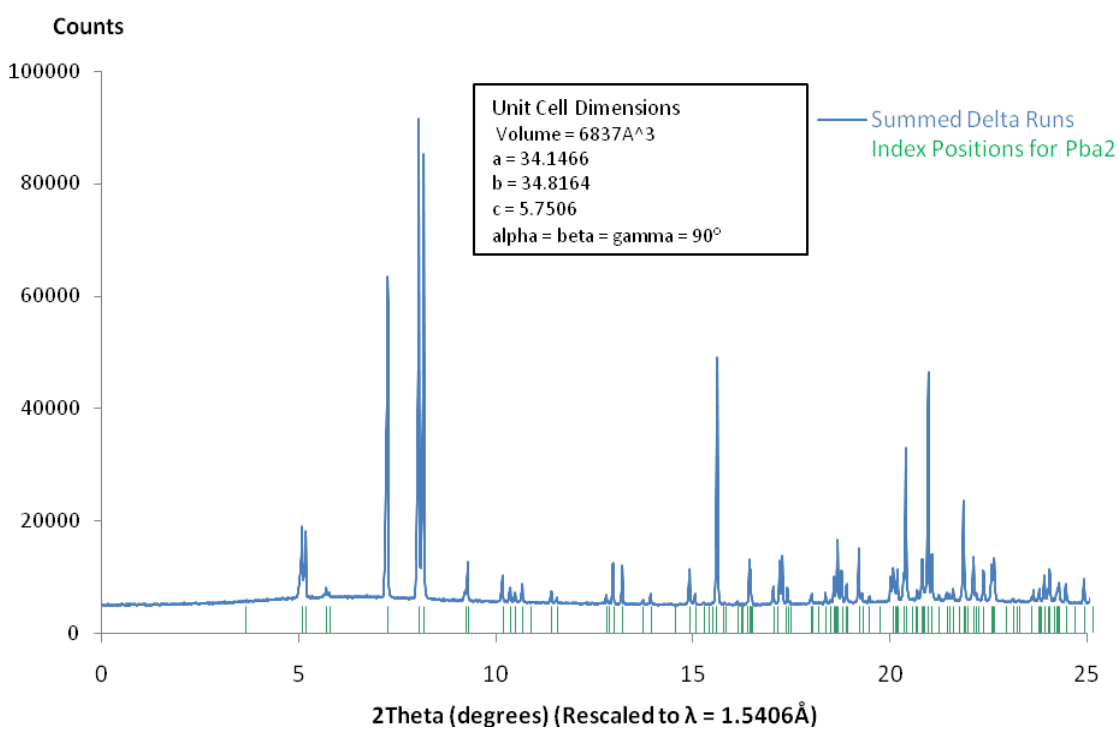


**Figure 15 - Phenylbutazone Delta Form in Space-group Pba2 (or Pbam)**



For the space-groups Pnn2 and Pnnm, which have the same general reflection conditions, the fulfilment<sup>11</sup> of general reflection conditions within this limited set of observations is shown in the following table. Similarly the fulfilment of general reflection conditions for Pba2 & Pbam is shown in Table 7.

**Table 6 - Fulfilment of General Reflection Conditions for Delta in Pnn2 & Pnnm**

Reflection Condition	Condition Observed (Yes/No)
h00, $h = 2n$	Yes
0k0, $k = 2n$	Yes
00l, $l = 2n$	Too few reflections to draw firm conclusion
0kl, $k + l = 2n$	Yes
h0l, $h + l = 2n$	Yes

**Table 7 - Fulfilment of General Reflection Conditions for Delta in Pba2 & Pbam**

Reflection Condition	Condition Observed (Yes/No)
h00, $h = 2n$	Yes
0k0, $k = 2n$	Yes
0kl, $k = 2n$	Yes
h0l, $h = 2n$	Yes

These observations indicate that space-groups Pba2 and Pbam are not ruled out. Nonetheless the index positions for these space-groups match the observed peaks less convincingly than is the case in Pnn2 or in Pnnm.

---

<sup>11</sup> A reflection condition was considered to be met when only the even plane indices indicated were observed; this does not necessarily denote that all theoretical even index values could be matched to an observed peak.

Refinement of the  $6837\text{\AA}^3$  solution was carried out in Expo2004 which has a Rietveld procedure built into its structure modelling package. A plausible structural model did not emerge, however the R factor of the refinement procedure dropped well below double digits for each of the four putative space-groups.

Refinement residuals for the four space-groups under consideration are displayed in the following table. For purposes of comparison the automated Rietveld algorithm was employed; this varies a fixed set of refinement parameters.

**Table 8 - Automatic Refinement of Delta PXRD Data in EXPO2004**

Space-group	Pnn2	Pnnm	Pba2	Pbam
Refinement No.	$R_p$ & $R_{wp}$ Values			
1	4.63 & 7.19	4.59 & 6.90	5.04 & 10.14	6.15 & 12.15
2	3.64 & 5.83	3.99 & 6.22	4.35 & 8.94	4.81 & 9.06
3	3.45 & 5.46	3.87 & 6.04	4.17 & 8.63	4.29 & 8.51
4	3.29 & 5.18	3.71 & 5.73	3.90 & 8.28	4.13 & 8.41
5	3.16 & 4.93	3.57 & 5.49	3.50 & 7.92	4.10 & 8.38
6	3.02 & 4.69	3.34 & 4.83	3.29 & 7.77	4.06 & 8.36
7	2.95 & 4.60	3.08 & 4.25	3.16 & 7.69	4.05 & 8.34
8	2.91 & 4.53	2.96 & 4.07	3.10 & 7.65	4.04 & 8.34
9	2.90 & 4.42	2.88 & 3.96	3.06 & 7.62	4.03 & 8.33
10	2.68 & 4.25	2.84 & 3.89	3.04 & 7.60	4.03 & 8.33
Terminal Value	2.47 & 3.93	2.75 & 3.75	2.96 & 7.54	4.03 & 8.33

The terminal output patterns including the residual plots are displayed in the figures overleaf. Both the Pba2 and Pbam plots show a large residual at the peak equivalent to a d-spacing of  $5.67\text{\AA}$  corresponding to  $2\theta = 8.36^\circ$  on the synchrotron diffraction pattern ( $\lambda = 0.8269\text{\AA}$ ) and  $2\theta = 15.61^\circ$  when adjusted to  $\text{CuK}\alpha$  radiation.

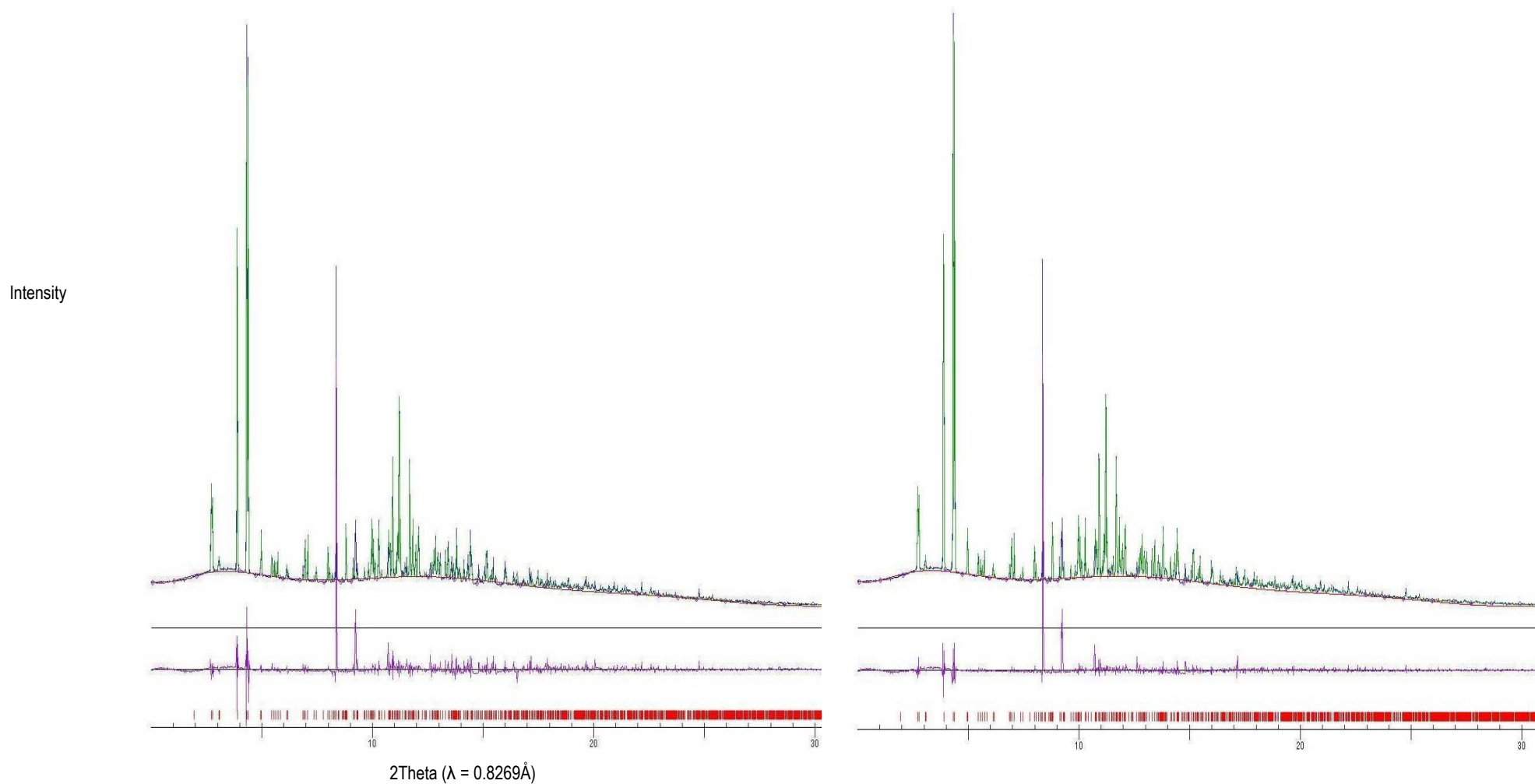
Although the refinement profile residual factor,  $R_p$ , is lower for the Pnn2 case, the residual plot shows the residual for the largest peaks to be smaller in the Pnnm case.

**Figure 16 - Terminal Residuals from Rietveld Refinements of Delta Form PXRD Pattern**

*(Y-Axis in counts, X-axis in 2θ, degrees, synchrotron radiation source, λ=0.8269Å. Index positions in red, residuals in purple, diffraction intensity in green)*

Space Group: Pbam

Space Group: Pba2

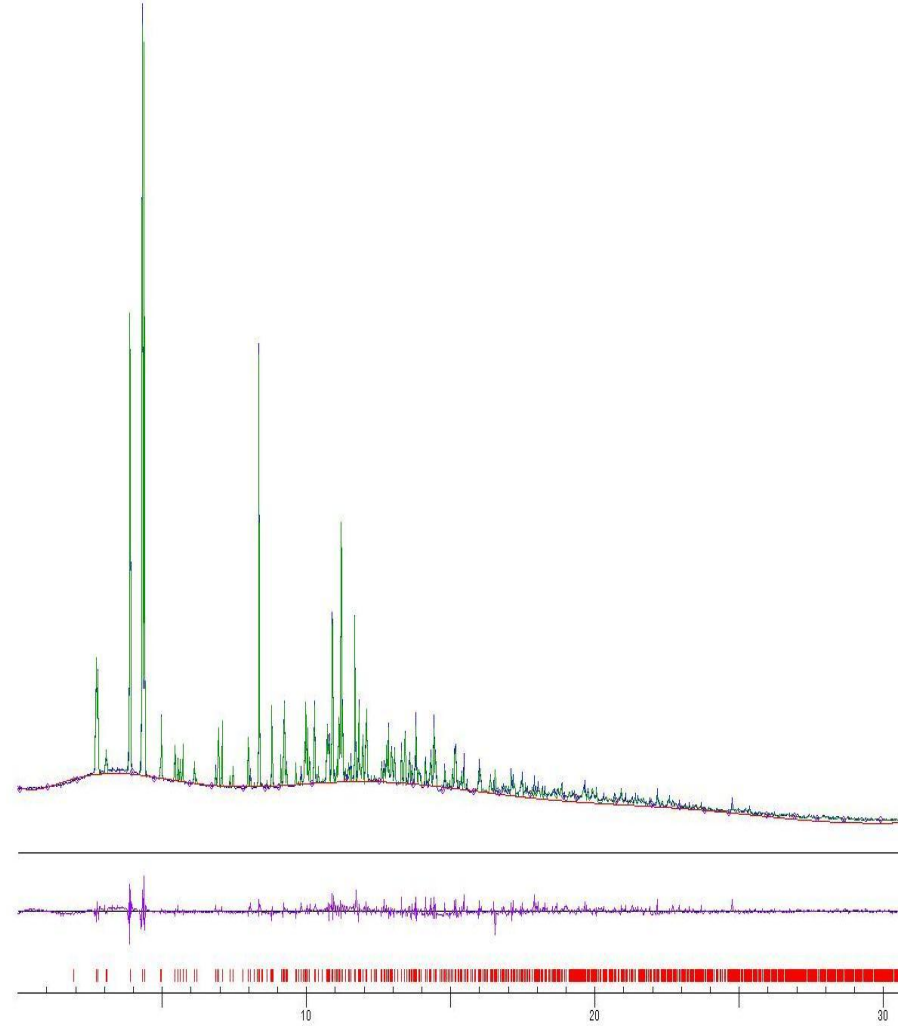
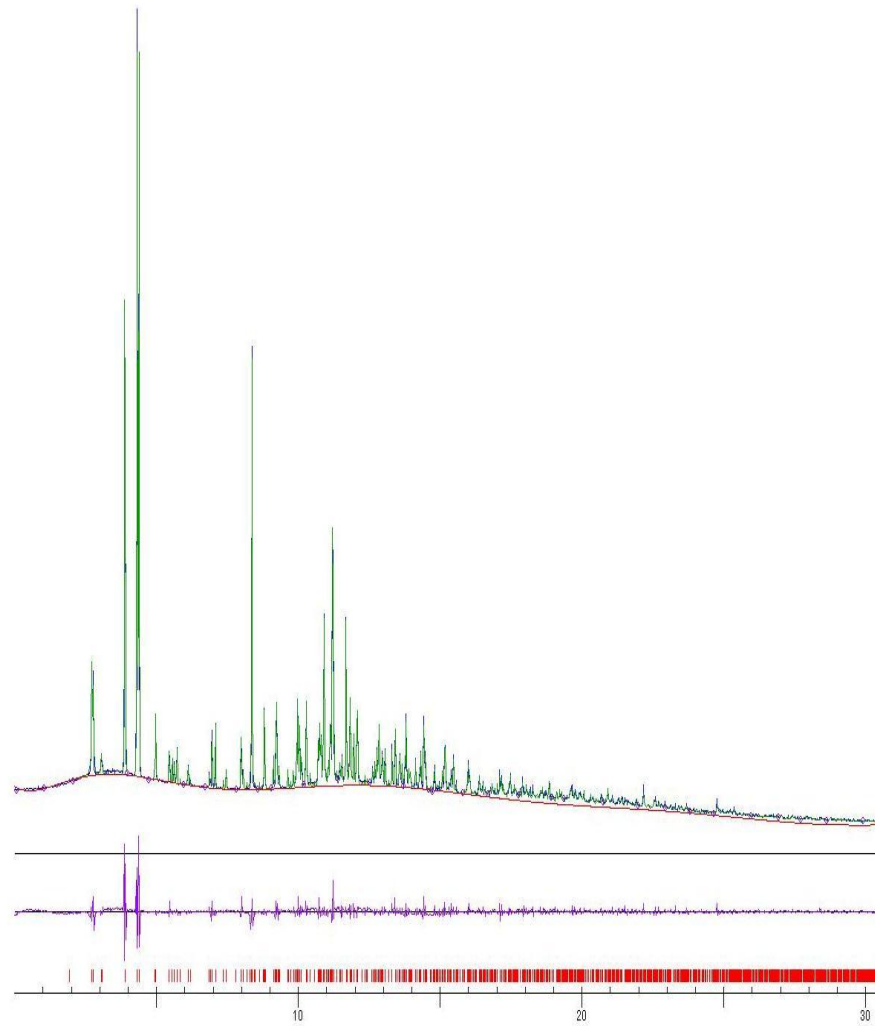




Space Group: Pnn2

Space Group: Pnnm

Intensity



2Theta (λ = 0.8269Å)

### 3.2.2 Solvates

Indexing of a number of PXRD patterns of solvates was attempted using data collected on in-house diffractometers. The unit cells of the solvates with methyl-tertiary-butylether and propylene carbonate were subsequently identified by single crystal diffractometry.

For the solvates with tetrahydrofuran and cyclohexanone index plots similar to those shown for the delta polymorph in the previous section were prepared. Indexing of the solvate with cyclopentanone was not attempted, however it is assumed to be effectively identical to the solvate with cyclohexanone; (Figure 6).

#### 3.2.2.1 Cyclohexanone Solvate

The indexing results for the cyclohexanone solvate included many monoclinic unit cell solutions with a short axis of approximately  $6\text{\AA}$  and a longer axis of  $27\text{\AA}$ , therefore resembling the solutions of the isostructural solvates with five other solvents identified by Hosokawa *et al.*

Chekcell's "best solution" test favoured a monoclinic unit cell with angle  $\beta$  unique and a volume of only  $2018\text{\AA}^3$ , approximately half that of the isostructural solvates solved by Hosokawa *et al.*, and with only the short dimension in common.

A solution of approximately double the size,  $4038\text{\AA}^3$ , is also proposed by Crysfire. Both these solutions are presented in the following table. In neither case is the software able to identify the space-group with high certainty.

C2/c, the space-group determined for the five isostructural solvates by Hosokawa *et al.*, was not favoured by Chekcell's "truecell" space-group determination algorithm.

**Table 9 - Tentative Unit Cell Dimensions of Cyclohexanone Solvate**

Cell Dimension Crystal System	a (Å)	b (Å)	c (Å)	$\alpha$ (°)	$\beta$ (°)	$\gamma$ (°)	Volume (Å <sup>3</sup> )
Monoclinic, $\beta$ unique Lines Indexed 20, FOM 16.1	27.51	5.78	25.71	90	99.09	90	4038
Monoclinic, $\beta$ unique Lines Indexed 20 FOM 8.0	20.20	5.78	17.29	90	94.07	90	2015 <sup>12</sup>

### 3.2.2.2 Tetrahydrofuran Solvate

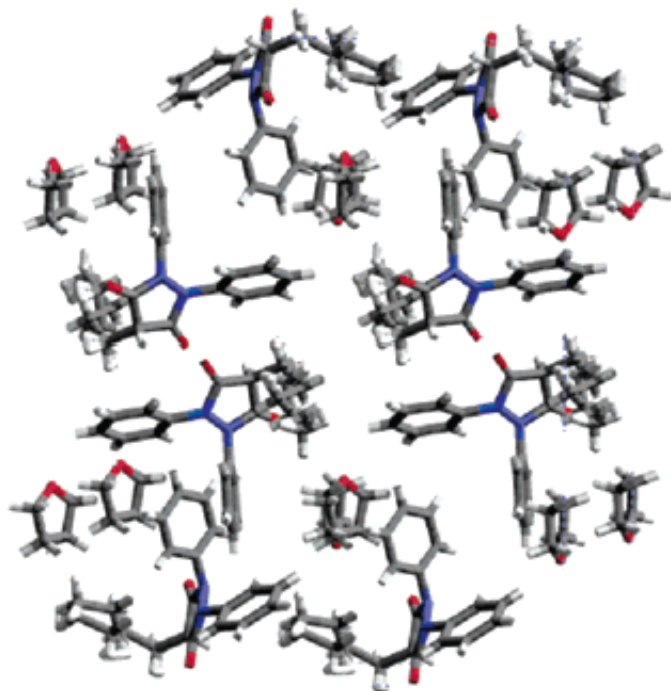
As mentioned in Section 1.3.2.2, Hosokawa and co-workers have submitted a structure to the Cambridge Structural Database for the crystal structure of a solvate of phenylbutazone formed with tetrahydrofuran. This solution indicates that the unit cell of the solvate contains a total of eight phenylbutazone molecules and four tetrahydrofuran molecules; i.e. the API:solvent ratio is 2:1.

An imputed PXRD pattern is also available on the CSD, which is based upon this SCXRD solution. This PXRD pattern does not match the diffraction pattern collected in-house. Thermogravimetric analysis was carried out on the solvate produced in-house. Making the assumption that the entire recorded weight loss corresponds to the loss of tetrahydrofuran bound-up in the crystal lattice of the solvate, an API:solvent ratio of approximately 2:1 was present in the in-house sample also. This does not support a hypothesis that there is more than one stable solvate structure of phenylbutazone with tetrahydrofuran, possessing different solvent:solute ratios.

---

<sup>12</sup> This is Chekcell's "Best Solution". Two nearly identical variants were determined – one with 19 lines indexed and FOM = 15, the other with 20 lines indexed but with FOM = 8.

**Figure 17 - Structural Model of Solvate with Tetrahydrofuran of Hosokawa *et al.***<sup>13, 14</sup>



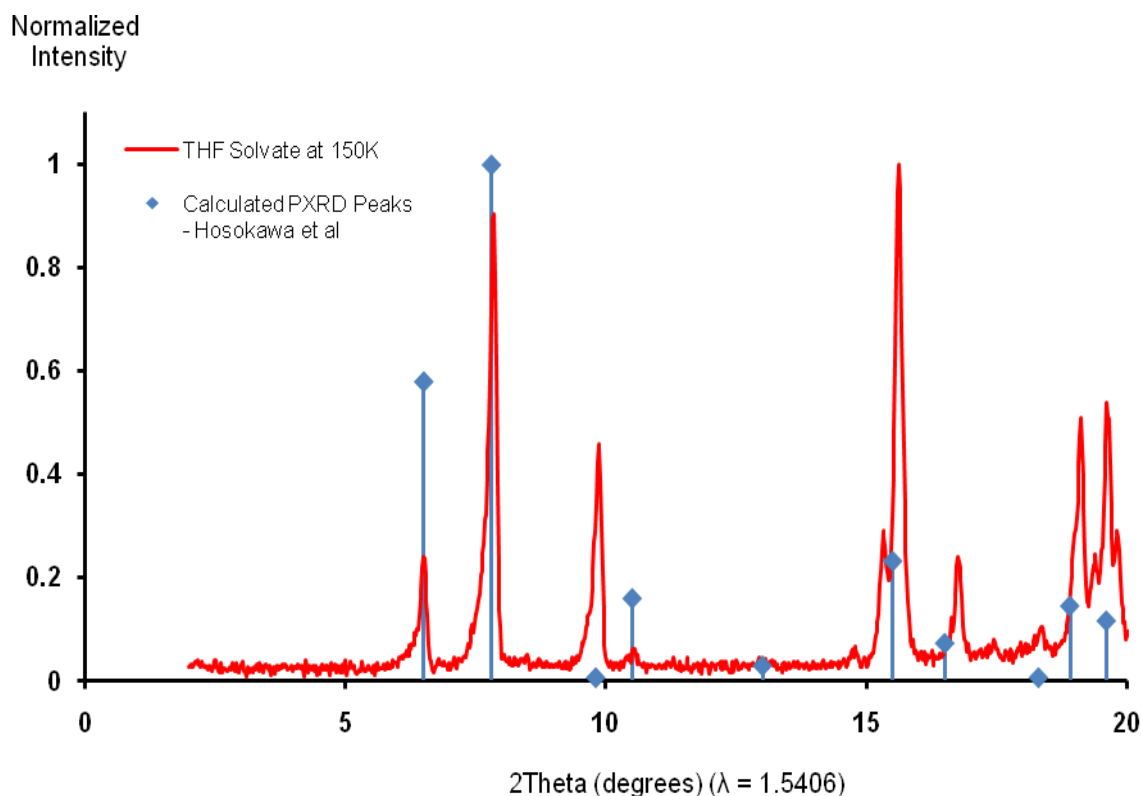
As a result of examination of the behaviour of the solvate at different temperatures by *in situ* X-ray diffraction experiments described in Chapter 5, a more plausible explanation for the diverging PXRD patterns came to light. The measurement temperature of the SCXRD experiments of Hosokawa *et al.* was 173K. When the in-house solvate was cooled to 150K, a different PXRD pattern to the ambient temperature pattern was obtained. Evidently this solvate undergoes a structural transition in the temperature range between 150K and 298K. While not identical to the calculated PXRD pattern based on the Hosokawa structure on the CSD, the in-house 150K pattern does bear a striking resemblance to it; (Figure 18). This suggests that the solvate under study is identical in terms of solvent:solute ratio, however that the solvate has more than one crystal form.

---

<sup>13</sup> The CIF file indicates that the atom positions of the butyl group of phenylbutazone and the atom positions of the tetrahydrofuran molecules are disordered.

<sup>14</sup> Reproduced from Crystal Growth and Design.

**Figure 18 - Comparison of THF Solvate Calculated Pattern & 150K Pattern**



### 3.3 Structure Determination from PXRD Data

In his 1998 IUCr monograph, [63], Giacovazzo acknowledges the difficulty of conclusive space-group identification from PXRD data. He concludes that:

*“The unequivocal definition of space-group is often difficult from powder data even when the unit cell parameters have been correctly defined.”*

He cites the difficulty of identifying systematic absences correctly, because of the presence of overlapping peaks, which make it difficult to determine if an absence is actually present.

Although the use of high-quality synchrotron data makes it possible to identify peak overlaps present in PXRD patterns collected on standard X-ray diffractometers, unless a complete structural model can be developed, some degree of uncertainty in the assignment of particular peaks to calculated index positions is liable to remain.

Achieving a complete structural model of phenylbutazone solely from PXRD data may be expected to be a daunting objective. Nonetheless the preponderance of literature and software available for the determination of complete crystal structures from powder X-ray diffraction data may cause the uninitiated to conclude that PXRD structure solution is almost routine for certain classes of molecule.

Pecharsky and Zavalij, [51], provide a number of examples of inorganic structures that have been solved successfully thanks chiefly to the ability to construct models of the structure under study from PXRD data alone, and then to refine the atom coordinates using methods such as Rietveld refinement. The ability of programs such as Mercury, [64], and Powdercell, [65], to calculate an imputed powder pattern from a completed molecular structure enables the integrity of a finished structural model to be confirmed independently.

However other crystallographers are notably more sanguine about the obstacles involved in achieving a complete structural solution from powder diffraction data, particularly for organic molecules above a certain size and complexity. Werner, [53], puts it this way:

*“In principle, all information available in a single-crystal diffraction pattern is also available in a powder diffraction pattern. Suppose all the pages in a book have been printed on top of each other on one single sheet. Obviously everything written in the book is present on the paper, but this does not mean that we are able to extract the information.”*

A recent list of structure solutions of a variety of molecular structures that have been arrived at from PXRD data is provided in a paper from the Istituto di Cristallografia, which is included in the same 2002 IUCr monograph on PXRD structure determination methods, [66].

Several software packages, including Expo, provide Cimetidine,  $C_{10}H_{16}N_6S$ , as an example of a small organic molecule whose structure is soluble from its powder diffraction pattern.

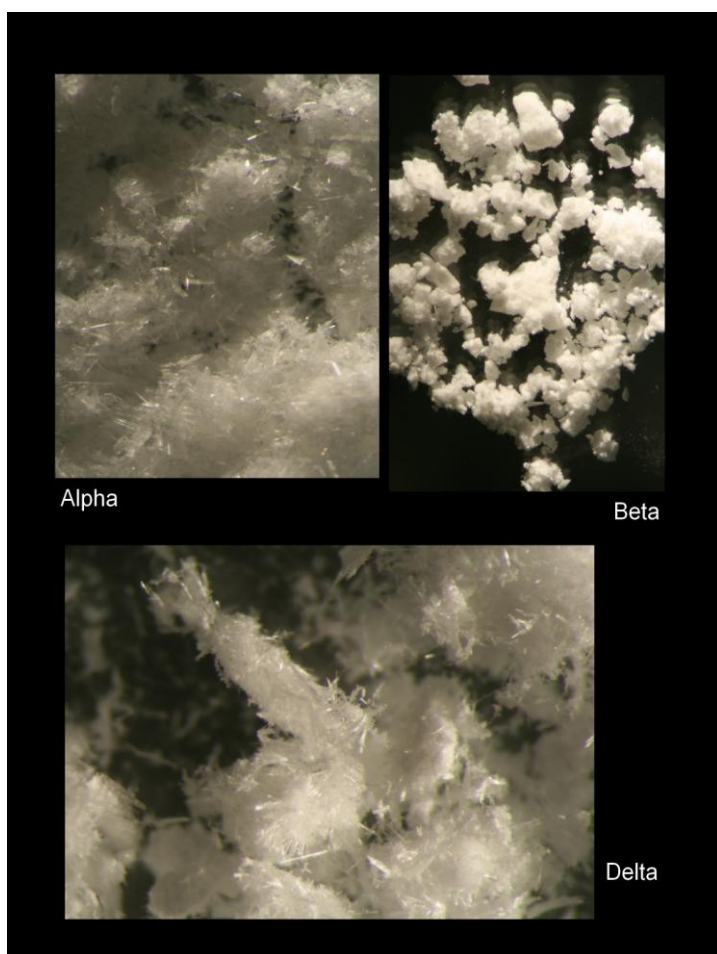
Despite the availability of high quality synchrotron powder diffraction patterns efforts to solve the structure of the alpha and delta forms of phenylbutazone using Expo, Fox and the Superflip procedure in Jana2004, were not successful, [67, 68]. Phenylbutazone,  $C_{19}H_{20}N_2O_2$  is considered too large to be solved by the reverse Monte Carlo and “pseudo” simulated annealing algorithms contained in the program, Espoir.

In consequence, structure solution of solvates of phenylbutazone from PXRD data was not attempted. The subsequent sections concern structure solution from single crystal X-ray diffraction data, SCXRD.

### 3.4 Collection of Single Crystal Diffraction Data

#### 3.4.1 Growing Suitable Crystals

The first step in structure determination by single crystal diffraction is the growth of suitable crystals. Mentions of the challenges involved in growing crystals of adequate quality for this purpose are not hard to find, [61, 69, 70].



Unless special care was taken, the crystallization of phenylbutazone generally resulted in samples unsuitable for single crystal diffractometry.

The alpha and delta form specimens shown to the left are the results of routine evaporative crystallization in a single solvent. The beta form sample was precipitated from warm methanol using water.

**Figure 19 - Phenylbutazone Polymorph Specimens**

For only one polymorph, the alpha form, was it possible to grow “macro” crystals that were translucent in polarized light in all but one orientation, in which no polarized light could pass through; an effect often referred to as extinguishing of the polarized light, [71].



**Figure 20 - Alpha Form Crystal under Polarized & Non-polarized Light**

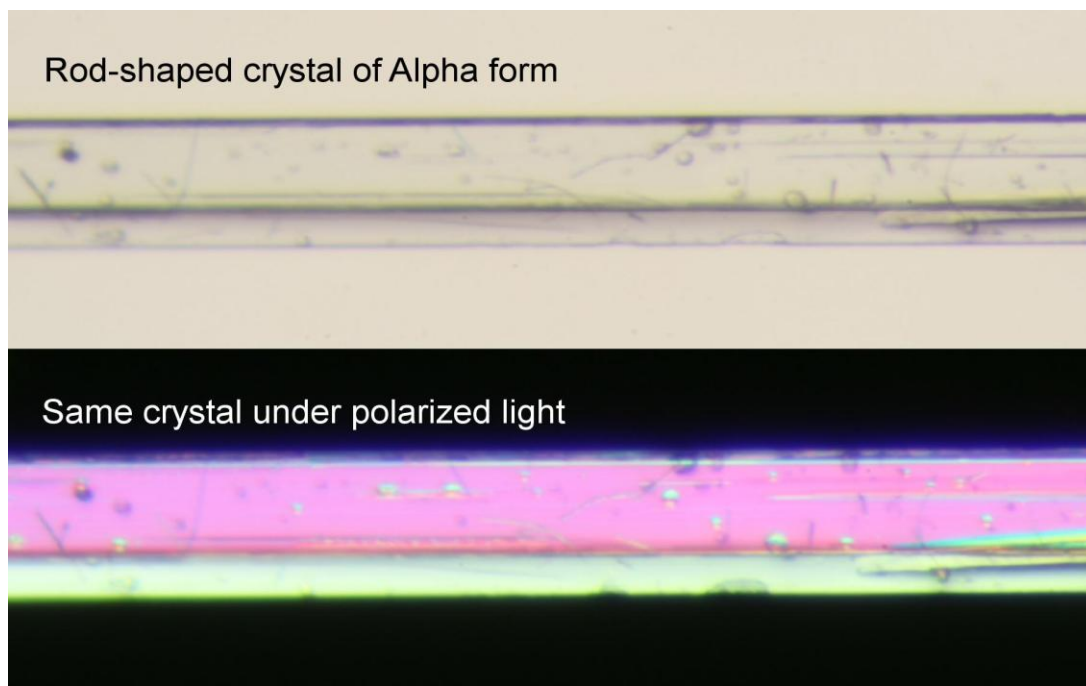
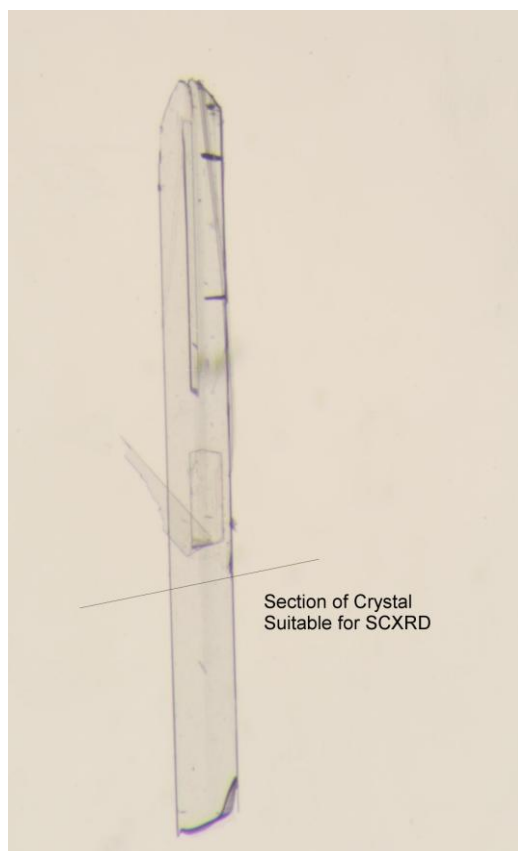


**Figure 21 – Alpha Form Crystal Selection for SCXRD**

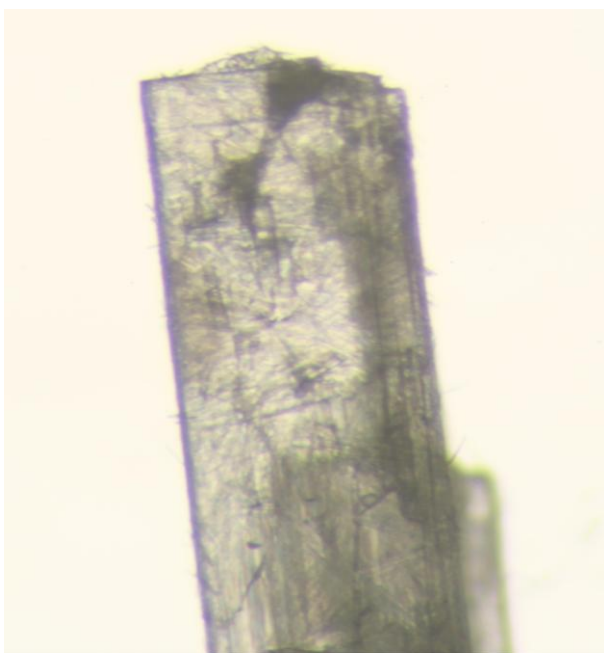


Although many of these large crystals displayed visible imperfections; e.g. air-bubbles, it was possible to locate specimens, from which adequate quality sections could be cut.

The standard route to the beta polymorph, precipitation from organic solution using water, is not conducive to the formation of large, single crystals; particularly when the solution is stirred. Formation of pure beta form was found to have occurred at the edge of a watch glass from which a highly volatile solvent had rapidly evaporated, resulting in the emergence of side-blooms. Regrettably these consisted of congealed, powdery deposits, inherently unsuitable for single crystal diffraction experiments. Kaneniwa *et al.*, [71], provide pictures of large, rod-shaped crystals of the beta form, which they were able to grow in ethanol solution. During this investigation, numerous crystallizations of phenylbutazone in methanol and ethanol failed to yield a similar result.

The typical crystal habit of the delta polymorph is a fibrous matrix of varying hardness, whose constituent strands rarely extend to a width of even 50  $\mu\text{m}$ . While these crystals yield a highly reproducible powder X-ray diffraction pattern, none has shown promise for single-crystal X-ray diffraction experiments.

**Figure 22 - Alpha Single Crystal after Heating**



The ability to produce the delta form by heating of the alpha polymorph of phenylbutazone gave grounds for optimism about obtaining a delta crystal suitable for SCXRD via heat-treatment of the alpha form.

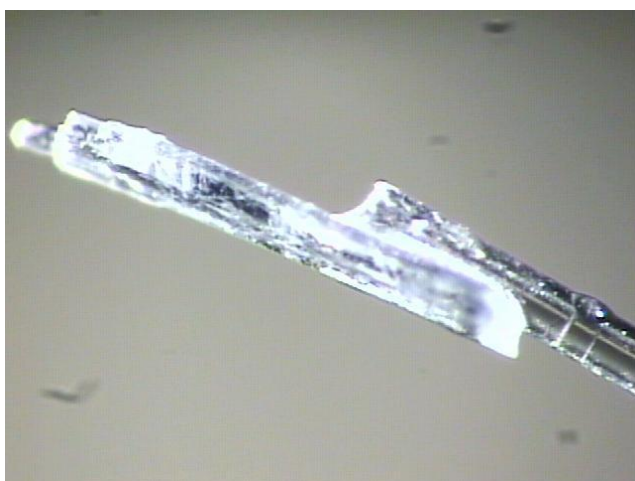
Unfortunately this technique leads to the formation of imperfect crystals such as the one shown opposite.

High quality single crystals of solvates were prepared from methyl-tertiary-butylether, propylene carbonate and cyclohexanone. By contrast attempts to grow single crystals of the solvates with tetrahydrofuran and cyclopentanone did not yield “macro” crystals.

The pictures shown in Figure 23 were taken using the camera installed on the single crystal diffractometer. The crystal is adhered to a cylindrical glass fibre mount by means of a small amount of an X-ray neutral, encapsulating oil, which also serves to prevent solvent escape from solvated crystals.

**Figure 23 - Single Crystals that Yielded Structure Solutions on the SCXRD Goniometer**

Methyl-tertiary-butylether Solvate

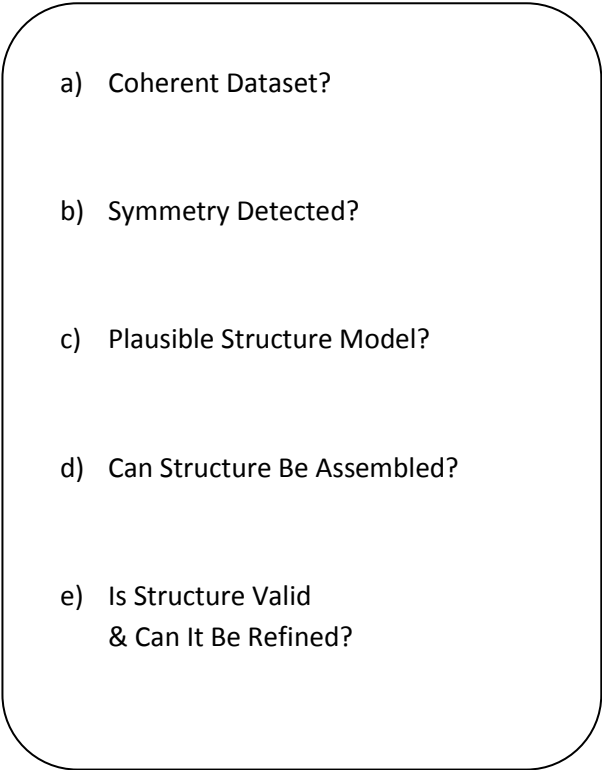


Propylene Carbonate Solvate



### 3.5 *Structure Determination from Single Crystal Diffraction Data*

Full SCXRD datasets were typically collected only in those cases where a plausible unit cell could be determined in the preliminary collection of the orientation matrix. The pre-screening of crystal specimens both by visual appearance under the microscope and according to the plausibility of the unit cell options determined during collection of the orientation matrix, helped keep the number of insoluble datasets in check.

- 
- a) Coherent Dataset?
  - b) Symmetry Detected?
  - c) Plausible Structure Model?
  - d) Can Structure Be Assembled?
  - e) Is Structure Valid  
& Can It Be Refined?

**Figure 24 - Checklist for Structure Solution**

#### a) **Dataset Coherence**

The presence of twinned crystal specimens was mooted as a cause of data processing difficulties in certain instances. Investigation of the datasets in question using the Bruker Gemini software program, designed to enable the processing of datasets from twinned crystal samples, part of the Shelxtl suite, did not lead to confirmation of this diagnosis, however. On only one occasion was it possible to identify a pattern in the raw dataset that pointed conclusively to a major crystal fault; a grouping of high reflection intensities along a particular  $h,k,l$  index, which became apparent during manual inspection of the raw reflection file. This anomaly was subsequently confirmed by the structure solution software packages, SIR, [72] and Jana, [73], with which the dataset in question was processed in parallel to the manufacturer-supplied software.

## **b) Symmetry Detection**

A more frequent occurrence was a failure to determine any symmetry above triclinic, even when data from a specimen believed to have a monoclinic lattice were being analysed; e.g. the alpha form of phenylbutazone. Although an adequate .hkl file could be generated and processed to yield an electron density map, this did not result in a set of atomic positions with features of phenylbutazone's molecular structure discernible in the subsequent 3-dimensional model; e.g. planar phenyl groups.

## **c) Structure Model Plausibility**

Typically the detection of a plausible space-group was the prelude to generation of a model, in which certain aspects of the anticipated structure could be recognized. For example, during the solution of structures of a number of solvates of phenylbutazone, the symmetry search yielded a space-group that had been determined for other phenylbutazone solvates, and the location of the drug molecule was readily distinguishable from the electron density map.

## **d) Structure Assembly**

The manner of structure assembly varies widely among different single crystal structure solution software packages. While this step is carried out manually in Shelxtl and in Jana, SIR2004 is capable of recognizing likely bond positions, and proved particularly adept at finding the location of phenylbutazone molecules more or less in their entirety, identifying all the ring moieties automatically. In all the solvated structures locating the solvent molecules proved challenging regardless of the software employed, and taxed the ability of the graphical user interfaces to situate consistent molecular forms.

### e) Structure Validation & Refinement

Having arrived at a plausible structural model, it remains to validate and refine the findings. In the case of determination of previously solved structures such as the alpha form of phenylbutazone, the model was validated by comparison with prior solutions. Prior solvate structure solutions are also available for comparison. In common with the PXRD datasets, raw files of reflections could be analysed in Excel<sup>®</sup> in order to confirm individual extinction conditions.

For example, during data reduction by Shelxtl, the space-group of the alpha form was identified as monoclinic with space-group number 14 and Hermann-Mauguin symbol,  $P2_1/c$ . The International Tables for Crystallography, Volume A, point out that various different forms of this space-group exist depending on choices of origin and unique axis. The dataset collected does not display reflection condition,  $h00: h=2n$ , but instead fulfils conditions:

- $00l: l = 2n$
- $0k0: k = 2n$
- $h0l: l = 2n$

This allows the space-group selection to be narrowed down to unique axis  $b$ , cell choice 1, which has the more precise space-group symbol of  $P12_1/c1$ .

#### 3.5.1 Refinement of SCXRD Solutions – Theoretical Background

The objective of the refinement of single crystal structure solutions is to improve upon the initial structure “solution” of calculated electron densities derived from measured intensities and estimated phases. These phase angles are calculated numerically (e.g. by direct methods) in order to make up for the absence of experimental phase information to accompany

intensity magnitudes measured at the detector; phase information that is subsequently required in Fourier synthesis of electron densities as can be seen in the three dimensional expression for electron density,  $\rho$ , shown below. The electron density values are used to construct a map such as the 2-dimensional example shown in Figure 25:

**Equation 12 - Expression for Calculation of Electron Density in Real Space**

$$\rho(xyz) = \frac{1}{V_c} \sum_h \sum_k \sum_l F_{hkl} \cos[2\pi(hx + ky + lz) - \phi_{hkl}]$$

Where:

$x, y, z$  = Unit cell coordinates

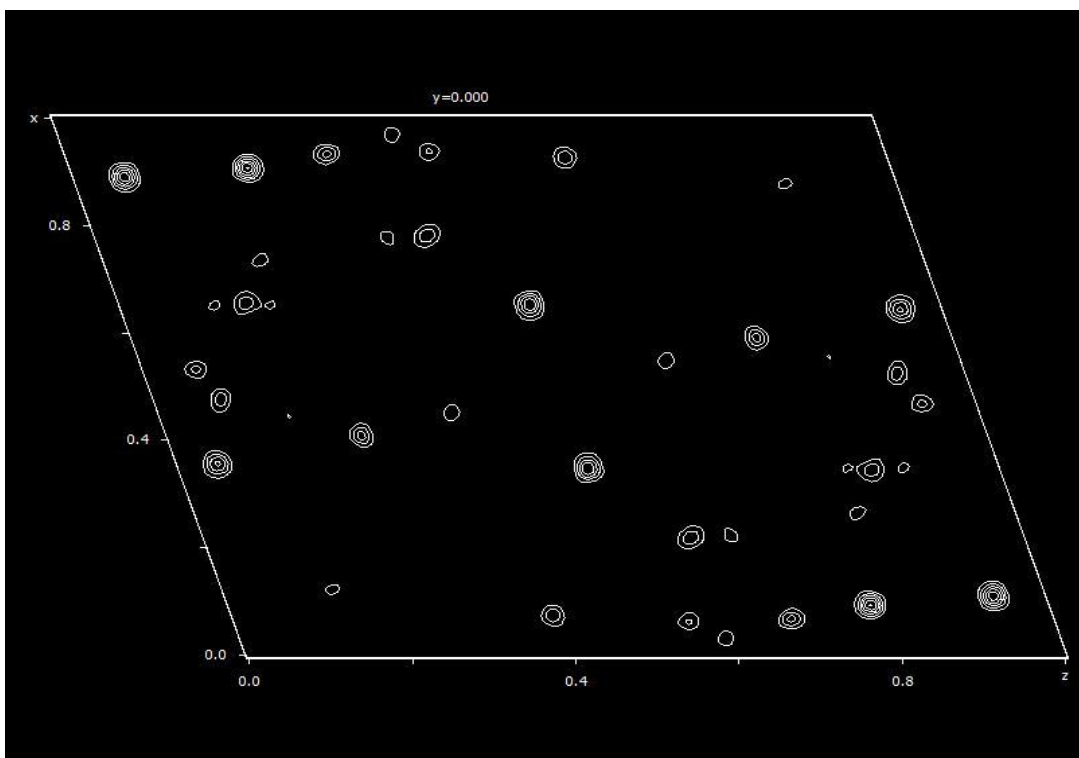
$V_c$  = Volume of the unit cell

$F_{hkl}$  = Observed structure amplitude for reflection plane,  $h,k,l$

$h,k,l$  = Plane indices

$\phi_{hkl}$  = Phase angle of diffraction vector for reflection,  $h,k,l$

**Figure 25 - Example Section of 2D Fourier Map of Alpha Form created in Jana2004**



Information about the phase angle is not provided at the X-ray detector, and phase values must be deduced in order to solve the crystal structure. This circularity is the essence of the so-called, “phase problem”. The use of “Direct Methods” is among the most common techniques to solve the structure of organic molecules, and was employed extensively during this study, [63].

From the electron density values, form factors are also determined. The expression for calculation of form factors for each atom,  $f_i$ , (alternatively termed atomic scattering factors), closely resembles the expression for the atomic Debye-Waller factor, (Equation 17), and is outlined by Shmueli and Massa among others, [61, 74]. Values of form factors for different elements are tabulated in the International Tables for Crystallography Volume C, [75].

Structure factors,  $F_c$ , which sum the estimated contribution of each atom in the unit cell in scattering the X-ray beam to arrive at a theoretical intensity value for each reflection plane, may then be calculated using the expression shown below:

**Equation 13 - Expression for Calculation of Structure Factor,  $F_c$**

$$F_c = \sum_i f_i \{ \cos 2\pi (hx_i + ky_i + lz_i) + i \sin 2\pi (hx_i + ky_i + lz_i) \}$$

The observed structure amplitudes,  $F_o$ , are typically obtained from the measured diffraction intensity,  $I$ , according to the following expression, in which the denominator term corresponds to the Lorentz Polarization correction:

**Equation 14 - Relationship between Intensity and Observed Structure Amplitude<sup>15</sup>**

$$F_o = \sqrt{\frac{I}{(1 + \cos^2 2\theta)/2 \sin 2\theta}}$$

---

<sup>15</sup> An absorption correction is typically applied to the raw intensities also



Differences between the observed structure amplitude,  $F_o$ , and calculated structure factors,  $F_c$ , result from errors in both the model and the data. The first step in refinement packages for SCXRD data is typically a least squares algorithm that minimizes the sum of the differences between the values of  $F_o$  and  $F_c$ . Certain refinement packages, such as CRYSTALS, [76], permit refinement, not only of the squared  $F_o$  values, but also their moduli, an important option, particularly where data intensity is weak. The expressions for calculation of the commonly encountered least squares residual factors are shown below:

**Equation 15 - Refinement Residual, R of Modulus  $F$  Values**

$$R = \frac{\sum_{hkl} (|F_{obs}| - |F_{calc}|)}{\sum_{hkl} |F_{obs}|}$$

**Equation 16 - Refinement Residuals,  $wR$  &  $wR_2$  of Squared  $F$  Values**

$$wR = \sqrt{\frac{\sum_{hkl} (F_{obs}^2 - F_{calc}^2)}{w \sum_{hkl} w F_o^2}}$$

$$wR_2 = \sqrt{\frac{\sum_{hkl} (F_{obs}^2 - F_{calc}^2)^2}{w \sum_{hkl} w (F_o^2)^2}}$$

The quantity,  $w$ , refers to the weighting factor applied to the individual measurement point. This is intended to take into account the fact that, in proportional terms, the measurement errors are larger for weak intensity readings than for strong ones. In the simplest case, a weighting factor of  $w = 1/\sigma^2$  is often employed, where  $\sigma$  is the standard deviation in the measured data; (Appendix 5).

For refined structures, the value of the residual,  $R$ , typically lies in the range of 0.05-0.15.

Only after least squares refinement, and achievement of a reasonable  $R$  value, do most refinement packages draw the user's attention to the atomic displacement of individual atoms in the structure. These are intended to account for the fact that atoms are not stationary, and that the measured electron densities at each atomic location in fact represent average values. Variations in atomic position are shown to decrease, as the measurement temperature is lowered, and result from:

- external displacement of the molecule as a whole, and
- internal, interatomic bond displacements.

Generally the latter have a much smaller effect than the former. Disorder in the structure may also be apparent, and is typically subdivided into two varieties:

- **Positional disorder** - this occurs when an atom or group of atoms (perhaps making up an entire molecule such as an incorporated solvent) is/are statistically distributed over two or more positions.
- **Orientalional disorder** - this connotes that a molecule is distributed over two orientations, usually related by a symmetry operation; e.g. rotation or inversion.

The treatment of atomic displacement is integral to the solution of the phase problem and the calculation of meaningful unitary structure factors. An overview of this topic is provided by Shmueli among others, and a harmonized, mathematical treatment of atomic displacement is set out in a publication of the IUCr, [74, 77]. In the development of the atomic Debye-Waller factor, (also known as the "atomic temperature factor"), these texts distinguish between:

- **Isotropic displacement** - uniform displacement in all directions, and
- **Anisotropic displacement** - directionally specific displacement

In the former case, a spherically uniform mean squared displacement is assumed for all atoms. By contrast, in the latter case, a Gaussian distribution is usually assumed, and the electron density values are distributed in the direction of the diffraction vector,  $k$ , giving rise to an ellipsoid. These “thermal ellipsoids” are unique to each atom in the structure:

**Equation 17 - Anisotropic Debye-Waller Factor, T**

$$T(k) = e^{\left(-8\pi^2 \langle u_h^2 \rangle \frac{\sin^2 \theta}{\lambda^2}\right)}$$

Where:

$u_k$  = Atomic displacement of diffraction vector,  $k$

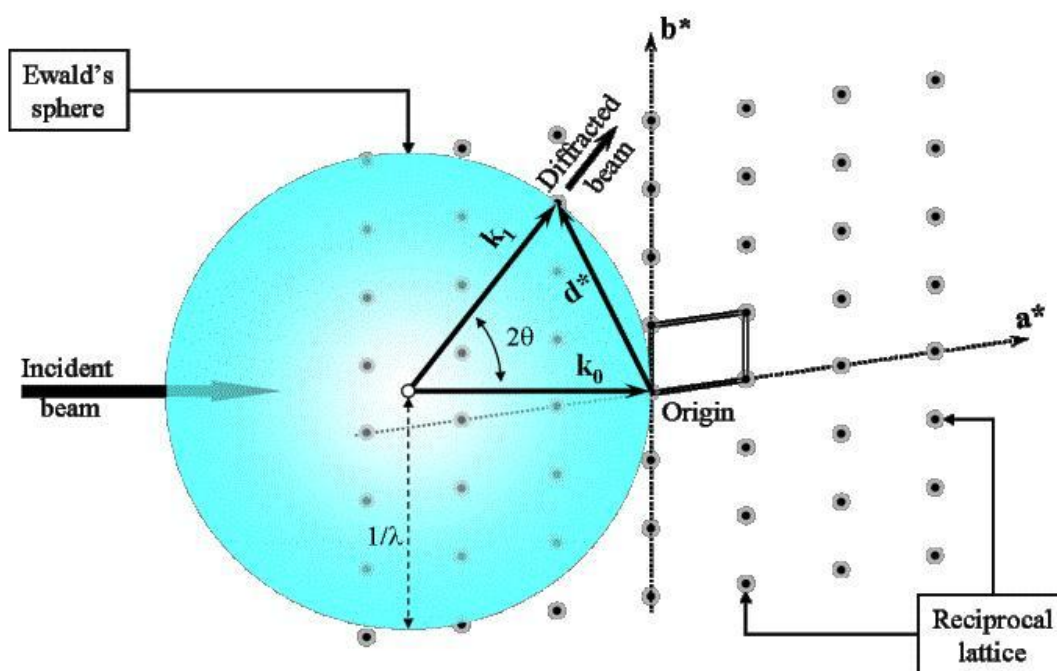
$\lambda$  = Wavelength of radiation source

$\theta$  = Diffraction angle

The quantity  $\sin \theta / \lambda$  is familiar from the Bragg equation as being equal to a distance from the origin in reciprocal space,  $d^*$ ; (more precisely  $1/2n \cdot d^*$ ). It is used, not only in calculations and plots of atomic displacement caused by thermal vibration, but also, in compilations of intensity statistics for SCXRD datasets, in which the several thousand individual reflections are typically subdivided into a series of concentric shells with the origin of the reciprocal lattice at its centre.

The length of the smallest reciprocal d-spacing that can be resolved in an experiment is given by the distance from the edge of the Ewald sphere to its centre, a fixed value of  $1/\lambda$ . Shelx, [78], presents the intensity data for each shell spacing using the term *resolution* to refer to the value  $\sin \theta / \lambda$ .

Figure 26 - Visualization of the Ewald Sphere<sup>16</sup>



In the example of the Bruker SCXRD dataset of the alpha polymorph of phenylbutazone (Mo  $K_{\alpha}$  radiation,  $\lambda = 0.7107\text{\AA}$ ) shown below, the reflection listing indicates the range of  $2\theta$  across which measurement was made, as well as the corresponding “resolution”. It is apparent from this calculation that much higher resolution is achieved at higher diffraction angles, an effect alluded to by Shmueli.

Table 10 - Phenylbutazone Alpha SCXRD Measurement Resolution

	$2\theta(^{\circ})$	Resolution ( $\text{\AA}$ )
Minimum	5.721	7.121
Maximum	54.690	0.774

<sup>16</sup> Reproduced from Pecharsky & Zavalij, *Fundamentals of Powder Diffraction*, 2005, Springer, New York, p151.

### 3.5.2 Summary of SCXRD Structure Refinements

The unit cell dimensions of phenylbutazone alpha form are shown in Section 3.2.1.1. No SCXRD solution was achieved for either the delta or the beta polymorphs owing to the absence of suitable single crystals.

Using SCXRD complete structure solutions were achieved for two of the four new solvates discovered during this investigation, and their unit cells dimensions are shown in the following table:

**Table 11 - Unit Cells of Solvates Determined by SCXRD**

Cell Dimension Solvate & Crystal System	a (Å)	b (Å)	c (Å)	$\alpha$ (°)	$\beta$ (°)	$\gamma$ (°)	Volume (Å <sup>3</sup> )
Methyl-t.-butylether Monoclinic, C2/c	25.708 (±0.005)	5.647 (±0.001)	27.610 (±0.006)	90	96.835 (±0.030)	90	3979.74
Propylene Carbonate <sup>17</sup> Monoclinic, C2/c	22.433 (±0.005)	5.993 (±0.001)	27.261 (±0.001)	90	92.990 (±0.030)	90	3660.01

Refinement of the raw structures to single digit residuals proved to be difficult for the solvate structure solutions, in particular; these both contain ambiguous solvent atom positions.

Efforts at manual refinement of Bruker Shelxtl .RES files using the academic version of Shelx were problematic, owing, not least, to syntax compatibility problems.

Using the refinement capabilities of CRYSTALS it was possible to lower the residual significantly simply by conventional least squares refinement. The special features in this package, most notably the ability to alter the selection of the intensity cut-off parameter,  $I/\sigma(I)$ , aided in lowering the residual for the alpha form solution into high single digits,

---

<sup>17</sup> Unit Cell Parameters changed slightly during refinement.

but only by sacrificing many of the reflections of which the model is comprised; sometimes to a total of below 1000 reflections.

Refinement against  $F$  and  $F^2$  was carried out; little or no improvement in  $R$  value was observed after switching to  $F^2$  refinement, and the weighted  $R$  values increased substantially. Results of refinement against  $F$  are therefore reported.

The value of the Goodness of Fit,  $GoF$ , gives an indication of how well the structural model fits the data. Values close to unity are considered ideal, while a value of below unity indicates that the model is better than the data, a situation referred to as “overfitting” of the model.

Adjusting the weighting factor,  $w$ , is a further technique that can be carried out in CRYSTALS in order to attempt to improve the  $GoF$  value, whose method of calculation is shown below:

**Equation 18 - Calculation of  $GoF$  Value**

$$GoF = \left[ \sum_{R=0}^{R=total} \frac{w(F_o^2 - F_c^2)^2}{N_R - N_p} \right]$$

Where:

$w$  = Weighting factor

$F_o$  = Observed structure amplitude

$F_c$  = Calculated structure factor

$N_R$  = Number of independent reflections

$N_p$  = Number of refined parameters

An overview of the refinement statistics for the three structure solutions of phenylbutazone polymorphs and solvates achieved during this investigation is shown in the following table:

**Table 12 - Refinement Statistics of Solved Phenylbutazone Structures**

	<i>R</i>	<i>wR</i>	<i>GoF</i>	<i>F<sub>o</sub>/F<sub>c</sub></i>	<i>I/Sigma(I)</i>	No. of Reflections
Alpha polymorph	8.149	5.678	1.191	1.242	7.0	1273
Methyl-t-butylether solvate	10.540	12.514	0.949	1.047	3.0	1500
Propylene Carbonate solvate	16.968	19.039	1.820	1.042	3.0	1761

Plots of residual factor, *R*, vs.  $\sin \theta / \lambda$  ( $1/2n.d^*$ ), are shown in the following figures for each of the three structure solutions:

Figure 27 - Refinement Analysis of Structural Models – Alpha Form

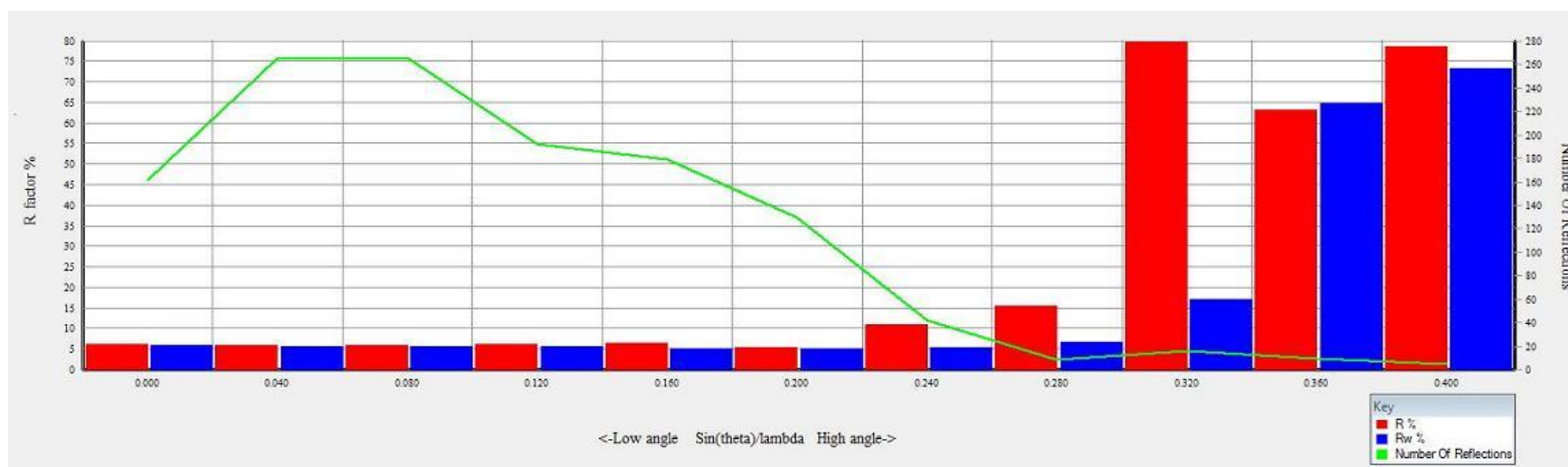
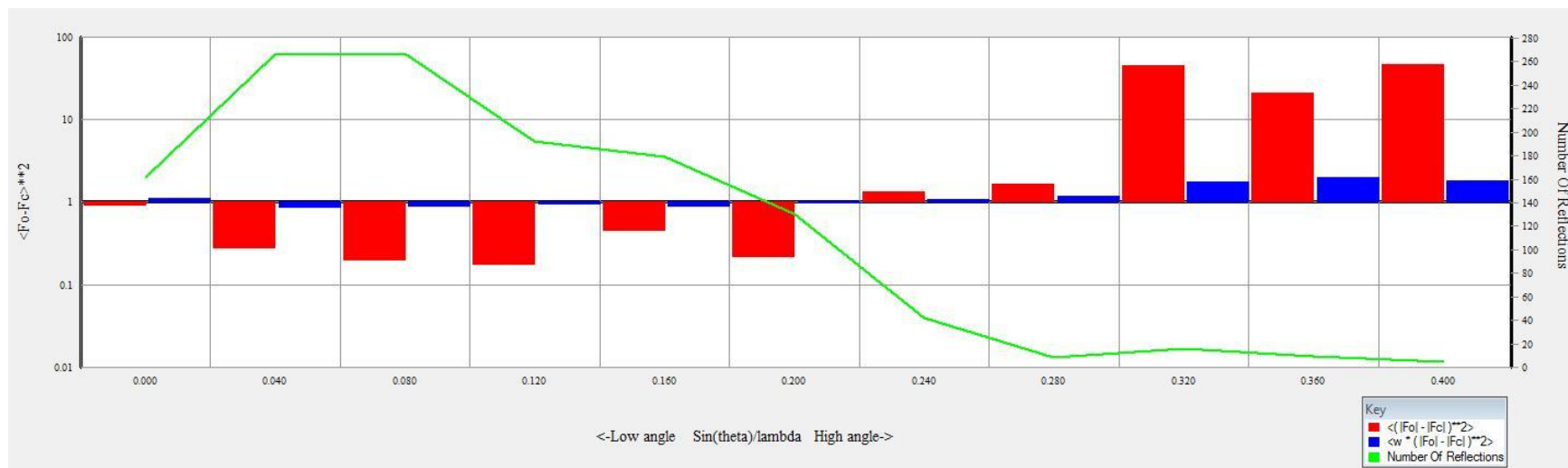




Figure 28 - Refinement Analysis of Structural Models - MTBE Solvate

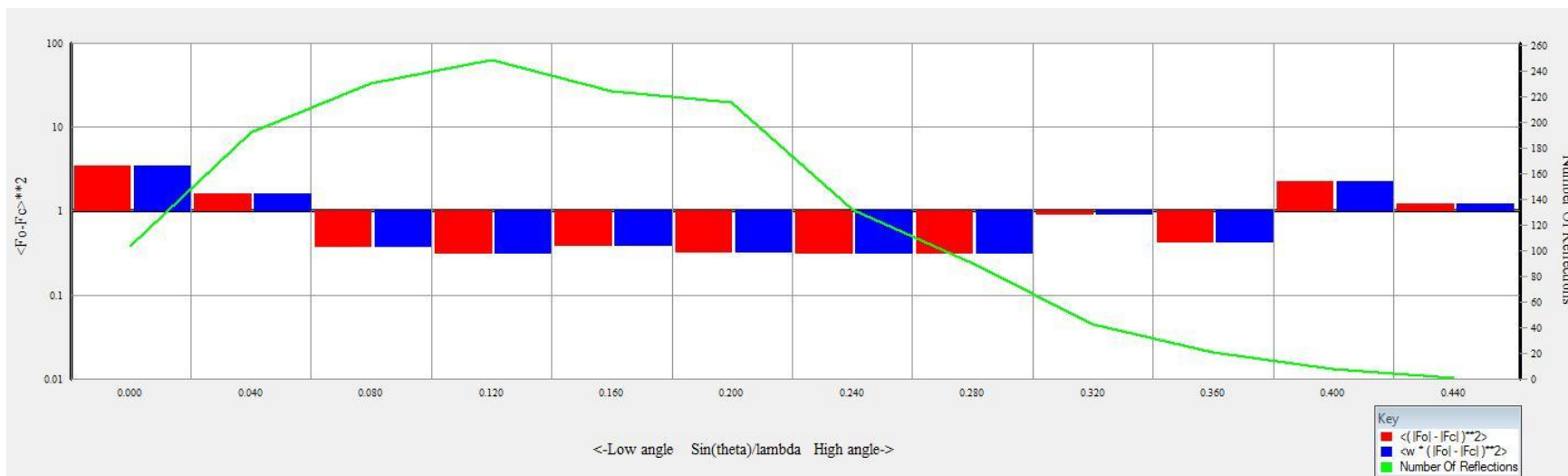
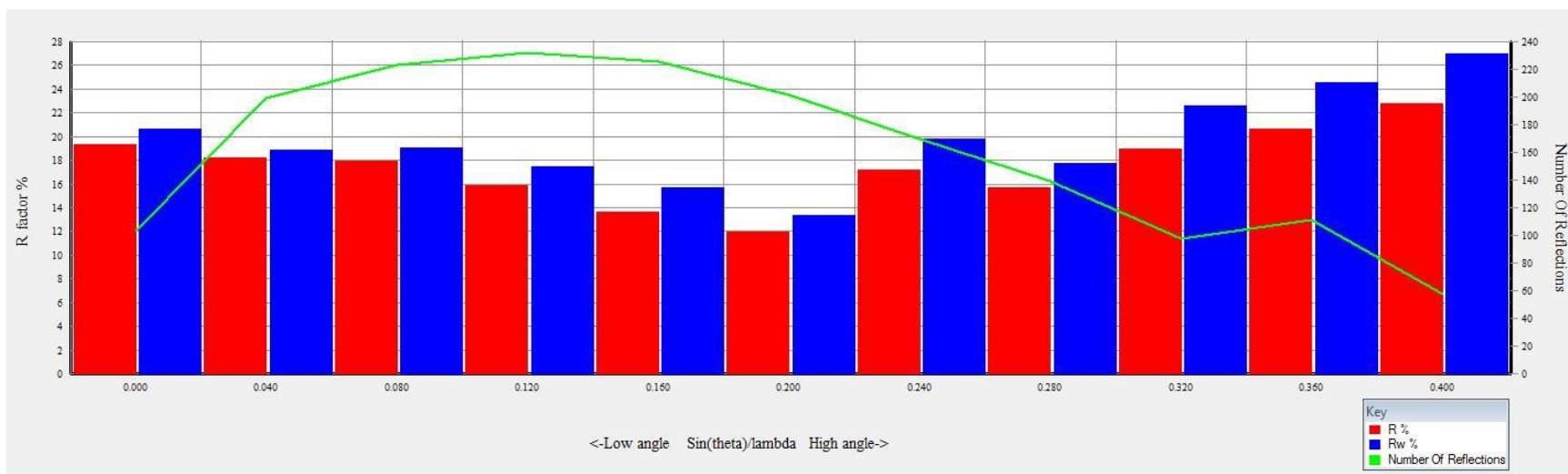
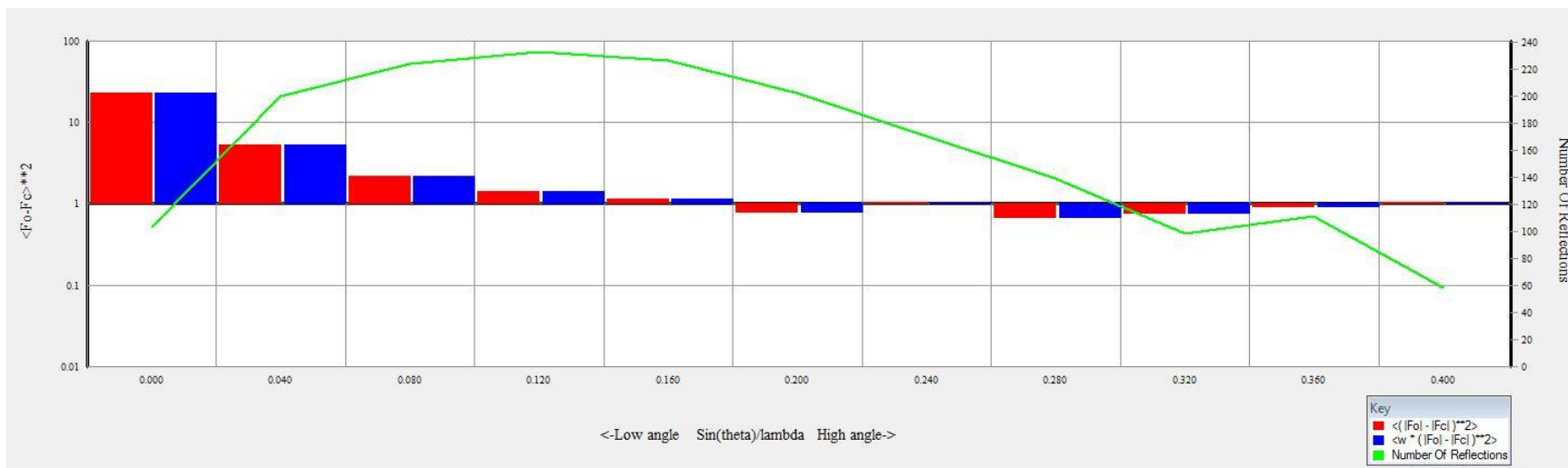


Figure 29 - Refinement Analysis of Structural Models – Propylene Carbonate Solvate

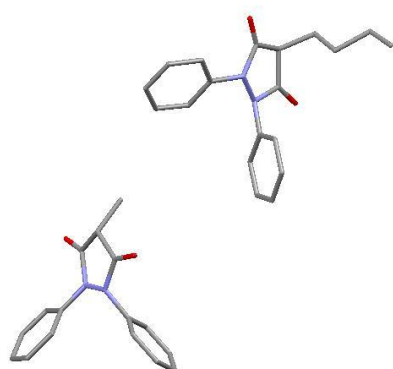


## 3.6 Structural Models

### 3.6.1 Alpha Polymorph

Singh and Vijayan show a truncated alkyl tail on one of the two phenylbutazone molecules in the asymmetric unit of their alpha form structure, which is available on the CSD:

**Figure 30 - Alpha Form Asymmetric Unit - Singh & Vijayan, 1978**



The in-house structure exhibits one molecule with a well-formed alkyl chain, the other contains less uniform alkyl-group bond distances and angles. A number of CIF files of solvate structures deposited into the CSD indicate disorder in this part of phenylbutazone's structure also.

In an effort to improve the refinement values of the alpha form structure solution, removal of poorly defined atoms was undertaken. The refinement procedure was then repeated, however little or no improvement in residual values was observed.

The following figures display the asymmetric unit and unit cell of the in-house alpha form solution. The oversize thermal ellipsoids from anisotropic refinement displayed in the foremost C4 chain of the asymmetric unit are an indicator of ill-defined atomic positions.

Figure 31 - Asymmetric Unit of Alpha Form

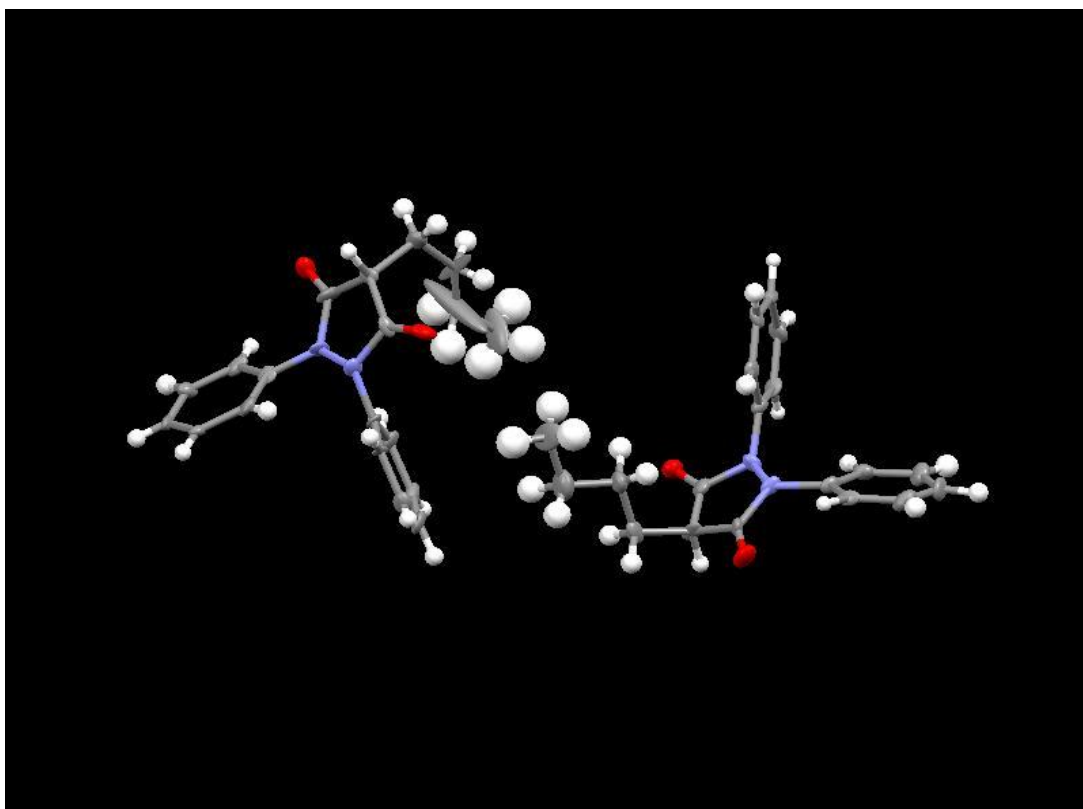
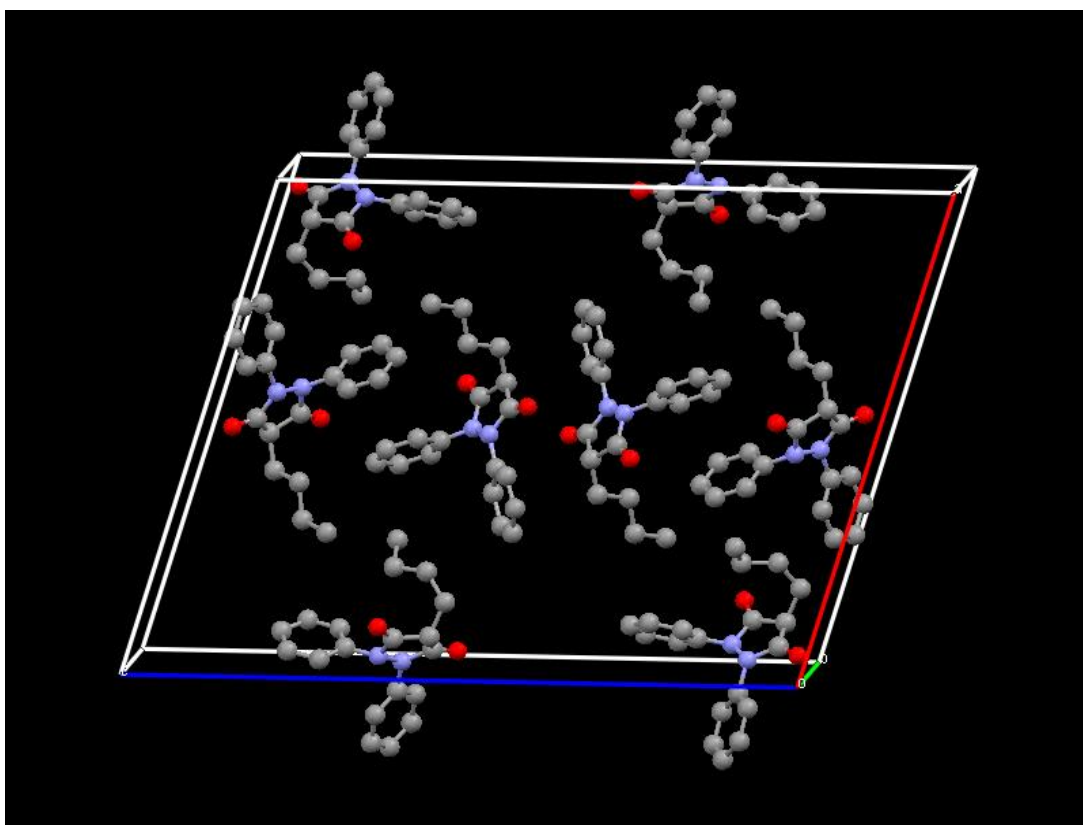
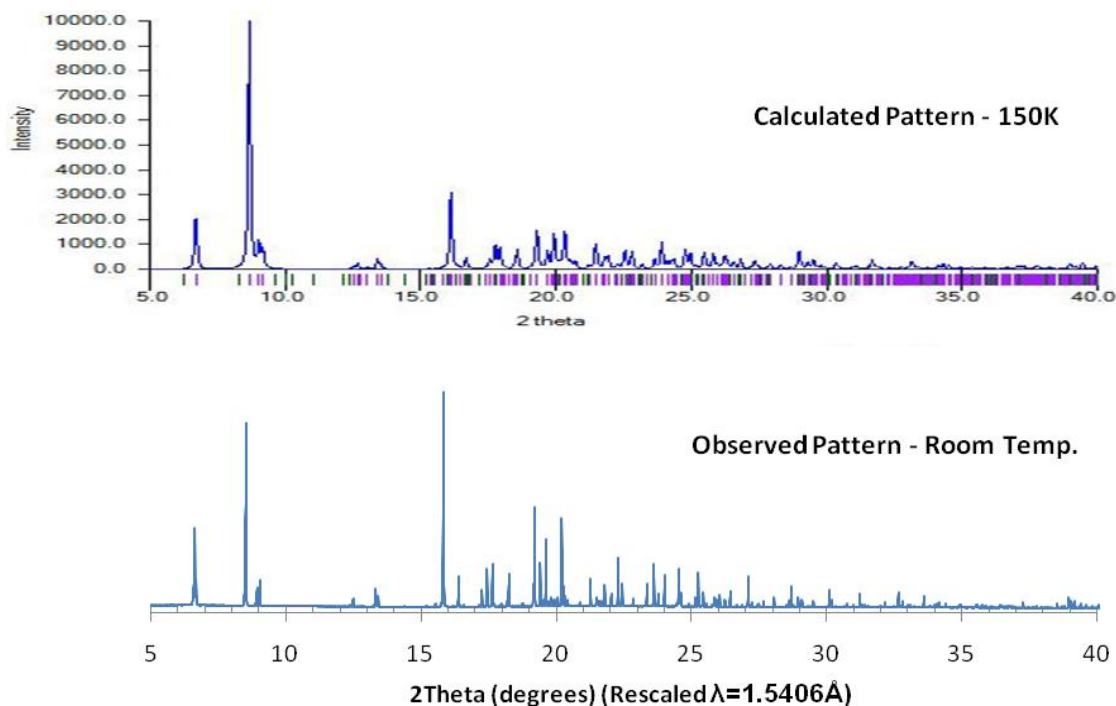


Figure 32 - Unit Cell of Alpha Form



As a further crosscheck of the refinement results, an imputed powder pattern was obtained from the refined .CIF file using Mercury. The calculated and observed peak positions display a good match to each other.

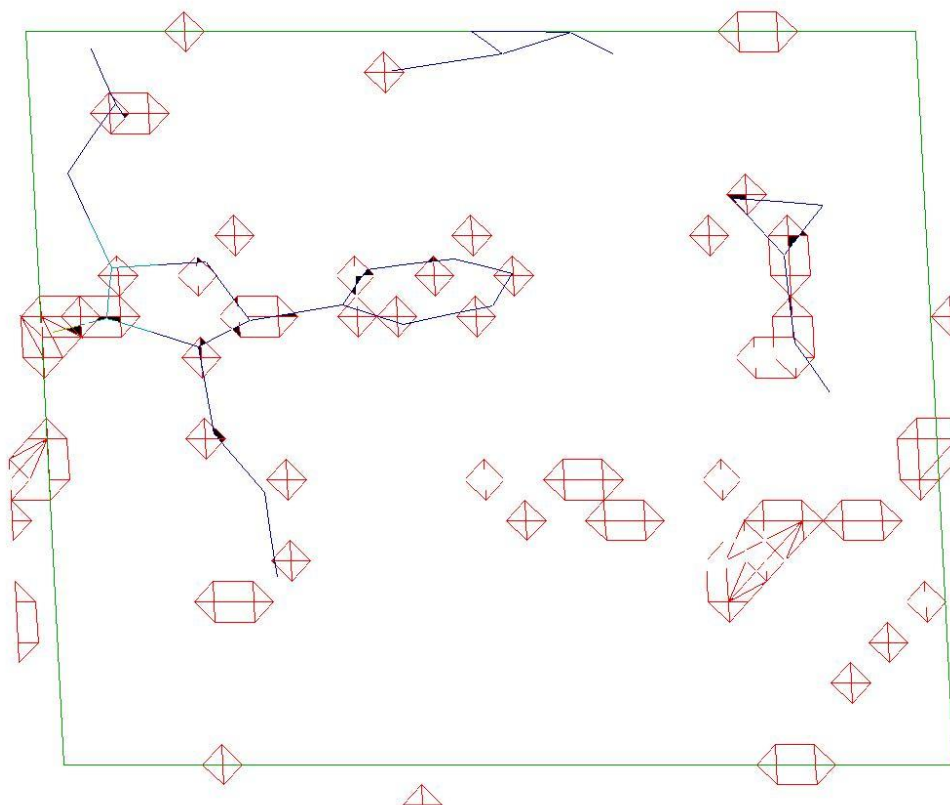
**Figure 33 - Comparison of Calculated & Observed PXRD Patterns of Alpha Form**



### 3.6.2 Propylene Carbonate & Methyl-tert.-butylether Solvates

The structures of the solvates with propylene carbonate and methyl-tertiary-butylether posed a different difficulty. In neither case were the solvent molecule positions clearly defined. After initial least squares refinement, the atomic positions of the phenylbutazone molecule were readily discernible, and displayed a well-ordered C4 tail. However the various remaining pockets of electron density did not provide unambiguous sets of atom positions for the solvent molecule.

**Figure 34 - Unrefined Model of Solvate of Propylene Carbonate – solved by SIR2004<sup>18</sup>**



From the standpoint of structure assembly, SIRWARE was the most adept at enabling plausible solvent structures to be completed. By contrast only partial assembly was possible in CRYSTALS, owing to constraints imposed by the software.

Although SIRWARE allowed more flexible atom positioning, upon carrying out least squares refinement on the solvate structure, attention was quickly drawn to the fact that imposed solvent atom positions did not correspond closely to areas of electron density in the underlying Fourier map; an obstacle that the software overcame by attaching large thermal parameters to those atoms. Disorder is also apparent in the positions of the solvent molecules, which is apparent from the additional solvent atom positions depicted.

The completed structural models of the two solvates are displayed in the following figures:

---

<sup>18</sup> Viewed normal to unit cell axis b.

Figure 35 - Asymmetric Unit of Methyl-tertiary-butylether Solvate

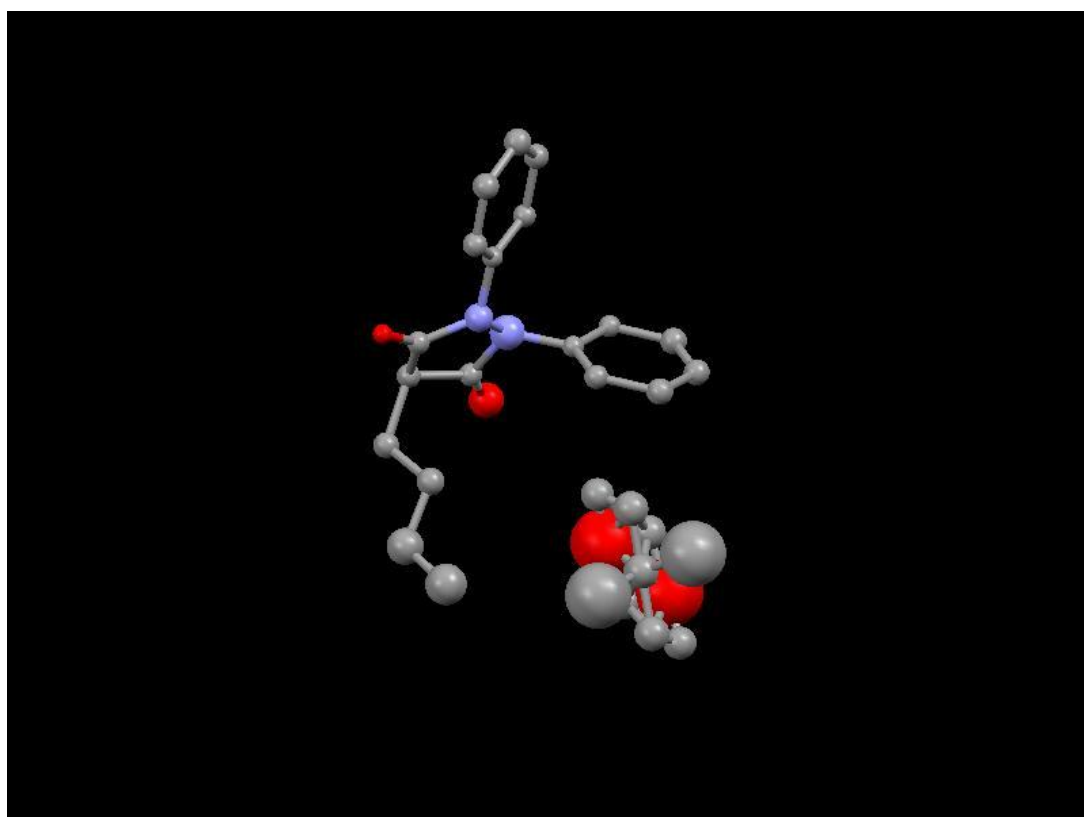
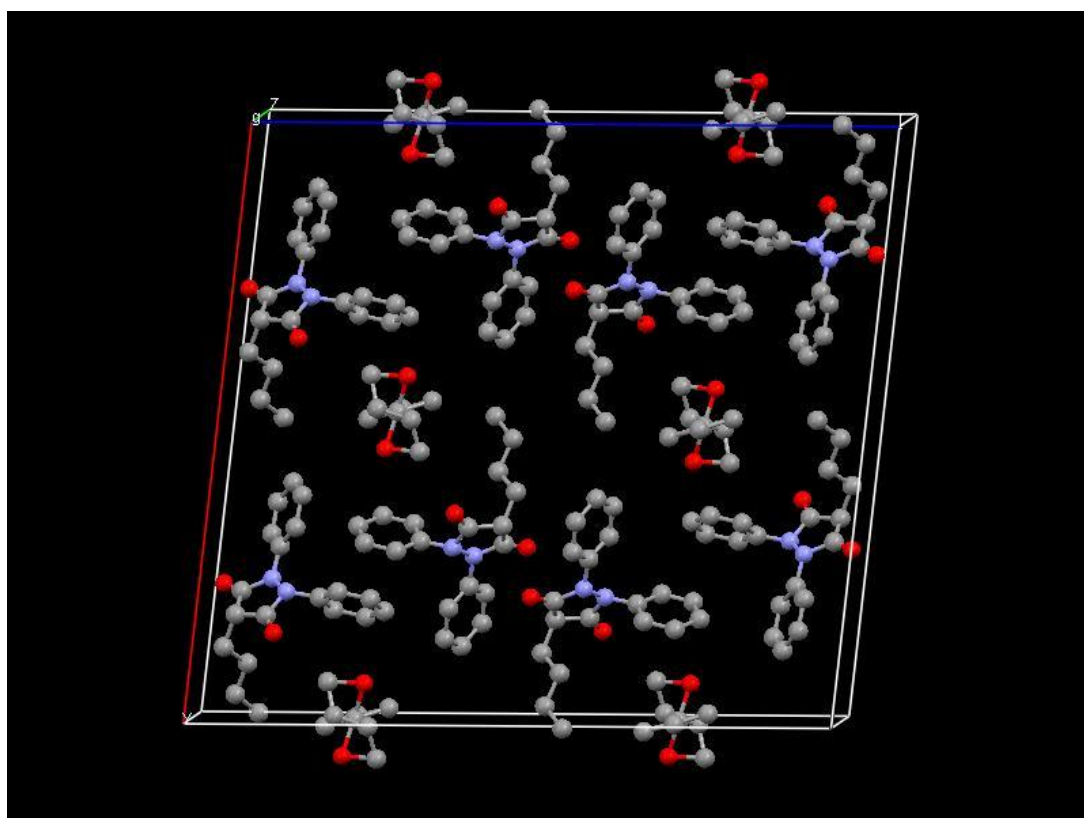
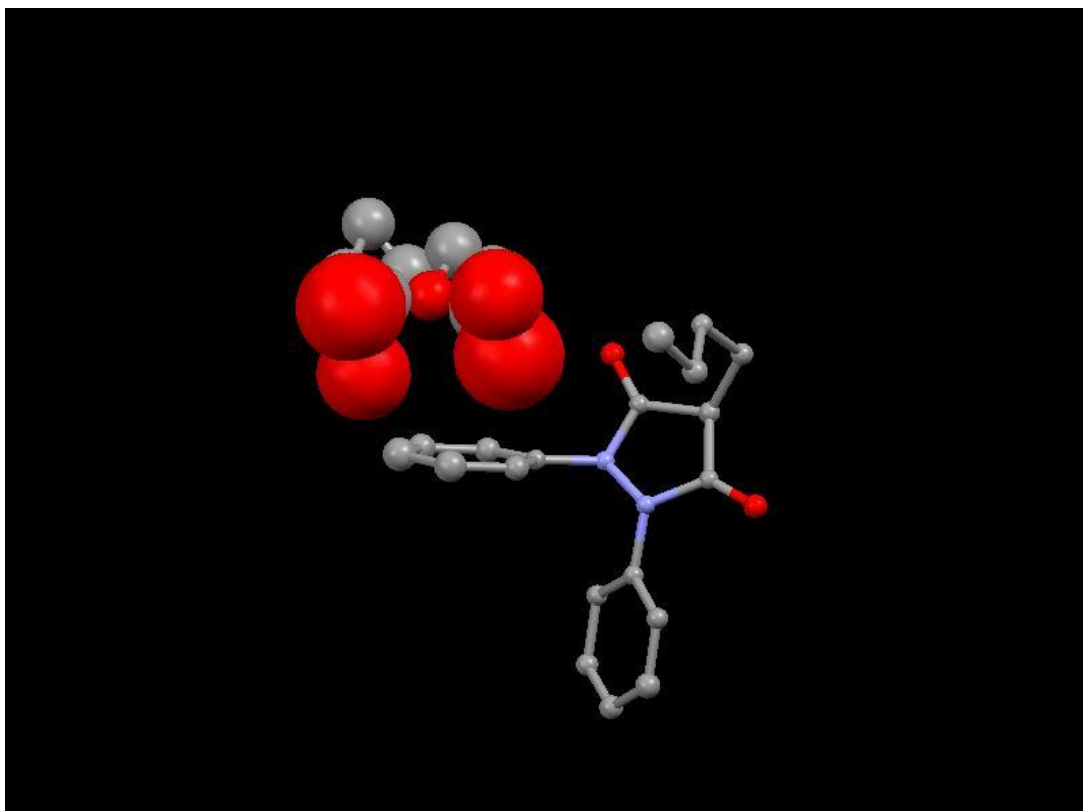


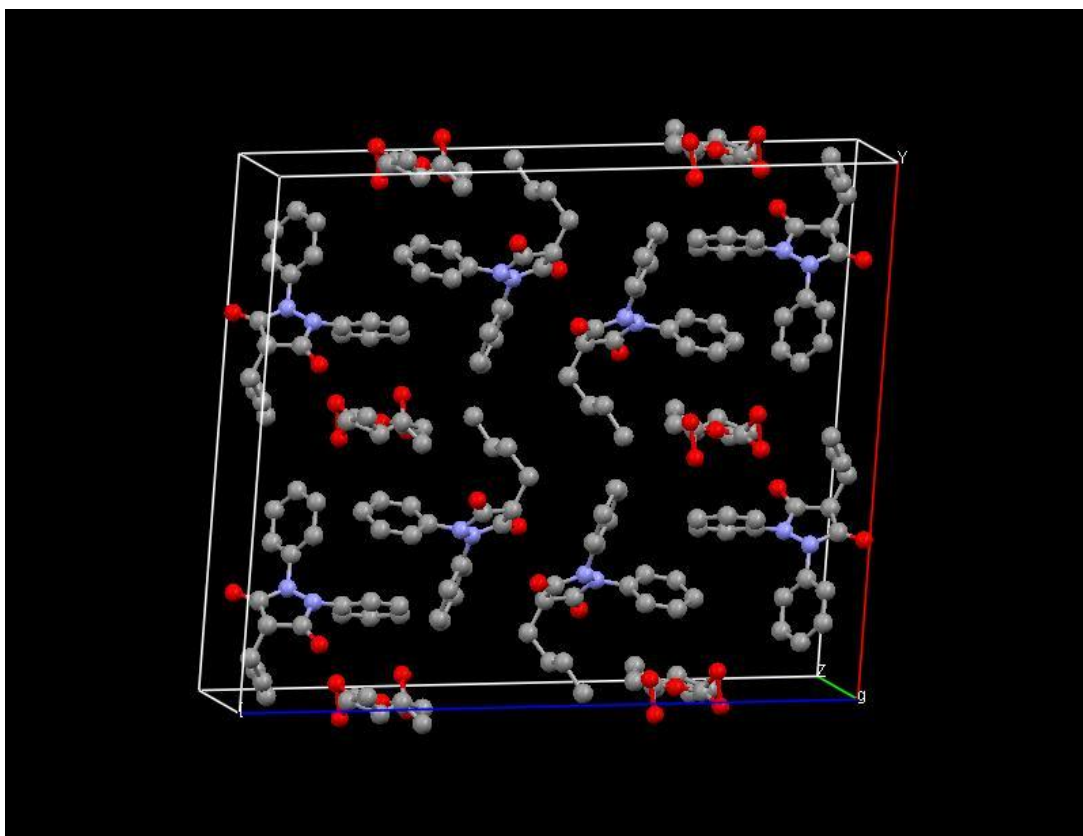
Figure 36 - Unit Cell of Methyl-tertiary-butylether Solvate



**Figure 37 - Asymmetric Unit of Propylene Carbonate Solvate**



**Figure 38 - Unit Cell of Propylene Carbonate Solvate**

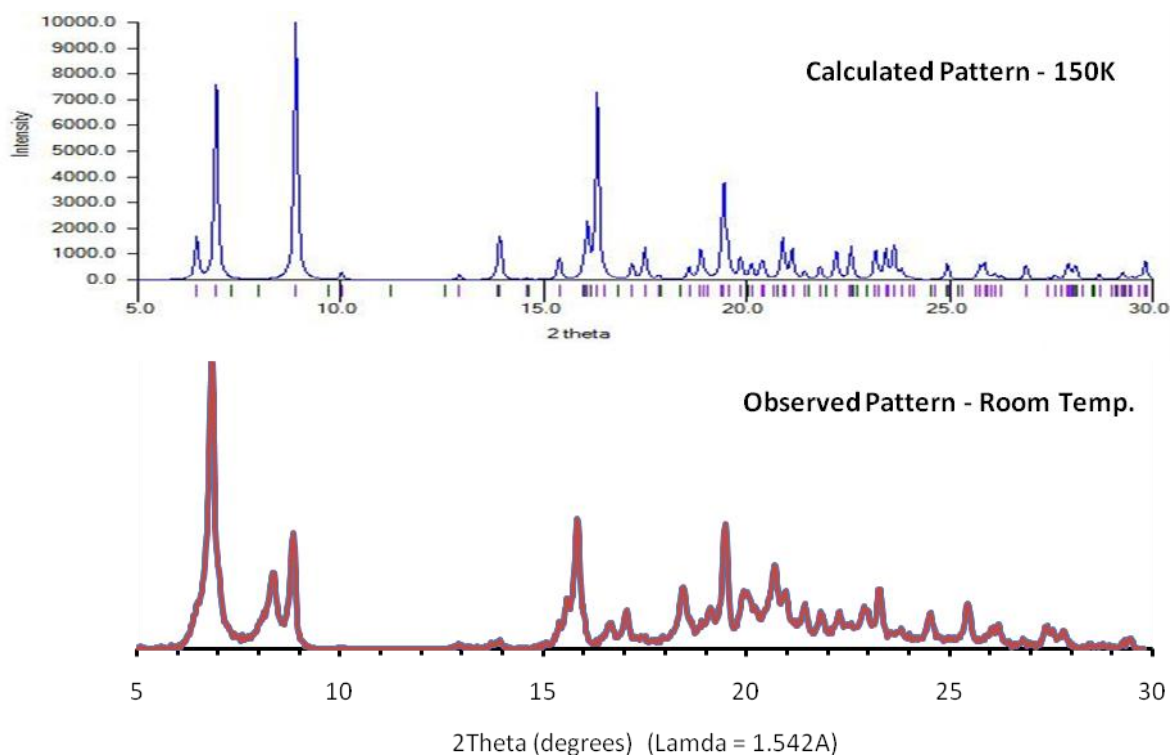




For these two solvate structures, comparison of the observed PXRD patterns and the imputed patterns calculated from the SCXRD-derived structure models reveals a number of discrepancies. For the solvate with methyl-tertiary-butylether:

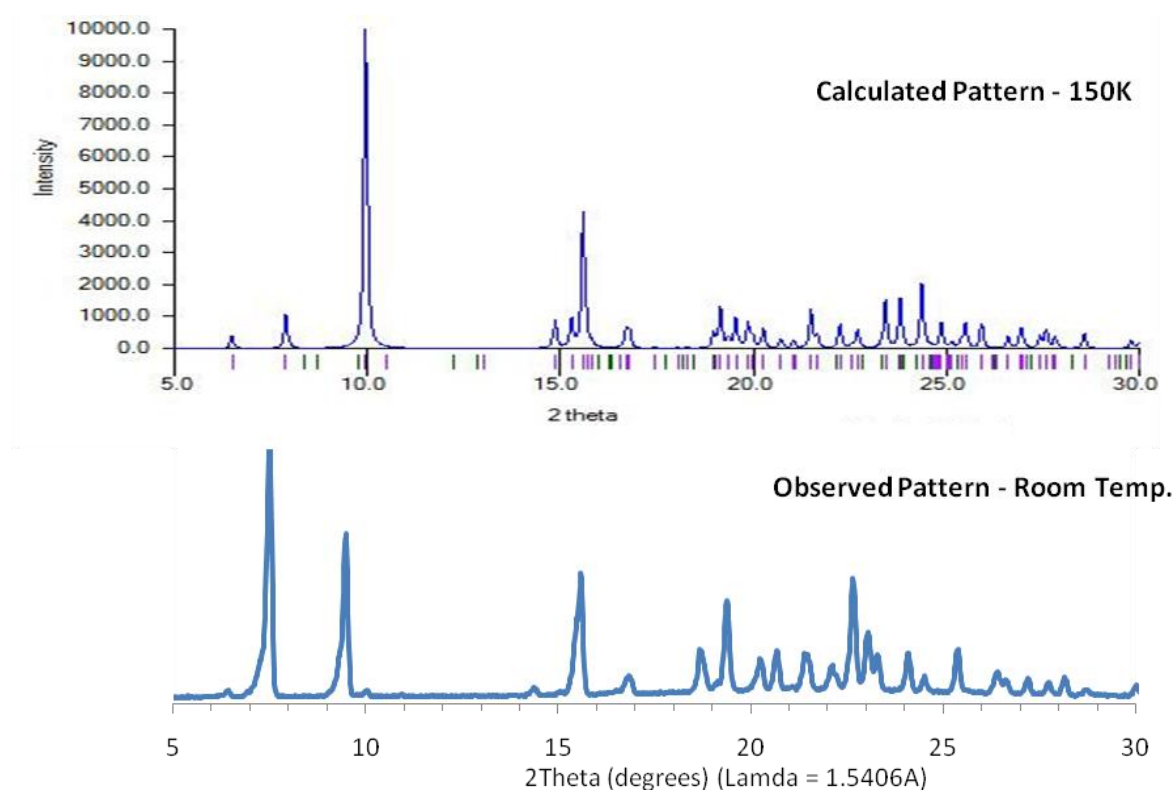
- The first two peaks in the observed pattern overlap – preferred orientation is a possible cause. Repeat PXRD experiments led to the same peak shape, however.
- A 2theta offset is apparent, which may be attributed to the difference in measurement temperature.
- The peak at  $2\theta = 8.3^\circ$  in the observed patterns is absent from the calculated pattern.

**Figure 39 - Observed & Calculated PXRD Patterns of MTBE Solvate**



The discrepancies in the observed and calculated PXRD patterns of the propylene carbonate solvate at low 2theta are less easily attributable to the difference in measurement temperature. Clearer correspondence between the two patterns is observed at higher angles.

**Figure 40 - Observed & Calculated PXRD Patterns of Propylene Carbonate Solvate**



The isostructurality of these and five other phenylbutazone solvates examined previously suggests that phenylbutazone forms an assembly that is, at least to some extent, structurally independent of the solvent molecule. However the differences in unit cell volume indicate that the solvent molecule is influencing the configuration of this assembly.

A comparison between the different solvates with space-group  $C2/c$  is provided in the following table:

**Table 13 - Overview of 7 Isostructural Solvates of Phenylbutazone**

SOLVENT	Benzene	Cyclohexane	1,4-Dioxane	Tetrahydrofuran	Tetrachloro- methane	Methyl-t.- butylether	Propylene Carbonate
Chemical Formula	C <sub>6</sub> H <sub>6</sub>	C <sub>6</sub> H <sub>12</sub>	C <sub>4</sub> H <sub>8</sub> O <sub>2</sub>	C <sub>4</sub> H <sub>8</sub> O	CCl <sub>4</sub>	C <sub>5</sub> H <sub>12</sub> O	C <sub>4</sub> H <sub>6</sub> O <sub>3</sub>
Molecular Weight	78.1	84.2	88.1	72.1	153.8	88.2	102.1
<b>SOLVATE</b>							
Chemical Formula	C <sub>19</sub> H <sub>20</sub> N <sub>2</sub> O <sub>2</sub> 0.5(C <sub>6</sub> H <sub>6</sub> )	C <sub>19</sub> H <sub>20</sub> N <sub>2</sub> O <sub>2</sub> 0.5(C <sub>6</sub> H <sub>12</sub> )	C <sub>19</sub> H <sub>20</sub> N <sub>2</sub> O <sub>2</sub> 0.5(C <sub>4</sub> H <sub>8</sub> O <sub>2</sub> )	C <sub>19</sub> H <sub>20</sub> N <sub>2</sub> O <sub>2</sub> 0.5(C <sub>4</sub> H <sub>8</sub> O)	C <sub>19</sub> H <sub>20</sub> N <sub>2</sub> O <sub>2</sub> 0.5(CCl <sub>4</sub> )	C <sub>19</sub> H <sub>20</sub> N <sub>2</sub> O <sub>2</sub> 0.5(C <sub>5</sub> H <sub>12</sub> O)	C <sub>19</sub> H <sub>20</sub> N <sub>2</sub> O <sub>2</sub> 0.5(C <sub>4</sub> H <sub>6</sub> O <sub>3</sub> )
Molecular Weight	347.5	350.5	352.5	344.5	385.3	352.5	359.5
<b>SOLVATE UNIT CELL</b>							
Research Group <sup>†</sup>	1	1	1	1	1	2	2
Crystal System	Monoclinic	Monoclinic	Monoclinic	Monoclinic	Monoclinic	Monoclinic	Monoclinic
Space-group	C2/c	C2/c	C2/c	C2/c	C2/c	C2/c	C2/c
Z	8	8	8	8	8	8	8
a	22.407	25.653	22.567	22.614	25.263	25.708	22.433
b	6.061	5.609	6.002	5.981	5.646	5.647	5.993
c	27.148	27.551	27.224	27.193	27.459	27.610	27.261
beta	91.107	98.621	93.444	93.819	99.117	96.835	92.990
Volume	3686.2	3919.5	3680.5	3669.9	3866.8	3974.7	3660.0
Calculated Density	1.25	1.19	1.27	1.25	1.32	1.18	1.31
<b>REFINEMENT</b>							
Reflections	3264	3479	3259	3237	3419	3662*	3103*
R1	0.0651	0.0567	0.0425	0.059	0.0452	0.1054	0.1679
wR2	0.1491	0.1347	0.1022	0.1309	0.1003	0.1251	0.1899

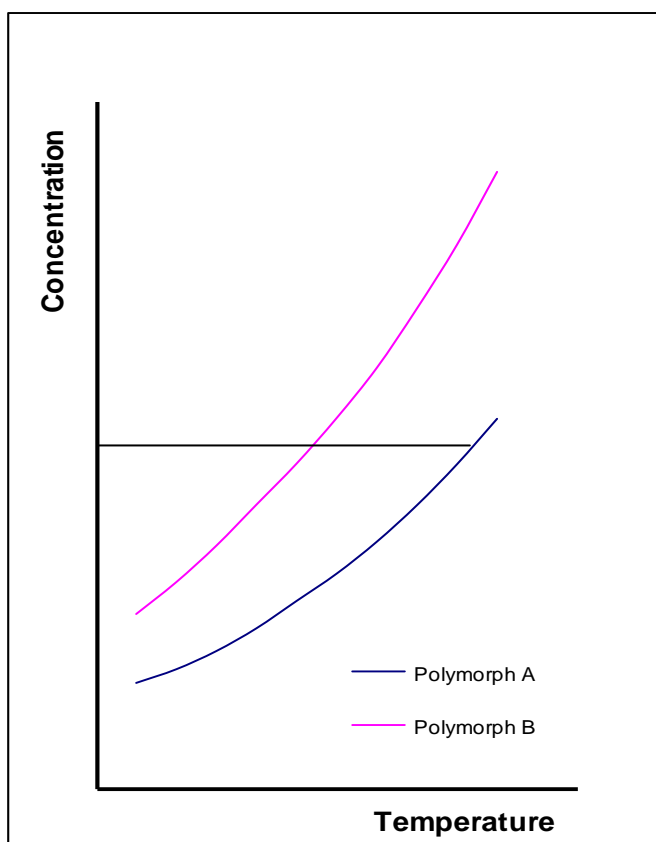
\*After merging of Friedel opposites, but before final refinement.

<sup>†</sup> 1 = Hosokawa *et al.*, 2004; 2 = Targett & Cockcroft, 2008.

## 4 Polymorphic Outcome of Solvent Crystallization

The importance of being able to predict and control the polymorphic form or forms that a molecule adopts upon crystallization was outlined in the introductory section. Although an exhaustive examination of the causes of polymorphic crystallization outcomes is undoubtedly worthy of an entire investigation in its own right, the most salient factors are introduced in this section. Particular attention is paid to the solubility behaviour of individual polymorphs, which forms the basis of the simplest model for the prediction of polymorphic outcomes of solvent crystallizations, the preferential solubility model.

### 4.1 Preferential Solubility Model



This model is analogous to the methodology used to predict how mixtures of two or more solutes with different solubility profiles will crystallize out of solution during solvent crystallization. In this important industrial technique, the temperature of a supersaturated liquor is adjusted to control the rate of crystallization of a target solute, [79].

Figure 41 - Solubility of Two Polymorphs vs. Temp.

It is straightforward to conceptualize the formation of a particular polymorph in terms of preferential solubility also. The graph depicts saturation concentrations of a pair of polymorphs, A & B, over a given temperature range. Moving from right to left along the line of constant concentration represented by the horizontal bar, once the temperature falls below the intersection with the blue saturation curve for the less soluble polymorph A, the solution is supersaturated with respect to this polymorph, and it can be expected to crystallize out of solution. As long as the temperature remains above the intersection with the pink saturation curve for polymorph B, no polymorph B is expected to crystallize.

It should be borne in mind, that below high saturation conditions, the dissolved solute molecules cannot be considered to possess even short range order, and should not be regarded as a mixture of distinct polymorphs, but rather as a collection of disordered solute molecules in solution. In the case of molecules such as phenylbutazone, this situation is complicated somewhat by the difference in the rate at which different polymorphs dissolve. There are also substance-specific factors to be considered, such as the influence of crystal habit and particle size on the rate of dissolution.

The crystallization behaviour of several molecules that exhibit polymorphism has been investigated by Kitamura *et al.*, [80-84], with a view to understanding the determining factors of the resulting polymorphic composition. The crystallization of glutamic acid has also been the subject of a recent *in situ* synchrotron study performed by a team that included researchers at the University of London, [85]. The study was completed within the framework of a research programme, based at the University of Leeds, entitled “Chemicals Behaving Badly”. Using a specially-designed, stirred crystallization apparatus in combination with an intense synchrotron beam, it has proved possible to discern the formation of bands of polymorphs in crystallization mixtures of glutamic acid.

## 4.2 Dissolution

In order to understand how valid the preferential solubility model is in determining polymorphic outcomes, it is first helpful to consider the dissolution behaviour of the solute. In the case of materials that exhibit polymorphism it was stated earlier that differences in the rate of dissolution between different polymorphs of the same molecule are regularly encountered. Solubility behaviour is of relevance in all steps of the usage chain in many industries, including pharmaceuticals, where it has bearing during:

- synthesis and crystallization of the active ingredient
- preparation of the dosage form; e.g. tablet production
- behaviour of the pharmaceutical ingredient in vivo

Pharmaceutical active ingredients elicit particular attention not least, because they are, in very many cases, insoluble in water, and therefore require modification and/or formulation in order that they may have the desired therapeutic effect. Yang *et al.*, [7], identify the entire class of API to which phenylbutazone belongs, non-steroidal anti-inflammatory drugs, as having very low aqueous solubilities.

### 4.2.1 Ideal Solution Theory

The thermodynamic treatment of the dissolution of solids considers the idealized effects of the forming and breaking of intermolecular bonds. For an ideal solution, comparison is drawn between the bond breaking process that occurs during dissolution of a solid and that which occurs during transition of the solid to the liquid phase at the melting temperature<sup>19</sup>.

---

<sup>19</sup> Constant pressure is generally assumed.

Frequently, however, dissolution is accompanied by additional, non-reactive bonding processes, which are typically exothermic; for instance the formation of hydrogen bonds or the creation of micelles. A commonly observed consequence of “mixing” bonding is the temperature rise upon mixing of two liquids<sup>20</sup>, commonly referred to as the heat of mixing. For dissolution of a solid in a solvent under ambient conditions, the heat of dissolution may be considered to be the sum of the heat of melting, usually an endothermic process, and the heat of mixing, usually an exothermic process:

**Equation 19 - Enthalpy of Solution of a Solid Solute**

$$\Delta H_{\text{solution}} = \Delta H_{\text{mixing}} + \Delta H_{\text{fusion}}$$

In the situations under consideration, the dissolution process occurs below the solute’s melting temperature, and an adjustment for the enthalpy terms is introduced in order to take into account the difference between the temperature at which the melting enthalpy has been measured and the temperature at which the dissolution process is taking place. For the heat of fusion this adjustment is calculated using the following integral, whose form is also valid for the enthalpy of mixing:

**Equation 20 - The Integral Form of the Kirchoff Equation**

$$H_{T_{\text{fusion}}} - H_T = \int_T^{T_{\text{fusion}}} C_p dT$$

Where:

$H_T$  = Enthalpy of solute at measurement temperature

$H_{T_{\text{fusion}}}$  = Enthalpy of solute at melting temperature

---

<sup>20</sup> Two liquids (or solutions) at the same starting temperature.

$T_{fusion}$  = Temperature of fusion

$T$  = Temperature of measurement

$C_p$  = Heat capacity at constant pressure

Typically it is assumed either that the heat capacity is constant over the temperature range in question, or that its variation is linear. Where the heat capacity is constant, the integral above simplifies to  $H_{T_{Fusion}} - H_T = C_p(T_{Fusion} - T)$ . Often this correction is small, and frequently it is neglected altogether. The definition of an ideal solution includes the assumption of complete dissociation by a given solute in all solvents, and the absence of a heat of mixing.

In ideal solution theory all individual characteristics of the solute are ignored; for example, the type of bonding present in the solute; ionic, covalent, containing a dipole, etc. Although a simplification, this approach serves as a basis for derivation of useful thermodynamic proportionalities for the bulk solution, which are readily observable; most notably the inverse relationship of the temperature of the solution to logarithmic solute concentration, which is captured in the van't Hoff relationship:

#### Equation 21 - The van't Hoff Equation

$$\ln[x_{solute}] = \frac{-\Delta H_{fusion}}{RT} + \frac{\Delta S_{fusion}}{R}$$

Where:

$[x_{solute}]$  = Mole fraction of the solute

$\Delta H_{fusion}$  = Heat of fusion of the solute

$\Delta S_{fusion}$  = Entropy of fusion of the solute

$R$  = The gas constant

$T$  = Absolute temperature



This expression is derived from the free energy change of mixing, which may also be calculated from the mole fraction of concentration according to:

**Equation 22 - Free Energy Change upon Mixing**

$$\Delta G = RT \ln [x_{solute}]$$

Rearranging this expression gives:

$$\ln [x_{solute}] = \frac{\Delta G}{RT}$$

For the ideal case, the enthalpy of mixing is equal to zero, and from Equation 19:

$$\Delta H_{solution} = \Delta H_{fusion}$$

Remembering the Helmholtz relationship; commonly expressed as follows:

**Equation 23 - General Form of the Helmholtz Equation<sup>21</sup>**

$$H = G - TS$$

Where:

$H$  = Enthalpy

$G$  = Gibbs free energy

$T$  = Temperature

$S$  = Entropy

The change in free energy upon dissolution may be expressed in terms of heats of fusion as follows:

$$\Delta G_{dissolution} = \Delta H_{fusion} - T\Delta S_{fusion}$$

---

<sup>21</sup> The Helmholtz free energy,  $A$ , is related to the Gibbs free energy,  $G$ , by the equality  $\Delta G = \Delta A + P\Delta V$ , where  $P$  and  $V$  refer to pressure and volume respectively. In processes where no expansion or contraction occurs  $\Delta V = 0$ , and the Gibbs & Helmholtz free energies may be considered equivalent.

Combining this with the terms of Equation 15 gives:

$$\ln [x_{solute}] = \frac{\Delta H_{fusion} - T \Delta S_{fusion}}{RT}$$

At the melting temperature, the free energies of the two states are assumed to be equal. This assumption is also made with respect to transitions between polymorphs, which are discussed in Section 5.1. This assumption allows the entropy of fusion to be calculated as follows:

**Equation 24 - Entropy of Fusion at the Melting Temperature**

$$\Delta H_{fusion} = T_{fusion} \Delta S_{fusion}$$

So that:

$$\ln [x_{solute}] = \frac{\Delta H_{fusion} - T \frac{\Delta H_{fusion}}{T_{fusion}}}{RT}$$

This simplifies to:

$$\ln [x_{solute}] = \frac{\Delta H_{fusion}}{R} \left( \frac{1}{T_{fusion}} - \frac{1}{T} \right)$$

This is the most commonly encountered form of the van't Hoff equation. The ideal solubility equation is derived from it. Kirchoff adjustments; (Equation 20) are applied, in order to account for the fact that:

- i. the solution is at a lower temperature than the melting temperature of the solute.
- ii. the heat capacity at constant pressure may vary over the temperature range under examination.

### Equation 25 - The Ideal Solubility Equation

$$\ln[x_{solute}] = \frac{\Delta H_{fusion}}{R} \left( \frac{1}{T_{fusion}} - \frac{1}{T} \right) + \frac{\Delta C_p}{R} \left( \frac{T_{fusion}}{T} - 1 \right) - \Delta C_p \ln \left( \frac{T_{fusion}}{T} \right)$$

$\Delta C_p$  is the difference in the heat capacity of the solute between the melting temperature and the measurement temperature. Not infrequently the Kirchoff correction terms are omitted.

The derivation is discussed further by Streng, [33].

### 4.2.2 Non-Ideal Solution Theory

As discussed in the previous section, the ideal solution is a largely conceptual entity. Ionic solutions conform most closely to its precepts. The most widely encountered theoretical method to predict the solubility of non-electrolytes was developed by J.H. Hildebrand, whose thermodynamic treatment is referred to as “regular solution theory”; [30, 31, 33, 86, 87].

A regular solution is defined as, “*one involving no entropy change when a small amount of one of its components is transferred to it from an ideal solution of the same composition, the total volume remaining the same.*”

Streng paraphrases thus: “*a regular solution can have a non-ideal enthalpy of formation but must have an ideal entropy of formation*”.

In prelude to a discussion of regular solutions it is typical to introduce the property of a solute known as its *activity*, a measure of the deviation of that solute from ideal behaviour:

### Equation 26 - Definition of the Activity of a Solute

$$a_x = [x] \gamma_x$$

Where:

$a_x$  = Activity of solute, x

$[x]$  = Molar concentration of solute, x

$\gamma_x$  = Activity coefficient of solute, x

The activity may be used in place of the concentration term in many thermodynamic expressions, in order to achieve a closer fit to measured data.

Regular solution theory considers non-ideal aspects of the solution such as its enthalpy of mixing, and defines an independent solubility parameter for each solute and solvent component on the basis of its heat of vapourisation and molar volume<sup>22</sup>:

#### **Equation 27 - Calculation of a Solubility Parameter for a Solvent Component**

$$\delta_x = \frac{\Delta H_{vap_x}}{V_x}$$

Where:

$\delta_x$  = Solubility parameter of component, x

$\Delta H_{vap_x}$  = Enthalpy of vapourisation of component, x

$V_x$  = Molar volume of component, x

These parameters are considered characteristic of a given molecule, and may be used for that substance in any given combination of solvent(s) and solute(s), in which the substance is included.

Regular solution theory expressly provides for solutions of multiple solvents and solutes.

This convenience factor has wide attraction, particularly in situations where mixtures of large numbers of solvents are commonplace; e.g. hydrocarbon processing.

---

<sup>22</sup> Certain sources also include a temperature correction term; i.e.  $\delta_x = \frac{\Delta H_{vap} - RT}{V_x}$

For a solution comprising a single solvent and a single solute, the activity of the solute is related to the Hildebrand solubility parameter as follows:

**Equation 28 - Activity of Solute in terms of Hildebrand Solubility Parameters**

$$\ln \gamma_{solute} = \frac{V_{solute} \phi_{solvent}^2 (\delta_{solvent} - \delta_{solute})^2}{RT}$$

Where:

$V_{Solute}$  = Molar volume of the solute

$\Phi_{Solvent}$  = Volume fraction solvent

$\delta_{Solvent}$  = Solubility parameter of the solvent

$\delta_{Solute}$  = Solubility parameter of the solute

$R$  = The gas constant

$T$  = Temperature of measurement

From the definition of the activity coefficient:

$$-\ln [x_{solute}] = \ln \gamma_{solute} - \ln a_{solute}$$

Combining the van't Hoff equation with the expression for the activity coefficient yields:

**Equation 29 - Hildebrand Solubility Equation**

$$-\ln [x_{solute}] = \frac{\Delta H_{fusion}}{R} \left( \frac{1}{T} - \frac{1}{T_{fusion}} \right) + \frac{V_{solute} \phi_{solvent}^2 (\delta_{solvent} - \delta_{solute})^2}{RT}$$

The Hildebrand solubility term is assumed to correct for the non-ideality of the solution, and the solute's activity term is therefore replaced by its concentration. Its value must always be positive; i.e. it lowers the value of solute concentration; (Figure 43).

Solubility parameters for commonly used solvents are widely available, and have been compiled in a handbook, [88]. By contrast values of solubility parameters and molar volumes have only been measured for a relatively small proportion of APIs.

For many organic molecules, including APIs, the definition of the solubility parameter in terms of heats of vapourisation is only of indirect relevance; many of these substances tend to undergo irreversible decomposition before boiling. Proponents of the Hildebrand approach state that it is necessary to consider a hypothetical sub-cooled liquid reference state in order to obtain solubility parameters for solutes that are solid at room temperature; the solute's solubility parameter may then be calculated from the solid's heat of sublimation. In many instances the solute's tendency to sublime is, however, minimal.

Various different methods have been devised to evaluate the solubility parameters of solutes experimentally, and they are often referred to as "cohesion" parameters, [29, 88, 89]. Streng employs heats of mixing in his derivation of solubility parameter values for solutes.

As well as the inherent solubility of a particular solute in a solvent or a mixture of solvents, a range of kinetic factors also play an important role in determining the rate at which dissolution occurs. These factors include:

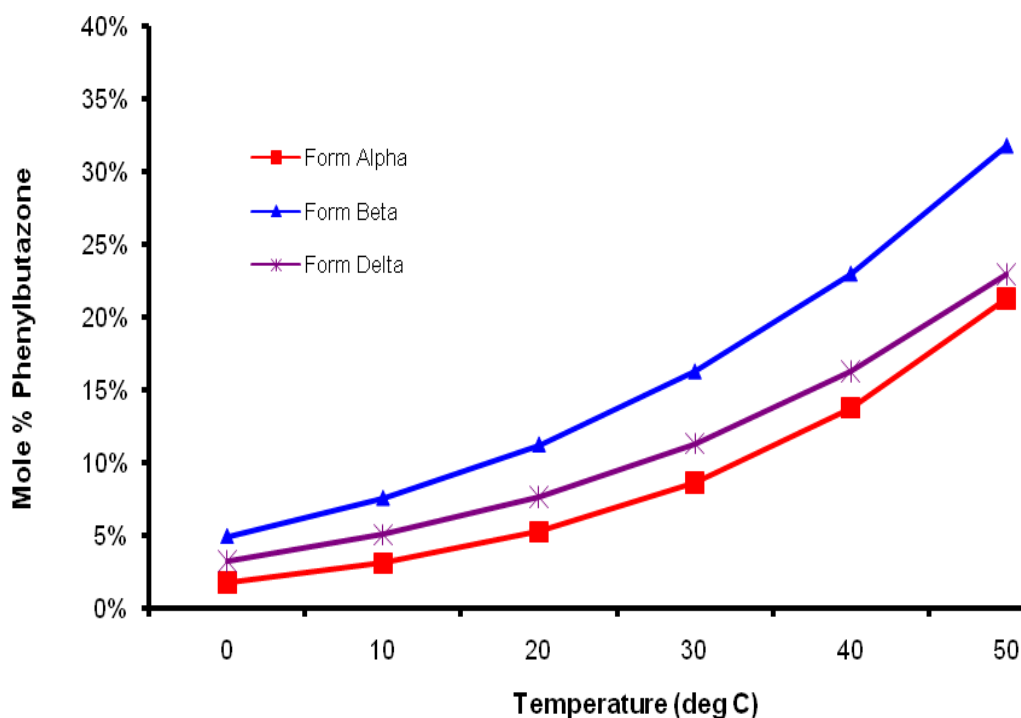
- the size of individual solute particles
- their wetting characteristics in a particular solvent or blend
- mixing conditions; e.g. agitation and/or stirring

Among the methods commonly used to capture the effects of these factors are the Ostwald-Freundlich equation, (also known as the Gibbs-Thomson equation), and the Noyes-Whitney equation, [79, 90].

### 4.2.3 Solubility of Phenylbutazone

Based upon the melting points and heats of fusion reported by Kaneniwa *et al.*; (Table 18), the ideal saturation solubility of phenylbutazone was calculated using the ideal solubility equation, (Equation 25), in its simplified form, which excludes measurement temperature adjustments. The heat of fusion of the different polymorphs increases in the order; beta, delta, alpha. A plot of ideal solubility against temperature is shown in the figure below.

Figure 42 - Ideal Solubility of Phenylbutazone Polymorphs vs. Temperature

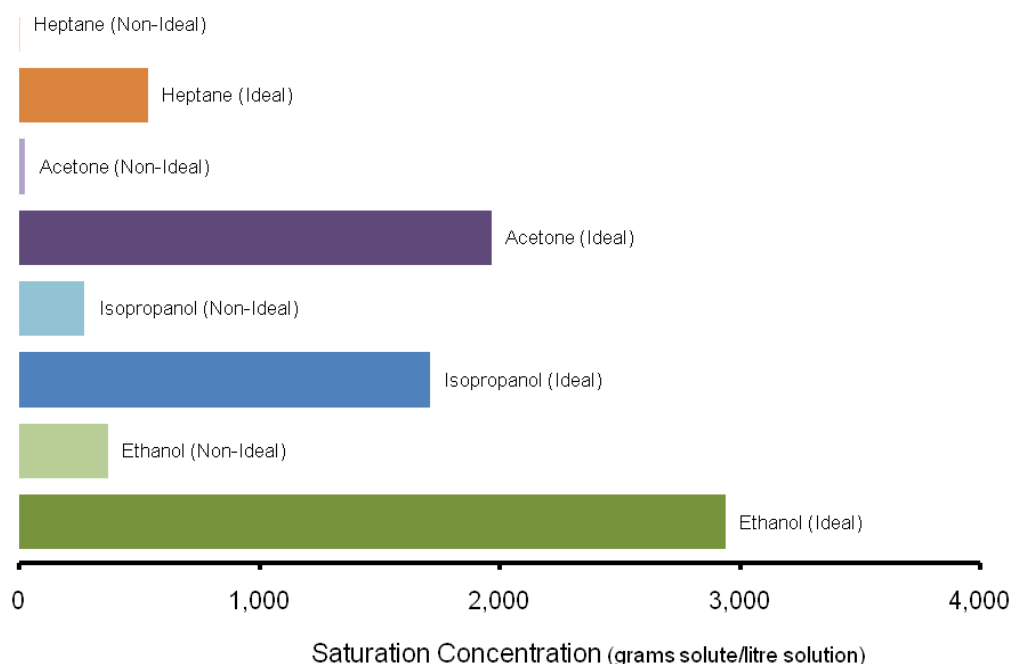


This method may be used to obtain the solubility for phenylbutazone in any solvent, simply by altering the molecular weight of the solvent, upon conversion from molar to mass units. The solubility ratios of the polymorphs calculated in this manner are in agreement with the range of 1.0-1.3 reported by Pudipeddi *et al.*, [91].

As stated earlier, this technique does not take into account specific solvent incompatibilities; for example phenylbutazone's insolubility in water. A better fit to observed data is to be expected from the modified van't Hoff equation incorporating Hildebrandt solubility parameters; (Equation 29). Insolubility of phenylbutazone in water, (solubility parameter  $\sim 48 \text{ MPa}^{1/2}$ ), is correctly predicted by regular solution theory.

The solubility parameter of phenylbutazone was reported by Rey-Mermet *et al.*, [29], without reference to the polymorphic form, but calculated using a range of different techniques, including induction from actual solubility measurements. Most routes indicate a solubility parameter in the region of 23-30  $\text{MPa}^{1/2}$ , but Rey-Mermet *et al.* point out that the value calculated from actual solubility measurements in methanol implies a solubility parameter of only 16.8  $\text{MPa}^{1/2}$ . The solubility of phenylbutazone (at  $\delta = 25 \text{ MPa}^{1/2}$ ) in a selection of solvents, according to ideal and regular solution theory, is shown in the figure below.

**Figure 43 - Ideal and Non-Ideal Solubilities of Phenylbutazone<sup>23</sup>**



<sup>23</sup> Thermal data for the delta form were used in these computations.

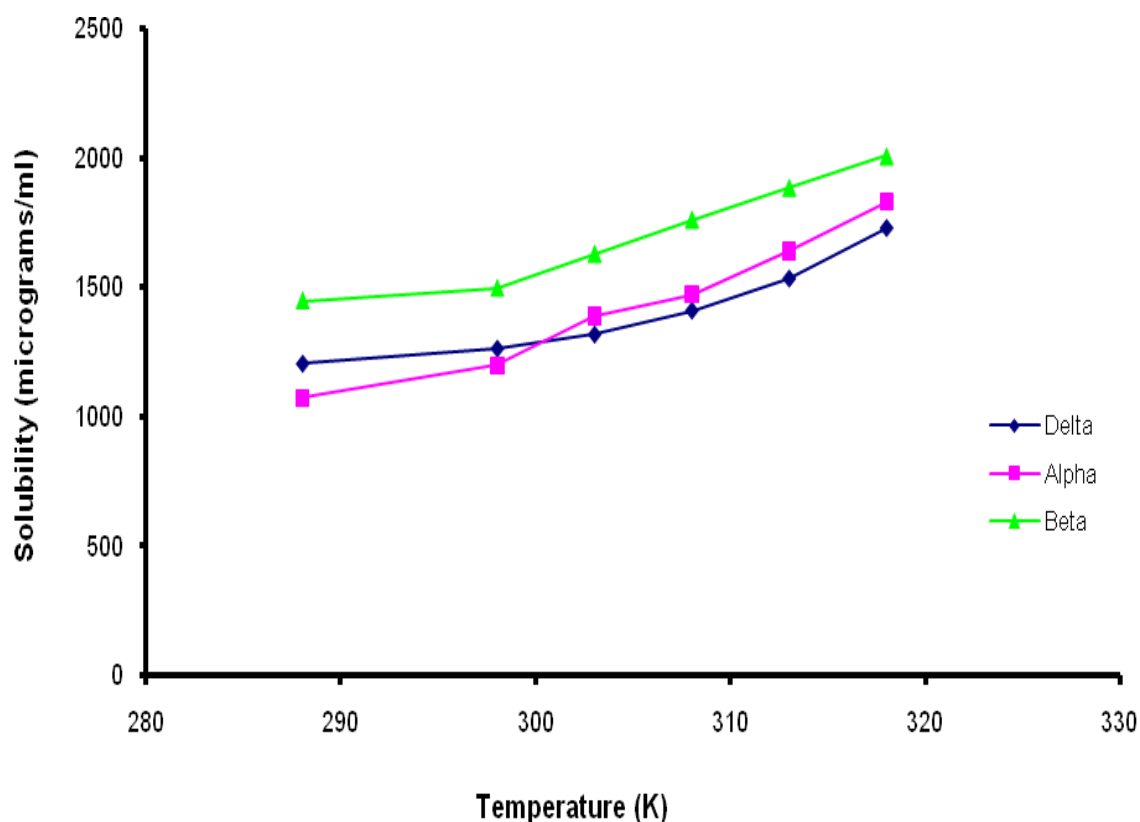


Quantitative solubility measurements were not conducted during this investigation. Solubility values in three organic solvents, including acetone, are provided by Datta and Grant, [92].

Several literature measurements of solubility in aqueous buffer solution indicate an equilibrium saturation concentration for the alpha, delta and beta polymorphs in the region of 1.0–1.5 mg/ml at room temperature.

The following figure shows solubilities of individual polymorphs over a range of temperatures, measured in a phosphate buffer solution of pH 6.8. This study implies that differences in the absolute solubility of solutions of the three polymorphs persist over time.

**Figure 44 - Solubility of Polymorphs in Phosphate Buffer Solution; Kaneniwa *et al.***



Changes in solubility of the polymorphs have been measured over time by the following groups:

- **Kaneniwa *et al.***, [26], indicate that the order of fastest initial dissolution rate is: beta, alpha, delta. Their rates of initial dissolution in buffer solution at different temperatures have been used in a technique to estimate the polymorphic transition temperature in Section 5.1.
- **Ibrahim *et al.***, [16] indicate that the solubility of the different polymorphs converges to a value of about 2.2 mg/ml at 36°C in phosphate buffer solution over a period of between 0.25-1.0 days, however the solution of the beta polymorph remains slightly more concentrated across the entire measurement period of 4 days.
- **Tuladhar**, [19], includes solubility curves collected over several days for the alpha, beta and delta forms dissolved in phosphate buffer at 37°C with and without the use of wetting agents. In these experiments an absolute solubility of 4-5mg/ml is determined. Both the beta and delta forms are shown to be slightly more soluble than the alpha form, and this gap remains after a period of 5 days. This solubility gap is eliminated through the addition of less than 1% of Tween<sup>®</sup>80, described variously as a dispersing agent and as an emulsifier, which consists primarily of polyoxyethylene sorbitan monooleate. In a separate study, Tuladhar *et al.*, [34], investigate the effect of particle size and compression on the dissolution of phenylbutazone, paying attention to the API's polymorphic form.

### 4.3 *Role of Solvent*

The crystallization experiments conducted during this investigation may be divided into the following classes:

- Solvent screening experiments to ascertain solvent mediated transitions and identify solvate formation
- Pure polymorph preparation according to developed procedures
- Single crystal growth in expectation of a particular form or forms

Solvent trials not only reveal the existence of solvated structures, but have brought to light the existence of new polymorphic forms as well. Furthermore different solvents are routinely observed to have a major impact on the morphology of the crystals formed, [70], a factor of major importance in the preparation of crystals suitable for single crystal X-ray diffraction. The objective of identifying conditions under which one polymorph of phenylbutazone crystallized in preference to another was also borne in mind.

The choice of solvent seldom features in thermodynamic treatments of solvent crystallization, and specific consideration of solvent would not be anticipated, other than in those situations where the use of a particular solvent is associated with a change in enthalpy, resulting from causes such as:

- Formation of a solvate
- Formation of ions
- Formation of hydrogen bonds
- Reaction between the solvent and solute; e.g. uncatalyzed esterification of a carboxylic acid group by an alcohol, [93].

In common with many small organic drug molecules, phenylbutazone forms solvate structures with many crystallization solvents, and exhibits wide variations in crystal habit depending upon the solvent employed. Ascertaining clear patterns between the solvent employed, and the polymorphic composition of crystallized samples was far from straightforward.

Under ambient conditions a number of solvents yielded pure alpha form, however in only very few instances was the pure delta form encountered. Moreover those solvents that gave rise to pure alpha form during one experiment could not necessarily be relied upon to yield pure alpha form upon repetition of the same experiment; the alternative outcome typically being a mixture of the alpha and delta polymorphs.

In the following table the polymorphic outcomes of evaporative crystallization of phenylbutazone at ambient temperature and pressure are summarized for a range of common crystallization solvents. Samples were mixed at conditions below saturation, and filtered, before being allowed to crystallize in glassware open to the atmosphere.

For a number of solvents, more than one experiment was conducted, and in several of these repeat experiments the effect of raising the starting temperature of the crystallization was observed.

The most common polymorphic composition is indicated as well as other compositions that were encountered – concomitant mixtures of polymorphic forms are indicated by the names of the polymorphs present, separated by a forward slash. Solvents in which three or more crystallizations were carried out are indicated by an asterisk.

**Table 14 - Crystallization Results of Solvent Screening of Phenylbutazone<sup>24</sup>**

<b>Solvent</b>	<b>Solubility</b> <i>(S=Sparingly, R=Readily)</i>	<b>Most Frequent Composition</b>	<b>Other Compositions</b>
Methanol*†	S	Alpha	Alpha/Delta, Delta
Ethanol*†	S	Alpha/Delta	Delta, Alpha
Iso-propanol	S	Alpha	
Acetone*	R	Alpha	Alpha/Delta
Methylethylketone*	R	Alpha	Alpha/Delta
Methyl-iso-butylketone	R	Alpha	
Cyclopentanone	R	Solvate	
Cyclohexanone*	R	Solvate	
Propylene carbonate	R	Solvate	
Methylacetate	R	Alpha	
Ethylacetate	R	Alpha/Delta	
Diethylether	S	Alpha	
Di-iso-propylether	S	Alpha	
Di-n-butylether	S	Alpha	
Methyl-tert.-butylether*	S	Solvate	Alpha/Beta/Solvate, Delta/Solvate, Beta <sup>§</sup> , Alpha/Delta/Solvate, Alpha/Beta/Delta
Chloroform	R	Solvate	
Tetrahydrofuran*	R	Solvate	
n-Heptane*†	S	Alpha/Delta	Alpha/Beta/Delta, Alpha/Beta, Alpha
Benzene	R	Solvate/Alpha	
Toluene*†	R	Alpha/Delta	Alpha/Delta/Beta, Delta
p-Xylene*†	R	Alpha/Delta	Alpha
o-Xylene*†	R	Alpha/Delta	Alpha/Beta/Delta

\*Three or more crystallizations were carried out using this solvent.

†Crystallizations at above ambient start temperatures were carried out using this solvent.

§Pure beta form occurred as a side bloom around the edge of the crystallization dish.

<sup>24</sup> Excludes crystallization experiments involving multiple solvents and/or antisolvents; e.g. methanol & water.

#### **4.4 Targeted Crystallization of Polymorphs**

Grant *et al.*, [94], state their belief that “*solvent-mediated polymorphic transformation is an efficient technique to obtain the most stable polymorph*”. Using the example of sulphamerazine, they go on to surmise that the selection of suitable solvent(s) to effect the desired polymorphic outcome of a given solute is determined by its degree of solubility and the strength of solvent-solute interactions; particularly hydrogen bonding. Rather than preferential solubility; (Section 4.1), the postulated mechanism of formation of a particular polymorph is kinetic control of nucleation events, influenced by stirring rate and temperature among other factors.

Blagden and Davey, [95], also emphasize the importance of solvent selection, whereby a specific solvent is chosen in order to give rise to a solvent/solute pairing, which favours a certain packing “motif” of the crystal lattice. During nucleation and lattice formation, these “motif” sub-units form the basis of the lattice of a specific polymorphic form. The addition of secondary, inhibiting, solvents is introduced as a simultaneous tactic by which to prevent the formation of unwanted sub-units, inasmuch as their formation can be anticipated.

Examples of the lack of predictability of the polymorphic composition of individual crystallization batches are not difficult to find. Threlfall, [96], recounts an experiment, in which preparation of specific polymorphs of twenty pharmaceutical active ingredients from well-described “recipes” was attempted, but which resulted in the expected outcome in only ten of the twenty cases.

In a further example of unpredictability, Threlfall draws attention to a method of preparing polymorphic form I of sulphathiazole using n-propanol, which had been employed for several decades, but which no longer yields that polymorph with regularity.

#### 4.4.1 Theoretical Background

The changes in crystallization outcomes of established preparation methods described by Threlfall, underscore the complexity of solvent/solute interactions. However the very fact that a particular solvent is specified in a recipe, and yields reproducible polymorphic outcomes over an extended period of time, lends support to the conviction of Grant *et al.* about the effectiveness of solvent selection methods.

In a review that explores the factors that give rise to different crystal forms, and concomitant mixtures in particular, Bernstein *et al.*, [97], employ the term “*occurrence domain*” to denote the set of crystallization conditions in which a particular polymorph is formed. Concomitant crystallization of two or more polymorphs is an instance in which the occurrence domains of two or more polymorphs happen to overlap. The review concedes that although, “*this domain exists for every substance, rarely if ever are its contents completely known*”.

In his more recent IUCr monograph on polymorphism, [1], Bernstein resorts to a probabilistic approach in order to explain the formation of a particular polymorph under a given set of conditions. In this framework preferential nucleation, rather than solubility, is the mechanism for the formation of a specific polymorph.

**Equation 30 - Probability Expression for Formation of Polymorph, *i*.**

$$P(i) = f(\Delta G_i, R)$$

The key variables are the free energy change associated with formation of polymorph, *i*, and kinetic rate function, *R*, for nucleation of the polymorph. As an example of *R*, Bernstein cites the rate expression principally attributed to Volmer and frequently referred to as the classical theory of nucleation from homogeneous solutions, which is expressed as follows:

### Equation 31 - Classical Nucleation Rate Equation from Homogeneous Solution

$$J = A_0 e^{-16\pi\gamma^3 v^2 / 3k^3 T^3 \sigma^2}$$

Where:

$J$  = Rate of nucleation

$A$  = Pre-exponential factor

$\gamma$  = Surface free energy

$v$  = Molecular volume

$k$  = Boltzmann constant

$T$  = Temperature

$\sigma$  = Degree of supersaturation

The expression for the rate of nucleation above is similar to the general Arrhenius rate equation, which is used to characterize the relationship between the kinetic rate constant,  $k$ , for various processes including crystallization, dissolution and reaction and the temperature at which those processes are carried out.

### Equation 32 - Arrhenius Expression for the Kinetic Rate Constant

$$k = A e^{-E/RT}$$

Where:

$A$  = Pre-exponential factor

$E$  = Activation energy

$R$  = The gas constant

$T$  = Temperature



The free energy term,  $\Delta G$ , is substituted out of the expression for the rate of nucleation; in the case of non-electrolytes; the Gibbs-Thomson relationship is frequently employed for this purpose. A full derivation is provided by Mullin.

Besides preferential nucleation, Bernstein also attributes the preferential appearance of one polymorph versus another to differences in the size of the activation energy barrier of formation of the individual polymorphs, a variable in the Arrhenius expression. Only the polymorph with the lower barrier would be expected to form, providing that the activation energy barrier of the other polymorph is not exceeded.

Unlike the comparison of activation barriers of individual polymorphs, inspection of the nucleation rate expression indicates that the values of  $J$  for a pair of polymorphs may intersect over a range of supersaturation degrees. Bernstein gives examples, which suggest that two polymorphic forms of a molecule may each display higher rates of nucleation at different degrees of supersaturation.

Threlfall postulates that crystallization processes may be divided into two categories, those which are under:

- **Kinetic control**, in which case the choice of solvent is important
- **Thermodynamic control**, in which case the choice of solvent is not relevant

The results of the solvent screening experiments of phenylbutazone; (Table 14), indicate that the polymorphic outcomes is more dependent upon the choice of solvent than the temperature at which crystallization is carried out. This suggests that the mechanism of formation of polymorphs of this substance is under kinetic control. More detailed experiments involving phenylbutazone's crystallization behaviour in a particular solvent are presented in the following section.

#### 4.4.2 Observed Crystallization Behaviour of Phenylbutazone

A recent study concerning the crystallization behaviour of phenylbutazone under conditions of supersaturation, [98], was carried out at the University of Minnesota. In these experiments, conducted on methanol solutions of phenylbutazone, supersaturated solutions were prepared in scintillation vials at temperatures close to the boiling point of methanol, and then allowed to cool until reaching the desired crystallization temperature, at which temperature they were maintained until crystallization had completed. The degree of supersaturation is defined as the ratio of actual supersaturation concentration to the saturation concentration.

The prevalent crystallization outcome is formation of the alpha or delta form or a mixture of the two. Datta and Grant point out the marked tendency of formation of the delta form at very high levels of supersaturation above a certain temperature. The results of that study are shown in the following table.

**Table 15 - Polymorphic Crystallization Outcomes – Datta & Grant, 2005**

Supersaturation Degree	1.5	2.0	2.5	3.5	5.0	7.0
Temperature (°C)						
-20	$\alpha$	$\alpha$	$\alpha$	$\beta + \delta$	$\beta$	$\beta$
4	$\alpha$	$\delta$	$\alpha + \delta$	$\alpha + \delta$	$\alpha$	$\alpha$
12	$\alpha$	$\alpha$	$\alpha$	$\alpha$	$\alpha + \delta$	$\delta$
20	$\alpha$	$\alpha + \delta$	$\alpha + \delta$	$\alpha + \delta$	$\delta$	$\delta$
30			$\delta$	$\delta$	$\delta$	$\delta$
40			$\delta$	$\delta$	$\delta$	$\delta$
50				$\delta$	$\delta$	$\delta$

Among the interesting aspects of this study is the finding that at sub-ambient conditions it is possible to encounter formation of the beta form of phenylbutazone during unstirred crystallization; an outcome also encountered by Kaneniwa *et al.*, [27].

Efforts to reproduce the formation of the pure delta form via the preparation of supersaturated solutions during the course of this investigation were not successful, owing primarily to the difficulty of achieving stable solutions with the high levels of supersaturation indicated.

Nucleation tended to occur spontaneously and crystallization would then progress to completion in the space of only a few minutes, yielding either pure alpha form or concomitant alpha/delta mixtures.

#### **4.4.3 Preparation of Pure Phenylbutazone Polymorphs**

The methods used to obtain pure polymorph samples are given in the following sub-sections.

##### **4.4.3.1 Alpha Form**

The use of ketone solvents typically resulted in formation of the pure alpha form.

Concomitant alpha/delta mixtures were nonetheless encountered on occasion; upon recrystallization in ketone solvent, these mixtures were converted to pure alpha form. Similar results were obtained using ester solvents.

##### **4.4.3.2 Delta Form**

Reliable solvent-mediated formation of the delta polymorph, the most stable polymorph, was an elusive goal. The most promising solvent was toluene, from which pure delta form was crystallized on more than one occasion. However repeated crystallizations from toluene at differing start temperatures most frequently resulted in the formation of concomitant alpha/delta mixtures. When a small amount of unsaturated toluene solution was crystallized

in a glass container, pure delta polymorph was obtained with some reproducibility; in most but not all cases a film of delta form was deposited on the floor of the container. By contrast pure delta form was obtained with complete reliability by heating of the solid alpha or beta forms at a temperature above their respective transition temperatures; (Section 5.2.1).

Efforts to obtain pure delta form under the conditions described by Tuladhar using n-heptane as crystallization solvent were not successful.

#### **4.4.3.3 Beta Form**

As outlined in Section 1.3.3, the beta polymorph was formed without the use of stirring in only one set of experiments. When using the solvent methyl-tertiary-butylether traces of the beta form occurred in a bloom that formed around the edge of the evaporation dish; the centre of the dish contained the alpha and/or delta polymorphs. This occurrence may be regarded as a case where Ostwald's Rule of Stages is obeyed; i.e. a crystallization event does not lead to the formation of the most stable polymorph, but rather to the polymorph, whose formation is accompanied by the smallest loss in free energy.

The formation of the beta form from warmed methanol solutions using water as antisolvent often yielded beta form in concentrations of 90% or higher. In this technique the formation of the beta form is favoured by the use of water-soluble solvents such as alcohols, which remain in a homogeneous mixture with water, while precipitation of the solute is taking place.

The results of a battery of control experiments intended to isolate the conditions, under which pure beta polymorph is formed, were less than conclusive. Raising the temperature, to which the methanol solution was heated, prior to precipitation of the phenylbutazone with water, did not lead to a clear pattern. Variations in the ratio of water to methanol had a more pronounced effect. These results are presented in the following table:

**Table 16 - Crystallization Outcomes of Stirred Methanol/Water Solution Experiments**

Batch	Precipitation Temperature	Methanol/Water Ratio	Outcome
1	55	1:1.25	Pure Beta
2	55	1:2.5	Pure Delta
3	55	1:5	Pure Beta
4	45	1:2.5	Pure Delta
5	62	1:2.5	Mostly Beta; <5% Delta

## 5 Transitions of Polymorphs and Solvates

### 5.1 *Predicting Transitions*

Transitions between polymorphs have been examined in detail for many materials, particularly in the context of studies of storage stability. In certain cases transitions occur at temperatures close to those of typical storage conditions, thereby raising the possibility that a delivery form may actually change partially or completely from the manufactured polymorphic form(s) to a different polymorphic form(s) along the supply chain.

A frequently cited example is that of the pharmaceutical, chloramphenicol palmitate, a material that undergoes solid-state transition; i.e. transition does not involve a melting event. A polymorphic transition occurs at around 340K, [99], and the various polymorphic forms display differing bioactivities.

Less frequently encountered are transitions, in which melting plays a role, [42]. In these cases a particular polymorph enters the liquid phase, from which a different form solidifies; a form exhibiting a higher melting point.

The majority of polymorph transitions are irreversible, but examples of reversible changes are mentioned in the literature. Desolvation events represent still another class of transition; these are generally irreversible also.

The existence of solid-state polymorphic transitions has been documented most extensively by Burger and Ramberger, [25, 100], and is implied in the thermodynamic treatment of polymorphic phases presented by Bernstein among others. But to what extent can thermodynamic properties of a polymorphic molecule actually enable the temperature of transition between polymorphs to be predicted?

Derivations of a thermodynamic model to predict the temperature, at which polymorphic transition occurs, typically start from the Helmholtz relationship; (Equation 23). For a molecule with two polymorphic forms A and B at temperature, T:

$$G_A = H_A - T S_A$$

$$G_B = H_B - T S_B$$

At the temperature of transition,  $T_{trans}$ , where polymorph A transforms to polymorph B, the free energies of the two polymorphs are assumed to be equal; i.e.  $\Delta G_{A \rightarrow B} = 0$  and the two equations above may be added to give the following expression:

$$0 = \Delta G_{A \rightarrow B} = \Delta H_{A \rightarrow B} - T_{trans} \Delta S_{A \rightarrow B}$$

The quantity  $\Delta G_{A \rightarrow B}$  has been widely estimated by considering the thermodynamic behaviour of the two polymorphs in solution, using measured solubility data in a particular solvent at the transition temperature,  $T_{trans}$ . When a pair of polymorphs is equally soluble, the polymorphs share the same free energy,  $G$ , and, at this temperature, solid-state transition between the two forms may be expected to occur. For such a transition the following relationship is derived from Equation 22:

### Equation 33 - Gibbs Free Energy Change for Polymorphic Transition

$$\Delta G_{A \rightarrow B} = RT_{trans} \ln \left( \frac{Sol_A}{Sol_B} \right)_{T_{trans}}$$

Where:

$R$  = The gas constant

$T_{trans}$  = Temperature of polymorphic transition, A  $\rightarrow$  B

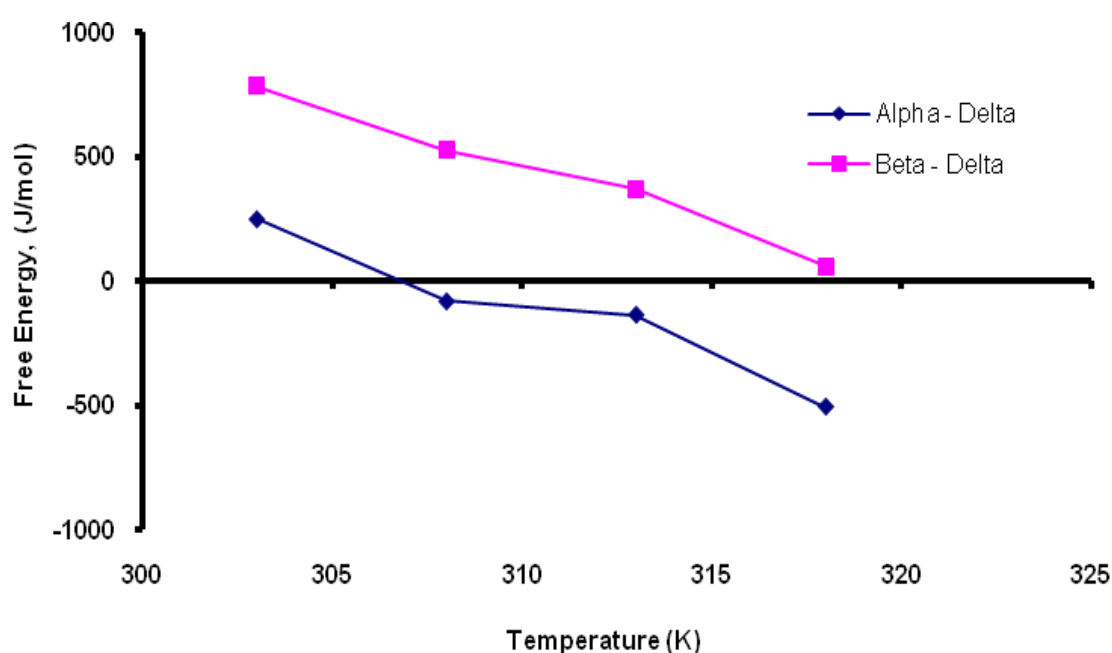
$(Sol_A)_{trans}$  = Solubility of polymorph A at transition temperature,  $T_{trans}$

$(Sol_B)_{trans}$  = Solubility of polymorph B at transition temperature,  $T_{trans}$

Evidently this method of calculating the transition temperature is most readily applied in cases where solubility data for individual polymorphs have been collected at several temperatures, and where the resulting solubility curves show an intersection. Gu and Grant recommend the use of dissolution rate values as an alternative to solubility values, [101].

For phenylbutazone both solubility and dissolution rate have been measured across a range of different temperatures in a variety of different solvents; (Section 4.2.3). Instances of solubility curves intersecting for the polymorphs are rare, but one example occurs in the measurements made by Kaneniwa *et al.*, [27]. Using these solubility values, plots of  $\Delta G$  vs. temperature have been prepared for both  $\Delta G_{\alpha \rightarrow \delta}$  and  $\Delta G_{\beta \rightarrow \delta}$ . These are shown in the following figure:

**Figure 45 - Free Energy Change vs. Temperature for Alpha-Delta and Beta-Delta Transitions**





According to this methodology, the transition from the alpha to the delta form is predicted to occur at about 307K. The transition of the beta to the delta form does not occur in the temperature range of dissolution measurements carried out by Kaneniwa *et al.*, however the trend in the lower temperature readings suggest that transition would be predicted to occur at about 320K (47°C).

Other groups have developed modified methods to calculate the transition temperature using solubility data:

i. **Urakami *et al.***, [102], derive an expression for the transition temperature,  $T_{trans}$ , using the solubility ratio for the two polymorphs at only one measurement temperature,  $T_1$ . In this approach the free energy difference between polymorph A and B,  $\Delta G_{A-B}$ , is calculated at the selected temperature  $T_1$ , however knowledge of the enthalpy of transition is required:

$$T_{trans} = \left[ \frac{[\Delta G_{A-B}]_{T_1}}{T_1 \Delta H_{trans}} + 1/T_1 \right]^{-1}$$

$$\Delta G_{A-B} = RT_1 \ln \left( \frac{Sol_A}{Sol_B} \right)_{T_1}$$

This yields the following expression for  $T_{trans}$ :

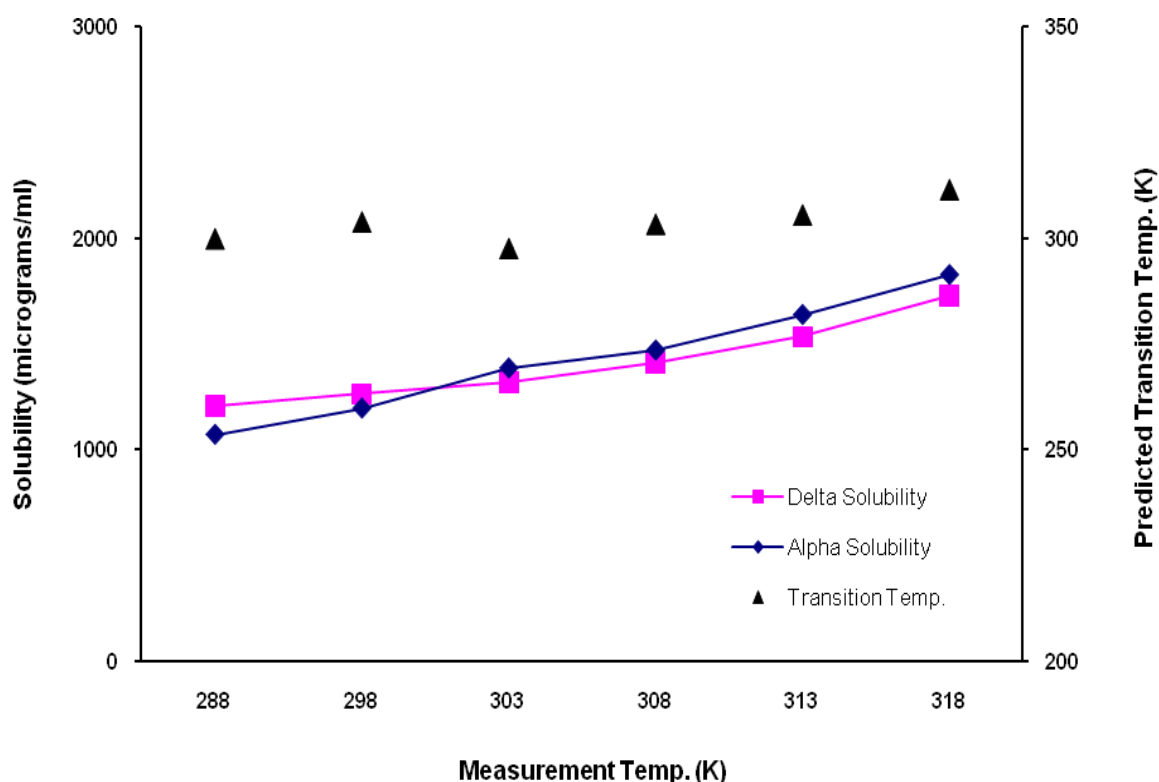
**Equation 34 - Transition Temperature Calculation after Urakami *et al.***

$$T_{trans} = \left[ \frac{R \ln \left( \frac{Sol_A}{Sol_B} \right)_{T_1}}{\Delta H_{trans}} + 1/T_1 \right]^{-1}$$

This method allows tabulated solubility ratios between polymorphs such as the values compiled by Pudipeddi *et al.*, [91], to be employed directly.

Again the solubility data in buffer solution measured by Kaneniwa *et al.* have been used to calculate the actual solubility ratio at a range of different temperatures. These solubility pairs for the polymorphs at each of the measurement temperatures are plotted in the following figure, together with the predicted transition temperature obtained from each pair of solubility values. Evidently this method does not rely on an intersection of the measured solubilities for the two polymorphs.

**Figure 46 - Solubility & Predicted Transition Temp. Vs Measurement Temp.**



ii. **Gu and Grant**, [101], modify the technique of estimation of  $\Delta G$  from solubility values by introducing the enthalpy of solution of polymorph A and B at the same temperature,  $T$ , in the same solvent; the enthalpy of transition is not employed:

$$\Delta S = (\Delta H - \Delta G) / T$$

The enthalpy term is then expressed as  $\Delta H_{sol_A} - \Delta H_{sol_B}$ , so that:

$$\Delta S_{B-A} = \left( \Delta H_{sol_A} - \Delta H_{sol_B} \right) - \Delta G_{B-A} / T$$

At the transition temperature,  $T_{trans}$ , the free energy is zero, and therefore:

$$\Delta S_{B-A} = \left( \Delta H_{sol_A} - \Delta H_{sol_B} \right) / T_{trans}$$

Rearranging:

$$T_{trans} = \left( \Delta H_{sol_A} - \Delta H_{sol_B} \right) / \Delta S_{B-A}$$

Substituting out the entropy term:

$$T_{trans} = \frac{\left( \Delta H_{sol_A} - \Delta H_{sol_B} \right)}{\left( \Delta H_{sol_A} - \Delta H_{sol_B} \right) - \Delta G / T}$$

Gu and Grant then replace the free energy term by the solubility ratio expression discussed earlier to give:

#### Equation 35 - Transition Temperature Calculation after Gu & Grant

$$T_{trans} = \frac{\left( \Delta H_{sol_A} - \Delta H_{sol_B} \right)}{\frac{\left( \Delta H_{sol_A} - \Delta H_{sol_B} \right)}{T} - R \ln \frac{Sol_B}{Sol_A}}$$

Using this expression<sup>25</sup> together with the heat of solution and solubility values presented by Kaneniwa *et al.* for the transition from form alpha to form delta of phenylbutazone, the transition temperature,  $T_{trans}$ , is calculated to be 369K.

---

<sup>25</sup> Reference temperature is 298K.

## 5.2 Measurement of Transitions

The storage stability of phenylbutazone's polymorphs has been examined over extended periods by Matsuda *et al.*, [24], who report no signs of transitions between polymorphs at room temperature over the course of several years. At temperatures above 40°C, however, the same group indicates that the beta and alpha forms change gradually to the delta form over a period of several months. These transitions are accelerated by the presence of atmospheric humidity.

Other groups confirm changes in form based upon DSC scans of the individual polymorphs; e.g. Müller, [18]. Endotherms that do not correspond to the main melting event are readily apparent on DSC scans of the alpha and beta forms of phenylbutazone carried out in-house on the Netzsch Jupiter<sup>®</sup>. To shed light on the transition behaviour of phenylbutazone's polymorphs and solvates, three types of experiment were undertaken:

- a) **Room Temperature Storage** - Long-term stability at room temperature was tested by repeated PXRD scans at intervals of a couple of months. Lozenge shaped samples, with one face open to the atmosphere, were stored in a large bell jar maintained at room temperature.
  
- b) **Isothermal Heating** – Powder samples were heated isothermally in an oven for periods of a number of hours, and then returned to sample holders, and re-examined by PXRD to ascertain whether a transition had occurred. The heating temperature was set a little below the melting temperature; prior DSC scans also provided indications of suitable temperature levels.

c) **Stepped Heating, *in situ* PXRD Scans** - Collection of PXRD patterns was conducted in sequence at temperatures up to the melting event, using a nitrogen stream for both heating and cooling. Polymorphs were examined in sealed capillaries, whereas solvates were examined in open capillaries to allow the solvent to escape. Thanks to the use of the wide-angle detector, it was possible to complete PXRD scans across an adequate 2theta range in time periods of 10-20 minutes. The temperature of the capillary was then increased incrementally, and allowed to stabilize at the new set point, involving the elapse of a matter of minutes, before the sample was rescanned. In certain cases the sample was recooled to check for reversible form changes. Low temperature measurements were also undertaken in search of sub-ambient temperature transitions.

## **5.2.1 Results for Polymorphs**

### **5.2.1.1 Room Temperature Storage**

No change was observed in the polymorphic composition of the alpha, beta or delta forms of phenylbutazone over a period of six months or more. This concurs with the findings presented in the kinetic study of Matsuda *et al.*.

### **5.2.1.2 Isothermal Heating**

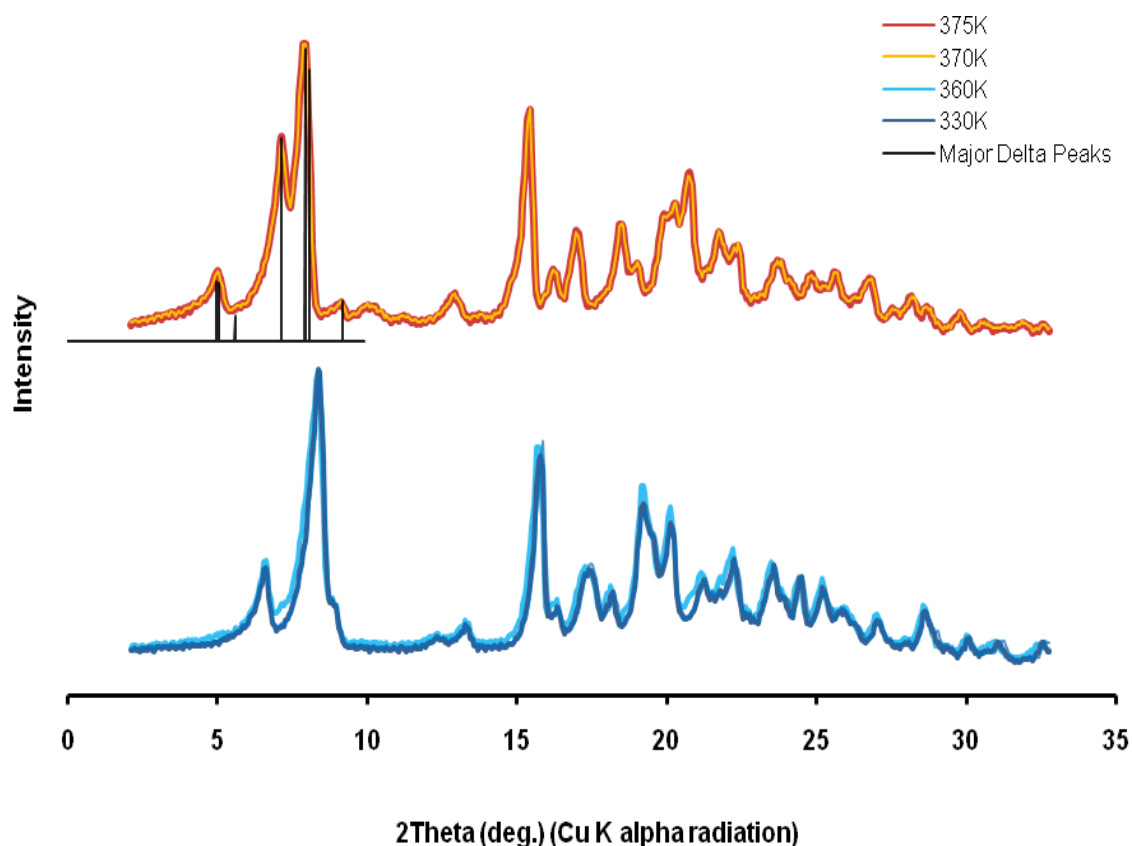
No change in the delta form PXRD pattern was apparent subsequent to the heating cycle. In the cases of the alpha and beta forms, a complete transition to the delta form occurred after heating at a temperature above the transition temperature within the space of an hour. No remaining traces of alpha and beta peaks are apparent in the respective PXRD patterns after the transition has taken place.

### 5.2.1.3 Stepped Heating, *in situ* PXRD Scans

For the alpha and beta polymorphs, complete transition to the delta form took place within the time frame of the temperature increase and equilibration steps. In both cases, the temperature at which transition occurred, matched the temperature of the observed non-melting endotherm in the corresponding DSC scan. The sequences of PXRD patterns are shown in the following figures.

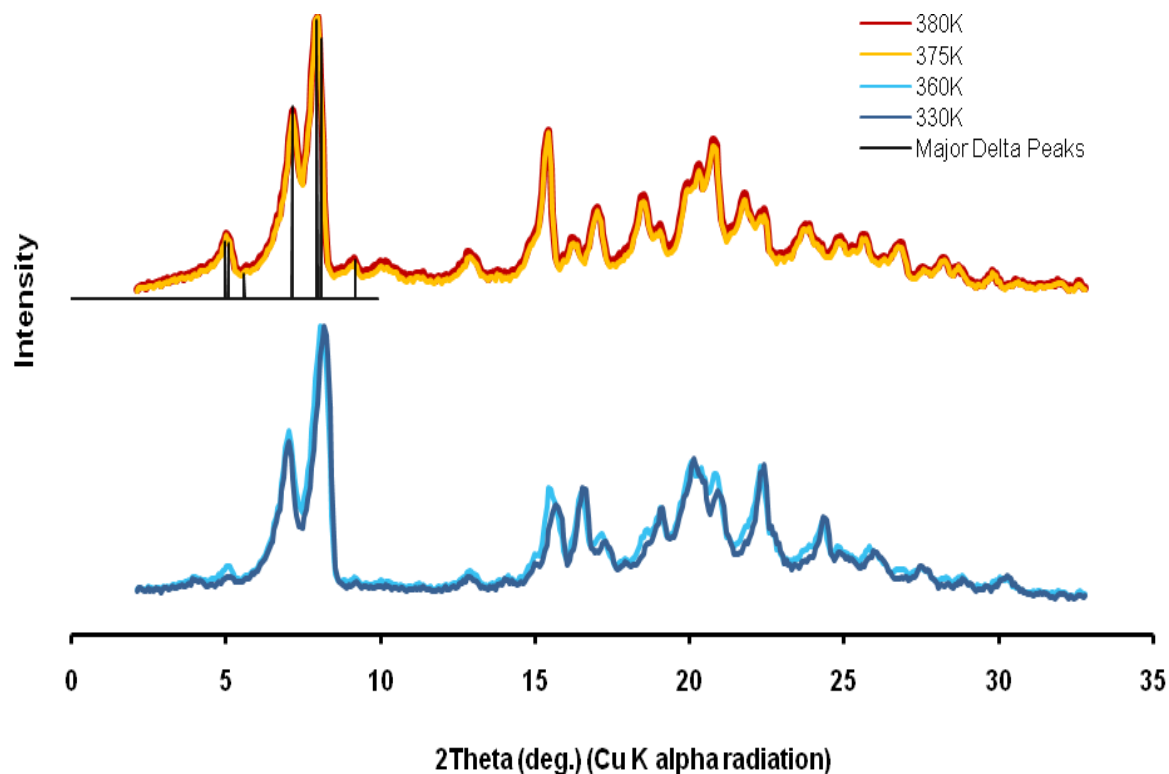
For both the alpha-delta and beta-delta transitions, subsequent to transition, the samples were recooled to below the transition temperature. In neither case was a reversion to the original polymorphic form found to take place.

**Figure 47 - PXRD Patterns of Alpha Form at Stepped Temperatures<sup>26</sup>**



<sup>26</sup> Post-transition patterns have been offset to improve visual clarity in many of the figures in this section

**Figure 48 - PXRD Patterns of Beta Form at Stepped Temperatures**



## 5.2.2 Results for Solvates

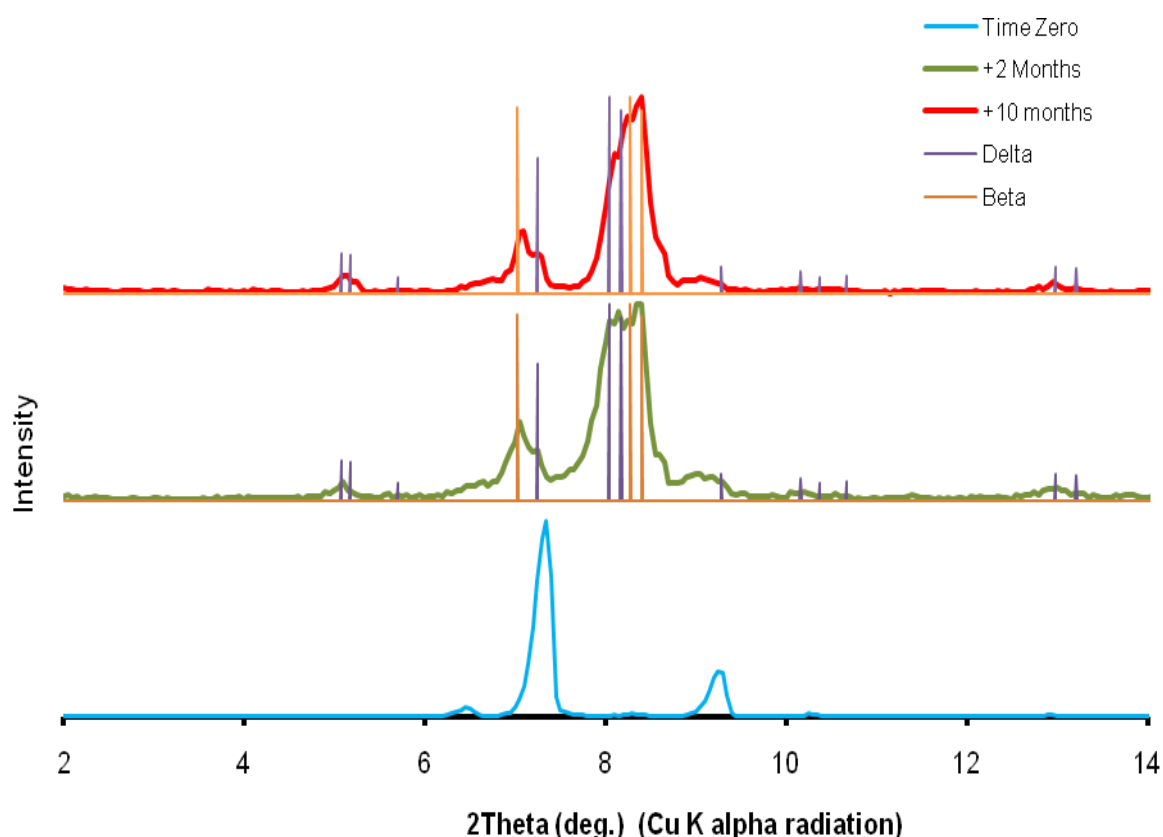
Apart from the sealing of capillaries for the collection of stepped temperature PXRD patterns, the procedures employed for the solvate samples were identical to those for the polymorphic forms.

### 5.2.2.1 Room Temperature Storage

Changes in crystal form were observed in certain of the solvates over a period of six months or less. Among the solvates that did exhibit changes, transitions gave rise to a mixture of known polymorphs; decomposition typically occurring from one measurement to the next with few major changes, if any, being observed in later PXRD patterns.

This behaviour is apparent in the series of PXRD patterns collected over a ten month period from a sample of the solvate with tetrahydrofuran, (b.p. 66°C). A transition of the solvate to a mixture of the beta and delta forms is observed to take place; the transition is largely complete within the period of a month.

**Figure 49 - Decomposition of Tetrahydrofuran Solvate over Time**

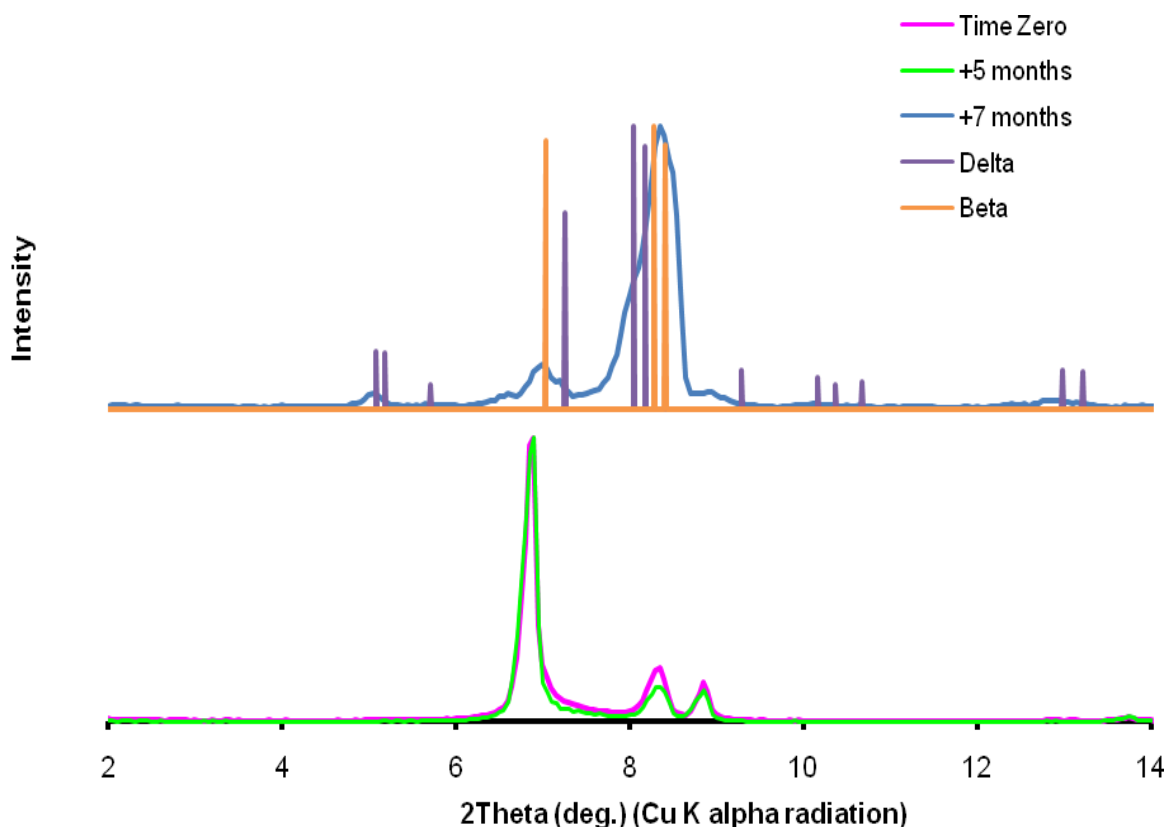


Transitions were also observed among other solvates formed with low-boiling solvents after periods of room temperature storage. Repetition of certain of these stability tests indicates that the period of decomposition of individual solvates is not constant. In one example, the solvate formed with methyl-tertiary-butylether, a transition took place in time periods of as little as one week, while in a few instances, batches of the same solvate remained unchanged for periods of several months, even when stored in an open sample container.



PXRD patterns of a specimen of the methyl-tertiary-butylether solvate collected over the course of 7 months are shown below; an amount of the solvate is evidently still contained in the decomposition product.

**Figure 50 - Decomposition of Methyl-tertiary-butylether Solvate over Time**

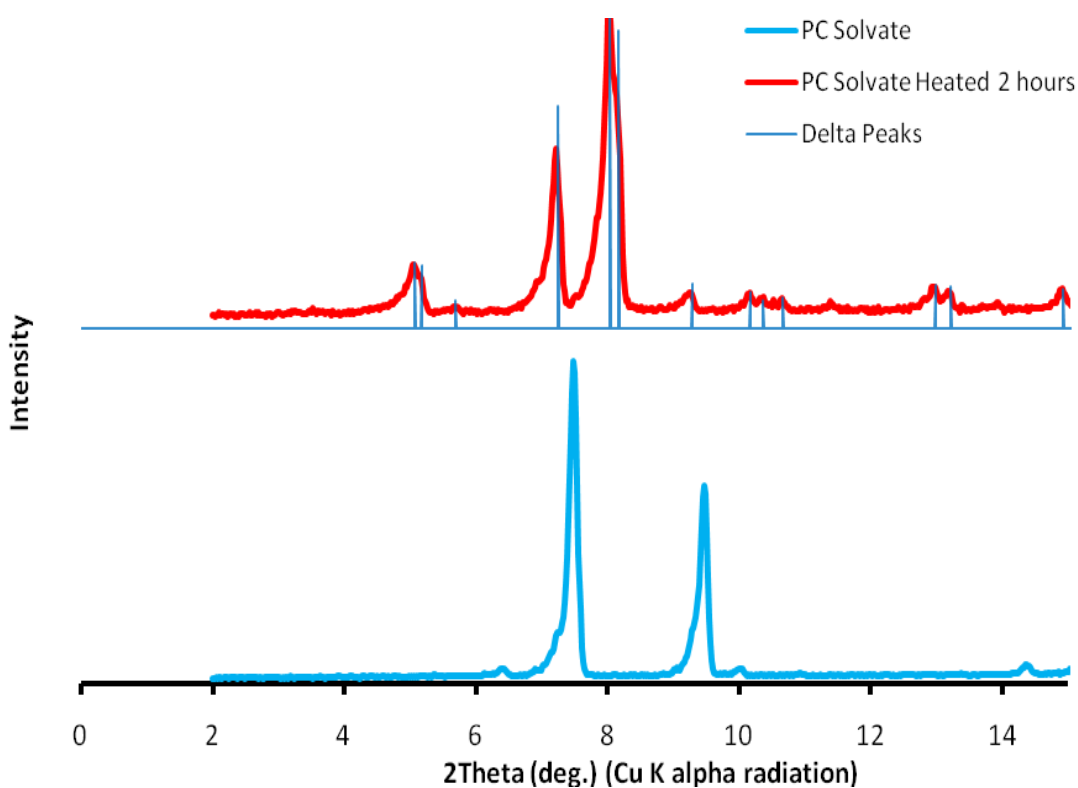


The solvate with cyclohexanone (b.p.156°C) was also tested, and was found to be unchanged after several months of storage. Similar behavior is presumed for the solvates with cyclopentanone and propylene carbonate, which also have boiling points well above the melting temperature of phenylbutazone.

### 5.2.2.2 Isothermal Heating

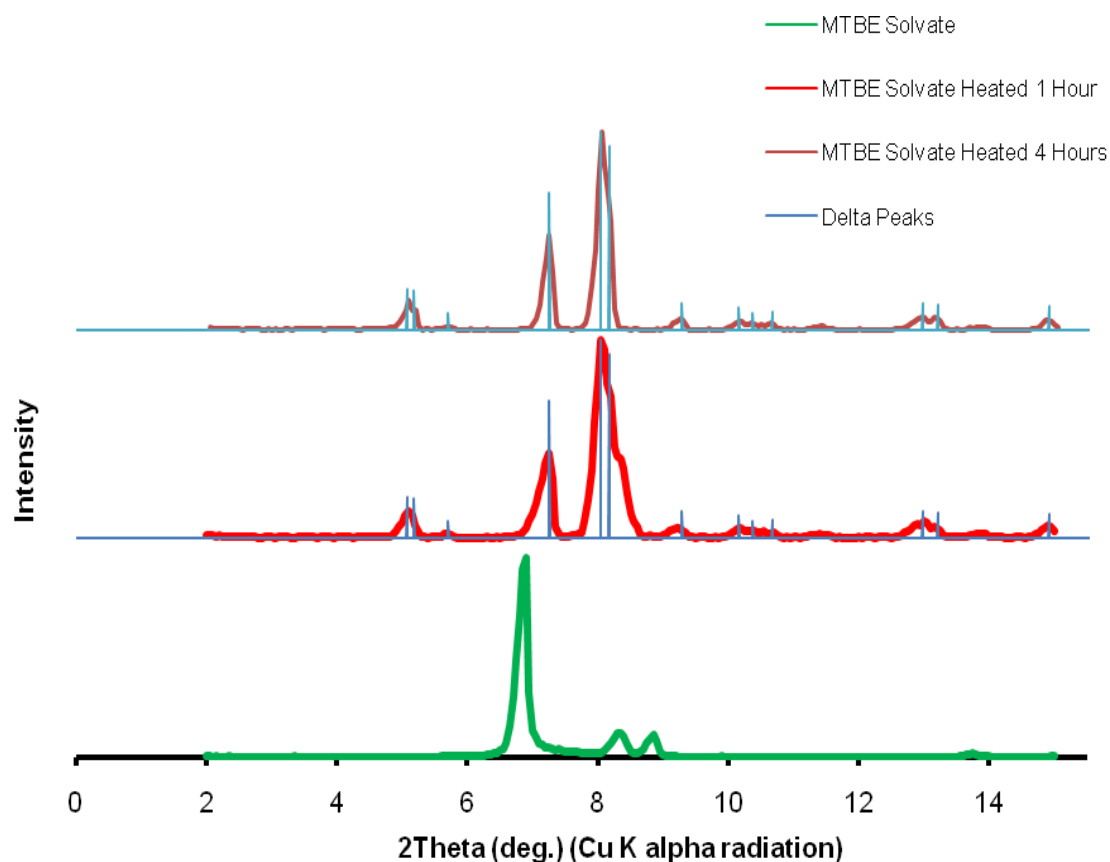
The solvates with cyclohexanone (b.p. 156°C) and with propylene carbonate (b.p. 240°C) undergo complete transition to the delta form after 2 hours of heating at 90°C. For the propylene carbonate solvate, the patterns before and after heating are shown below.

**Figure 51 - PXRD Patterns of Propylene Carbonate Solvate before & after Heating**



A sample of the solvate with methyl-tertiary-butylether was heated isothermally at 90°C. After an hour there is no sign of the major solvate peaks, however there is a visible shoulder in the delta peak at  $2\theta = 8.15^\circ$ , suggesting that another form is present; its position,  $2\theta = 8.3^\circ$ , matches the largest peak position of the beta form. After two hours of heating, the peak shoulder has disappeared. The sequence of patterns is shown in the figure overleaf.

**Figure 52 - PXRD Patterns of MTBE Solvate before & after Heating**



### 5.2.2.3 *In situ* PXRD of Solvates at Elevated Temperatures

There was no indication of the emergence of intermediate phases or polymorph mixtures in the stepped heating experiments conducted on phenylbutazone's solvates.

In the case of the tetrahydrofuran solvate, complete transition to the delta form took place in a single temperature increase interval. Whereas for the solvate with cyclohexanone changes in the PXRD pattern were observed as the melting point of the solvate was approached; the solvate's melting point was found to be a little below the melting temperature of pure phenylbutazone. These results are presented in the figures displayed overleaf.

**Figure 53 - PXRD Patterns of Tetrahydrofuran Solvate up to Transition to Delta Form**

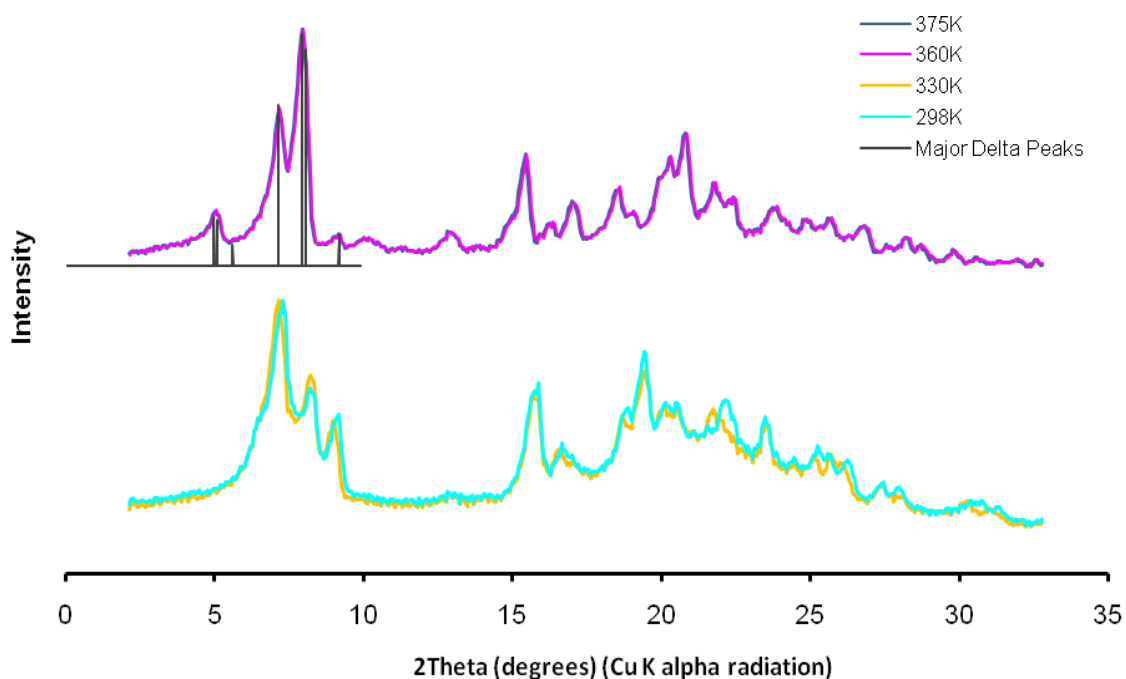
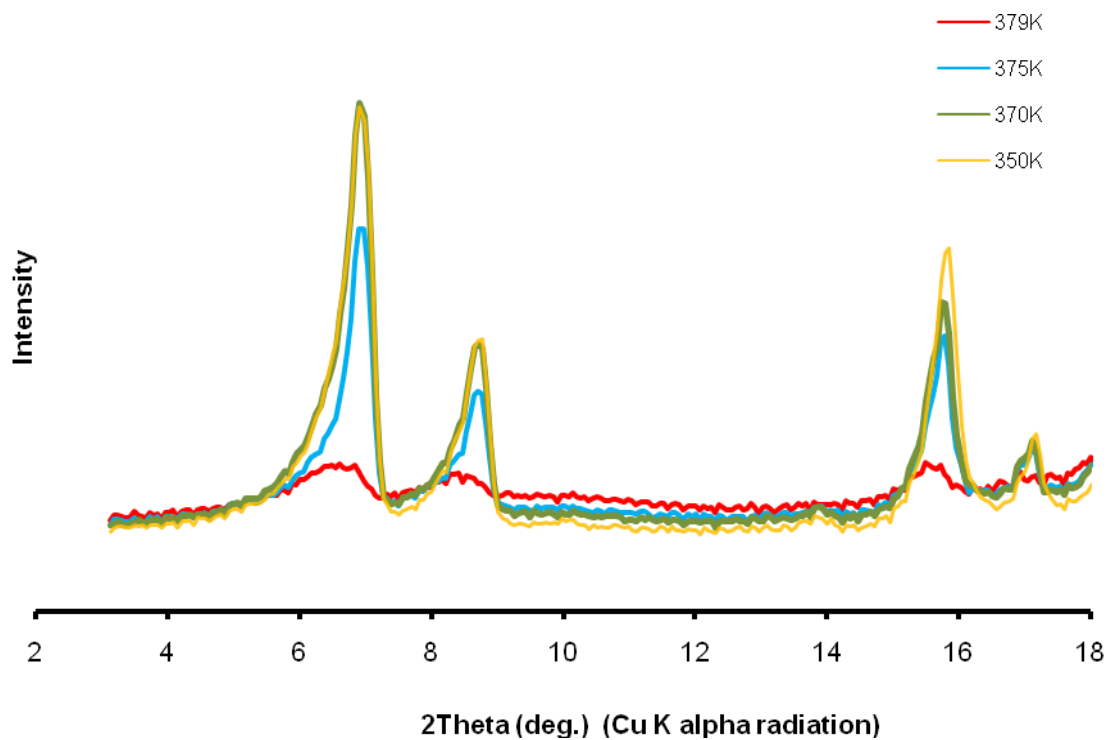


**Figure 54 - PXRD Patterns of Cyclohexanone Solvate up to Melting Temperature**



### 5.3 Kinetic Considerations

Carstensen, [90], postulates that polymorphic transitions may be divided into four classes of mechanism:

- a) Probability of transition of individual molecules is independent; the fraction converted to the end product increases linearly from 0 to 1 over time.
- b) The rate of transition is proportional to the amount of the starting form that has not yet changed form up to extinction of the start material.
- c) The rate of nucleation of the new form changes over time<sup>27</sup> (in addition to the extinction of start material characterized in class b).
- d) The above factors apply, and the geometry of nucleation events is taken into account; diffusion effects may also be considered.

The extent of conversion of the start product into the end product is expressed in a proportional range between zero and one; typically designated by the Greek letter alpha, [103]. For transitions of crystal forms occurring in the solid state, in which species X changes into species Y upon heating,  $\alpha$  is commonly determined by the following techniques:

- DSC - enthalpy flow is integrated over time; conversion is equivalent to the ratio of the integral enthalpy input to the total enthalpy input of the transition.
- TGA - weight loss over time as a proportion of total weight loss is calculated.
- PXRD - peak intensity changes are used to calculate actual polymorph concentrations at each point of the transition.

---

<sup>27</sup> Galwey and Brown introduce five different types of nucleation mechanism each with its own expression for the rate of nucleation, namely: exponential, linear, instantaneous, power and branching.

While the first two methods provide only an analogue of the concentration, the use of PXRD enables actual concentration values to be measured using conventional quantitative PXRD methods, [104-107]. Unlike thermal analysis, PXRD also provides explicit confirmation of the species present, and reveals the emergence of any intermediate phases.

Examples of the use of powder X-ray diffraction to follow polymorphic transition events are less common, not least because of the inherent complication of the extended counting time required to collect a diffraction pattern over an adequate range of  $2\theta$ .

Using in-house diffraction equipment, the shortest measurement interval for a complete  $2\theta$  range is the 5-10 minute scan time of the wide angle detector available for use with the transmission geometry diffractometer. For materials such as phenylbutazone, which change form within the space of a few minutes, this represents a limitation. Studies of this nature have mostly been carried out on synchrotron beam lines with detection apparatus capable of recording a complete diffraction pattern in a minute or less, [108, 109].

Clearly thermogravimetric analysis is suitable only in those instances, where the transition under study is associated with a change in weight; e.g. desolvation or certain chemical reactions. DSC is the most frequently encountered method.

Once a set of conversion data has been obtained, it may be used to identify the kinetic rate expression for the transition under examination. In “model-fitting” techniques, which are summarized by Khawam and Flanagan, [110], among others, [111], the general form of the kinetic rate expression combines the terms of the Arrhenius equation for the rate constant,  $k$ ; (Equation 32), with a rate function,  $f(\alpha)$ , which can be shown to fit the conversion curve of the transition under investigation. The general form of the reaction rate equation may then be expressed as follows:

### Equation 36 - Generalized Reaction Rate Equation

$$\frac{d\alpha}{dt} = f(\alpha)Ae^{-E/RT}$$

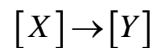
Where:

$\alpha$  = Proportional conversion to end product

$t$  = Time from start of transition

$f(\alpha)$  = Rate function that fits observed conversion of the reaction components

For the case of constant nucleation with extinction of start material described earlier, the general form of the function for the change of species one, X, into species two, Y, is described in mathematical terms as follows:



Where:

$X$  = Moles of species one

$Y$  = Moles of species two

$[X]$  = Molar fraction of species one

$[Y]$  = Molar fraction of species two

Taking into account that complete extinction may not occur, the start and end mass balance expressed in absolute molar terms is as follows:

Start:  $X_0 + Y_0 = \text{constant}$

End:  $X_{end} + Y_{end} = \text{constant}$

And:  $X_0 + Y_0 = X_{end} + Y_{end}$

Expressed in proportional terms:

Start:  $[X]_0 + [Y]_0 = 1$

End:  $[X]_{end} + [Y]_{end} = 1$

And:  $[X]_0 + [Y]_0 = [X]_{end} + [Y]_{end}$

The mass balance at any point in the transition is simply:

$$[X] + [Y] = 1$$

For the general case, the conversion of species one into species two is given by:

$$\alpha = \frac{Y - Y_0}{Y_{end} - Y_0}$$

If complete transition to the end product  $Y$  takes place from zero start concentration, then  $Y_0$  equals zero, and the expression above simplifies to:

$$\alpha = \frac{Y}{Y_{end}}$$

Expressed proportionally:  $\alpha = [Y]$

Assuming that complete conversion occurs,  $Y_{end} = X_0$ , and the rate at which transition occurs is directly proportional to the proportion of start material that is present; the highest rate of transition is at the start of the transition and declines for the duration of the transition, until  $X$  falls to zero.



The rate function may then be expressed as follows:

$$\frac{d\alpha}{dt} = k[X]$$

In proportional terms  $[Y] = 1 - [X]$  so that the rate expression may be re-expressed in terms of only the end-product or the proportional conversion:

$$\frac{d\alpha}{dt} = k(1 - [Y])$$

Or: 
$$\frac{d\alpha}{dt} = k(1 - \alpha)$$

Substituting the rate constant,  $k$ , by the terms of the Arrhenius equation gives:

#### **Equation 37 - First Order Reaction Rate Equation**

$$\frac{d\alpha}{dt} = (1 - \alpha) A e^{\frac{-E}{RT}}$$

This corresponds to a first order “order of reaction” model for the decomposition. Matsuda *et al.*, conclude that the transition of the beta to the delta form follows this kinetic model.

This derivation does not specifically take into account the nature of the nucleation of a given polymorph. Apart from DSC scans, which are shown in the next section, no real-time information is available about the manner in which the alpha and beta forms of phenylbutazone transform to the delta polymorph. Nucleation mechanisms may therefore only be inferred from DSC-based conversion curves.

Hot-stage microscopy is one technique employed to observe polymorphic transitions in order to ascertain how nucleation takes place, however it does not form part of this study.

From hot-stage microscope experiments Bernstein, [1], presents graphical examples of nucleation occurring in polymorph specimens. In these examples nucleation occurs either in a diffuse manner throughout the sample, or at a front that moves through the crystal.

Nucleation by interface advance gives rise to power law rate expressions, [112], as distinct from the “order of reaction” model derived earlier in this section.

As their name suggests, power law models raise the conversion factor,  $\alpha$ , by a power factor; e.g.  $n(\alpha)^{(n-1)/n}$ . They provide a good fit to integral conversion measurements for transitions that accelerate from start to finish.

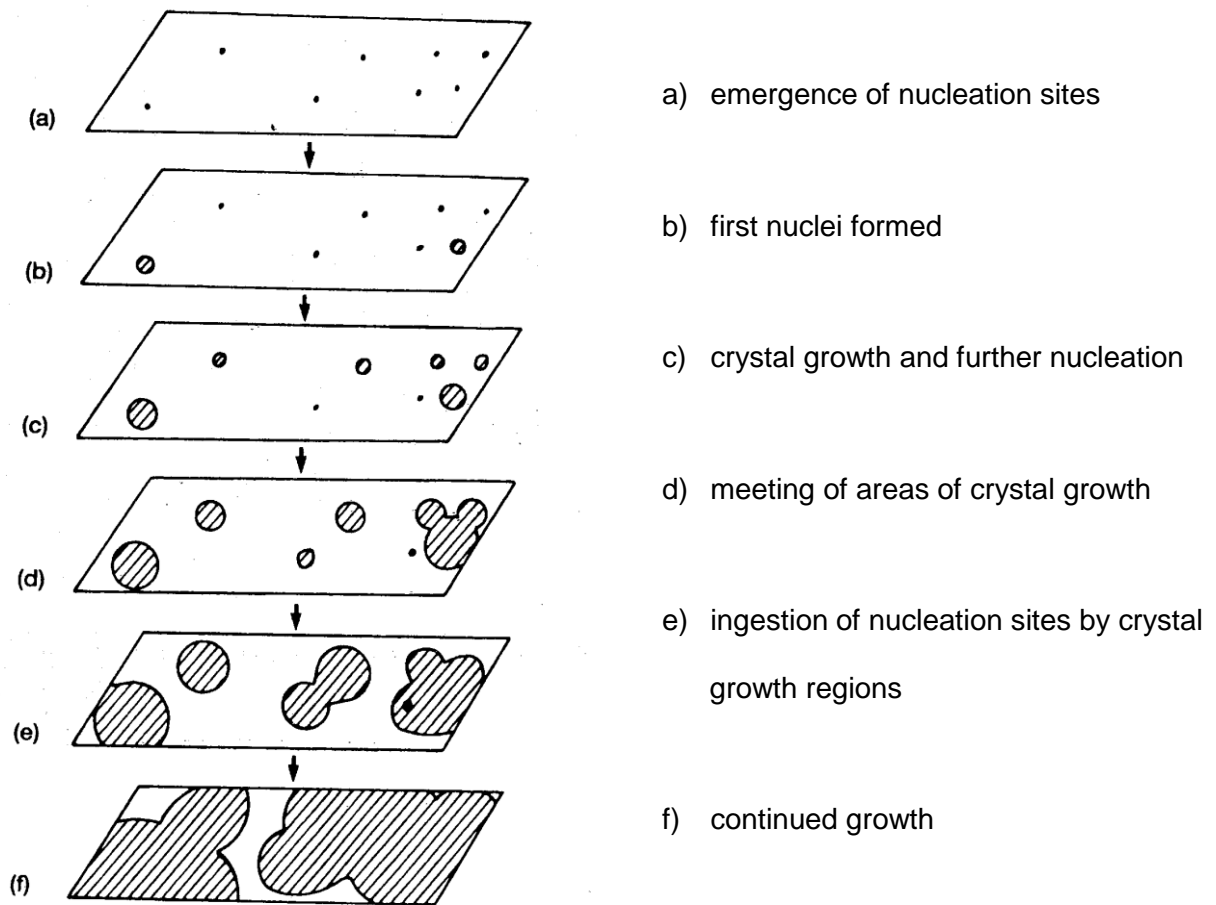
In the case of “order of reaction” models, acceleration of the transition from start to finish does not occur, because the rate of transition is proportional to the amount of start material remaining.

Bernstein identifies two alternative nucleation mechanisms for transitions of this nature:

- Random nucleation throughout the crystal
- Nucleation at specific defects or crystal edges

Brown, [103], identifies six stages in the progress of nucleation and growth across the surface of a material undergoing transition with nucleation initially taking place randomly; these are depicted for the 2-dimensional case in the figure displayed overleaf.

Figure 55 - 2D Nucleation and Growth Model<sup>28</sup>



This sequence gives rise to an acceleratory phase and a deceleratory phase. The following terminology is frequently used to describe these phases:

- “the induction period” at the commencement of the transition
- “the acceleration period” up to the inflection point of the conversion curve
- “the decay period” of slowing conversion until conversion is complete

<sup>28</sup> Reproduced from M.E. Brown, *Introduction to Thermal Analysis*, 2<sup>nd</sup> ed., 2001, Kluwer, Dordrecht, p.184.

For transitions with this mechanism the cumulative conversion follows an S-shaped, “sigmoid” curve such as the one observed for the alpha-delta transition; Figure 57. A fuller derivation of this mechanism is provided by Galwey and Brown among others, [113].

The Prout-Tompkins equation and, more commonly, the Avrami-Erofeev equation (also known as the JMAEK equation) are used to fit sigmoid-shaped conversion curves:

**Equation 38 - “AN” Form of the Avrami-Erofeev Rate Equation**

$$kt = [-\ln(1 - \alpha)]^{1/n}$$

Where n is an integer typically between 2-4.

Whichever method is chosen to follow the progress of the transition under study, the heating programs employed are either:

- Non-isothermal measurements typically along a constant heating gradient
- Isothermal heating at a particular temperature over an extended time period

In this investigation only ramped temperature measurements were carried out, and calculation of the Arrhenius parameters was not undertaken. Accurate evaluation of the kinetic parameters and the reaction order is inherently more difficult in non-isothermal experiments because the rate constant,  $k$ , changes during the course of the transition, owing to its dependence on the measurement temperature; ( Equation 32).

Among techniques for establishing the rate relationship suitable for single experiment sets, The Handbook of Thermal Analysis presents a method which it attributes to Freeman & Carroll, [114, 115]. In this procedure the following equality is plotted, using the axis terms indicated. A line of best fit is then determined for the plotted points.

### Equation 39 - Non-isothermal model fitting function of Freeman & Carroll

$$\Delta \ln(d\alpha/dT) = n \ln(1 - \alpha) - \frac{E_a}{R} \Delta(1/T)$$

From this expression the following terms are obtained for use as the axis coordinates:

$$\frac{\Delta \ln(d\alpha/dT)}{\Delta \ln(1 - \alpha)} \text{ and } \frac{\Delta(1/T)}{\Delta \ln(1 - \alpha)}$$

A good fit between the measurement points and the best fit line confirms that the rate function is indeed of the form;  $f(\alpha) = (1 - \alpha)^n$ . Although this technique requires only a small amount of experimental data, Brown points out that it is not conclusive; a straight line can be indicative of a number of different models including those with power law and Avrami-Erofeev rate equations.

This technique is employed to fit the conversion values for the alpha-delta polymorph transition, which is examined in the following section.

## 5.4 Transitions of Phenylbutazone during Constant Gradient Heating

### 5.4.1 Polymorphs

#### 5.4.1.1 Alpha Form

A DSC scan of a sample of the alpha form, heated in a rising temperature programme at a constant ramp rate of 10K/minute, displays two clear endotherms; see Figure 56.

*In situ* X-ray diffraction experiments explicitly identify the endotherm that commences at approximately 85°C as corresponding to a transition from the alpha form to the delta form. The second endotherm corresponds to the melting event.

**Figure 56 - Alpha Form Transition & Melting Endotherm by DSC**

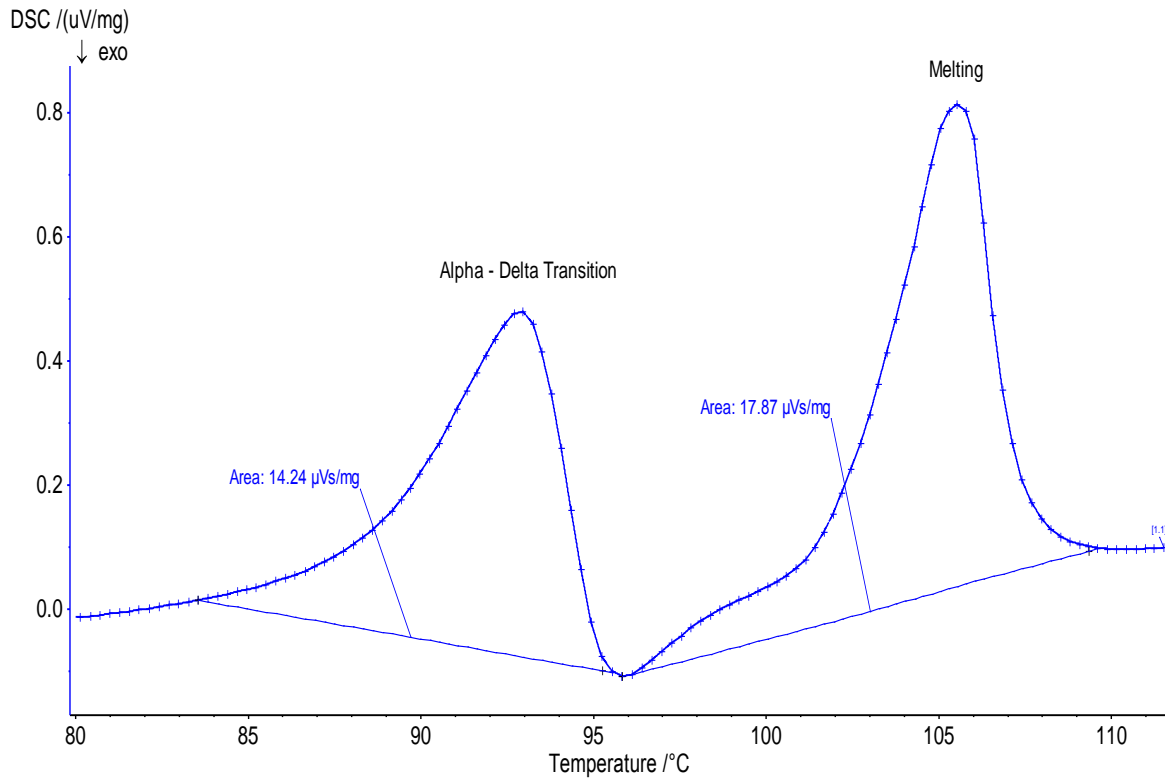
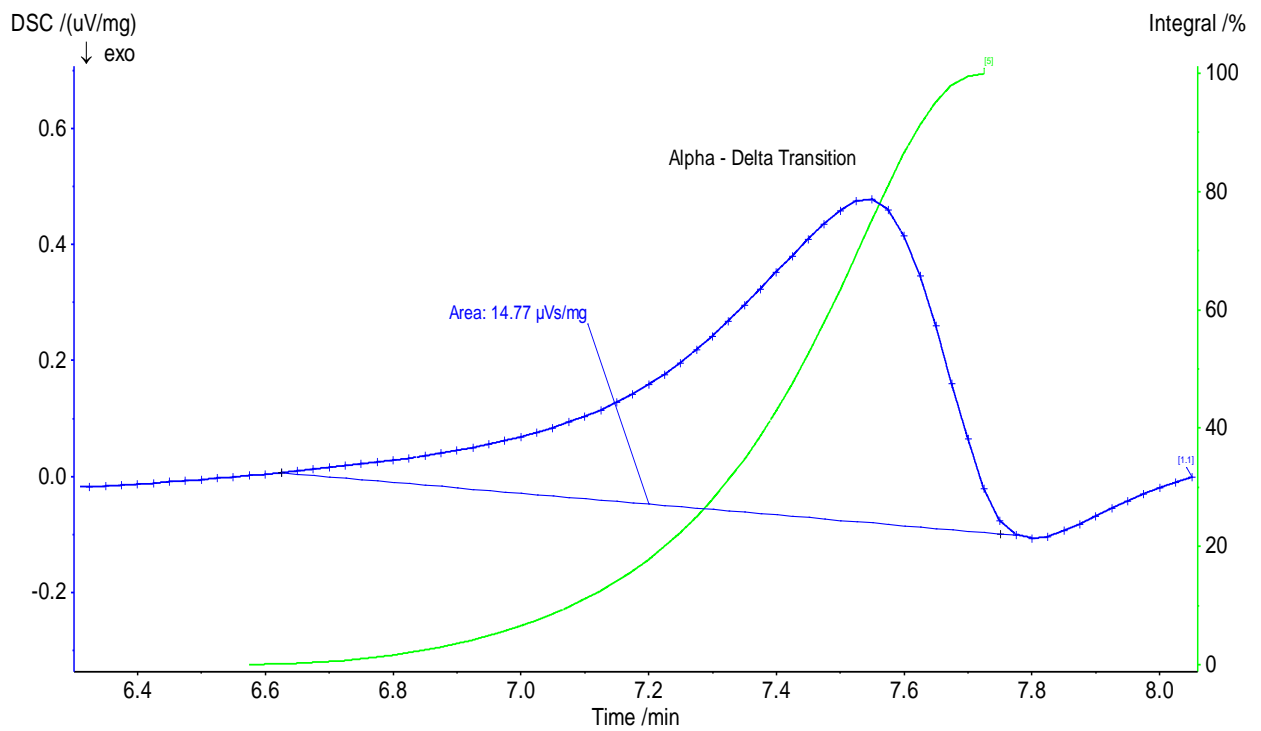


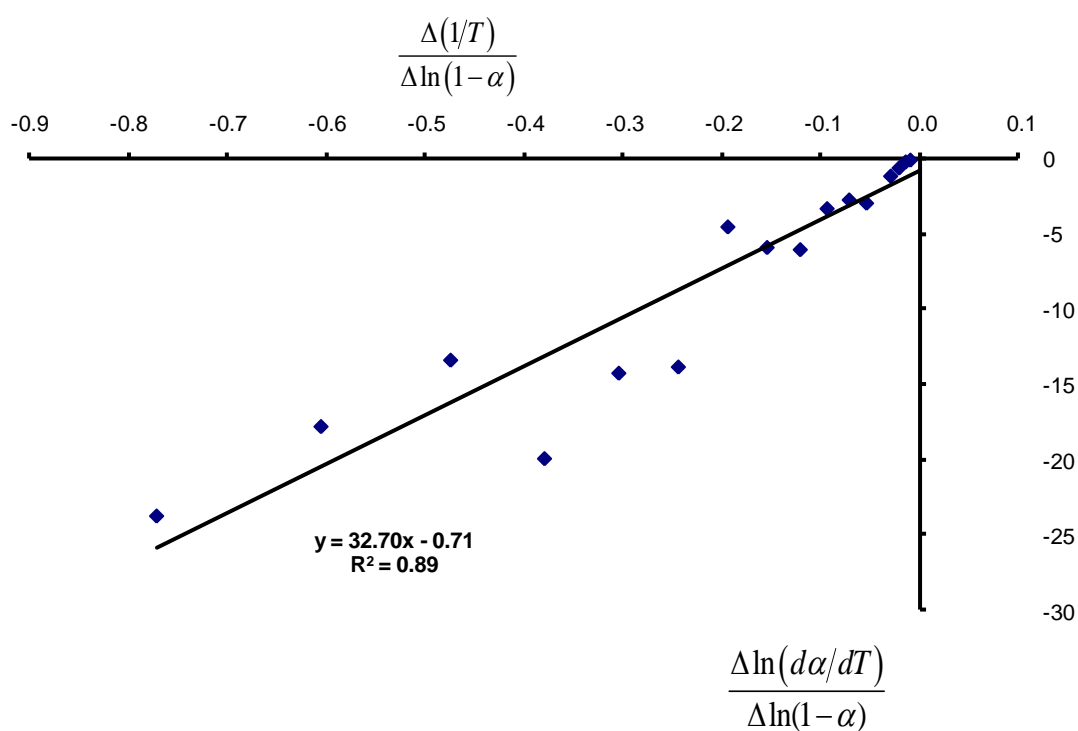
**Figure 57 - Conversion Curve of Alpha-Delta Transition Endotherm**



From the *in situ* X-ray diffraction patterns, it is apparent that all the alpha form is transformed into delta form. The integral enthalpy change across the endotherm over time is therefore taken to be analogous to the proportional conversion,  $\alpha$ , displayed in Figure 57.

The integral conversion plot appears to follow a sigmoid curve. Applying the Freeman & Carroll method described in the preceding section, yields the following plot from the end of the induction period of the transition, whose termination has been arbitrarily fixed at  $\alpha = 1\%$ .

**Figure 58 - Plot of Kinetic Expression of Alpha-Delta Conversion after Freeman Carroll**

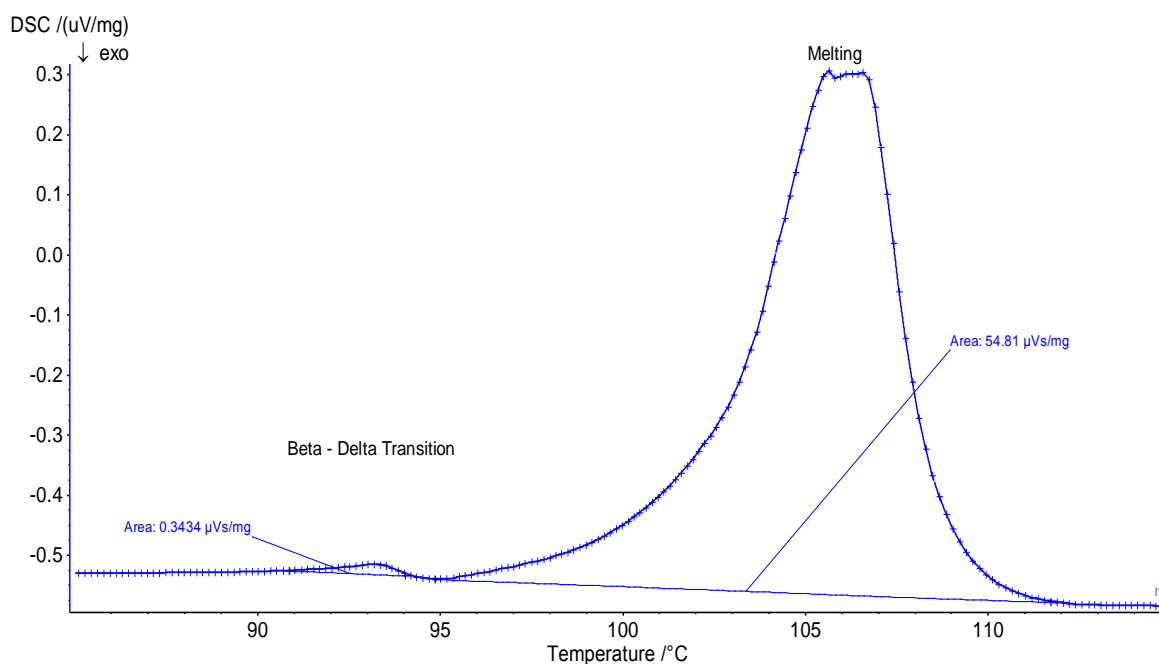


The high value of the coefficient of determination,  $R^2$ , of the line of best fit indicates that a kinetic function of form,  $f(\alpha) = (1 - \alpha)^n$ , is valid for this transformation. The sub-unitary value of  $n$ , given by the axis intercept, coupled with the sigmoid shaped conversion curve suggests that an Avrami-Erofeev model is applicable to this transition. This supports the conclusion of Matsuda *et al.*, and is consistent with a nucleation and growth mechanism.

### 5.4.1.2 Beta Form

The DSC scan of the beta form was measured at a temperature increase rate of 5K/min. It displays a clear melting endotherm apparent in the figure below, but only a very minor endotherm at the temperature where *in situ* X-ray diffraction experiments identify that the beta form transforms to the delta form. These diffraction patterns confirm that little or no delta form is present at the temperature at which the corresponding DSC endotherm commences, and that complete extinction of the beta form occurs by the end of the transition event. Owing to the small size of the transition endotherm, confirmation of the first order kinetics postulated by Matsuda *et al.* was not attempted. Variations in the enthalpy of this transition are discussed in the next section.

**Figure 59 - Beta Form Transition & Melting Endotherm by DSC**



In situations such as these Bernstein, recommends the use of hot-stage microscopy, noting that “*there may be optically observed phase changes that are barely detectable by other analytical techniques such as differential scanning calorimetry.*”



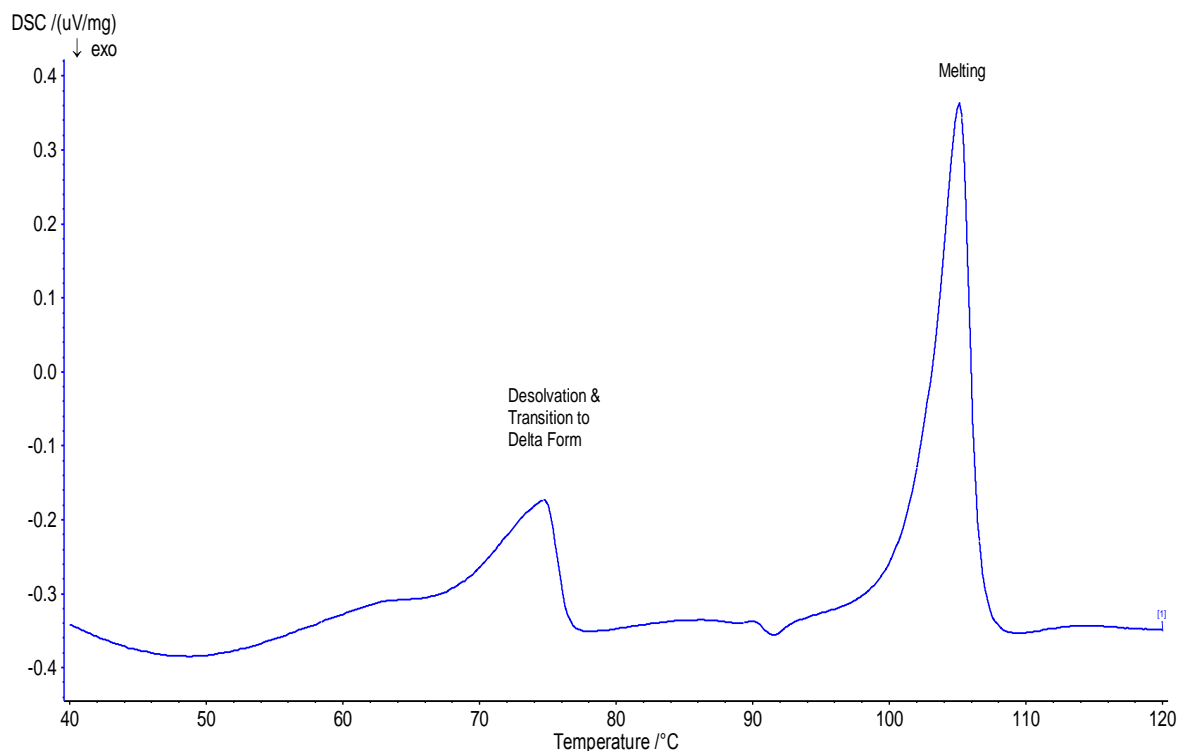
### 5.4.1.3 Delta Form

The delta form was not observed to transition to other polymorphs upon heating during X-ray diffraction experiments. Its DSC scan displays only a melting endotherm; (Appendix 2).

### 5.4.2 Solvates

For the solvate formed with tetrahydrofuran (b.p. 66°C), the behaviour upon heating was similar to that of the alpha and beta polymorphs. At a temperature ramp rate of 5K/min, the solvate transformed to the delta form of phenylbutazone without a visible melting event. Subsequently the sample melted at 105°C, the melting temperature of the delta polymorph.

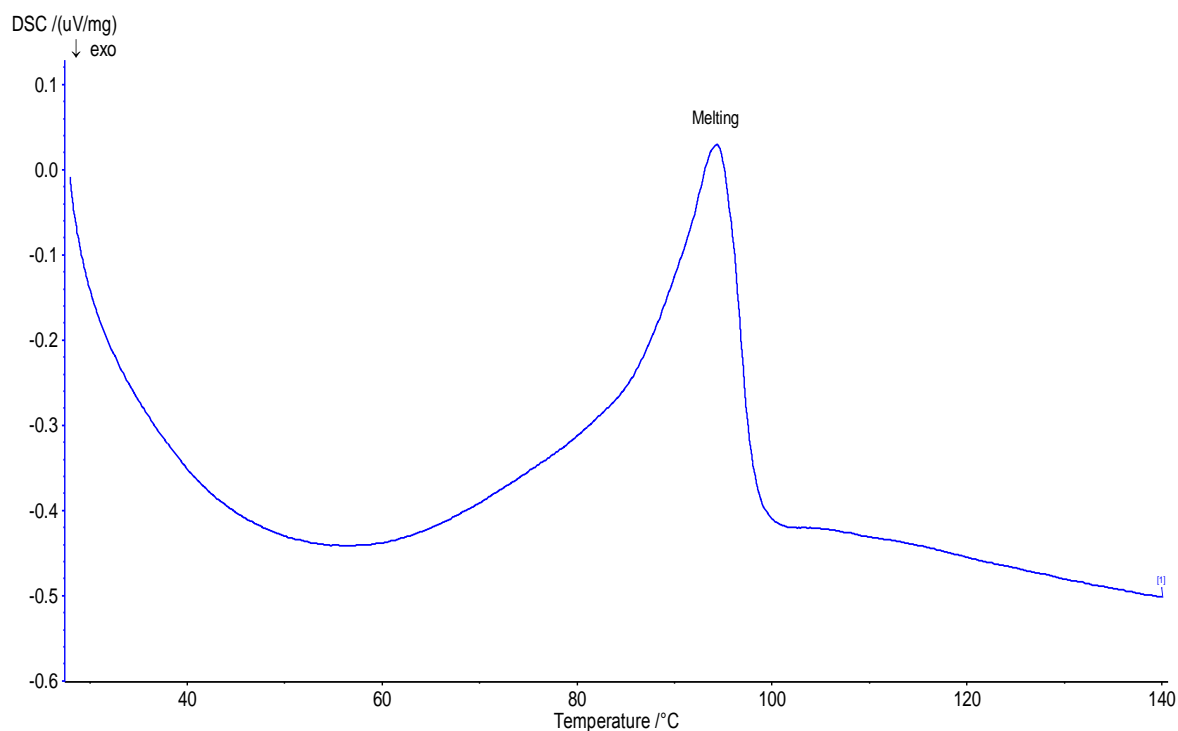
**Figure 60 - DSC Scan of Tetrahydrofuran Solvate**



Similar behaviour was observed of the solvates with methyl-tertiary-butylether, (b.p. 55°C) and with the high-boiling solvent, propylene carbonate (b.p. 240°C).

For the solvate formed with cyclohexanone, (b.p. 155°C), at a temperature ramp rate of 5K/minute, no transition is observed before melting, which occurs at 95°C; i.e. below the melting point of the delta form. The reduction of the melting temperature is also apparent in the corresponding *in situ* PXRD patterns; (Figure 54).

**Figure 61 - DSC Scan of Cyclohexanone Solvate**



## 5.5 Discussion of Results

### 5.5.1 Polymorphs

From the elevated temperature X-ray diffraction patterns of the alpha and beta polymorphs; (Section 5.2.1.3), it is readily apparent that full transition to the delta form has taken place, and that transition is completed in a matter of minutes after a particular temperature increase step has been carried out. At the temperature step immediately below the transition event, there is no indication from the PXRD patterns that even partial transformation takes place within the space of the half hour needed to achieve equilibrium and collect the PXRD pattern.

Rising temperature heating of the alpha and beta polymorphs across the same temperature range in the differential scanning calorimeter shows up the presence of an additional endotherm to the melting endotherm, albeit only a very small one in the case of the beta form.

From the shape of these additional endotherms it is assumed that the transition event is completed in about a minute. The following table summarizes the temperatures of transitions between forms of phenylbutazone measured by different groups:

**Table 17 - Temperatures of Transition of Phenylbutazone's Polymorphs**

Investigator(s) Transition Temperature (K)	Present Investigation	Burger & Ramberger <sup>29</sup> [25]	Matsunaga, Nambu & Nagai [17]	Müller [18]
Alpha to Delta	360-70	350	373-376	366.4
Alpha to Beta	Not observed	330 ± 20	n/a	n/a
Beta to Delta	365-68	360	n/a	368.1

In their compilation of transition events of pharmaceutical active ingredients, Burger and Ramberger, indicate that at about 330K the alpha form changes to the beta form, which in turn changes to the delta form. A transition from the alpha to the beta form did not become apparent during the stepped temperature PXRD experiments conducted in-house.

The divergences in measured transition temperatures may result from differences in the heating gradient of the different experiments. Forni *et al.*, [116], demonstrate the impact that heating rate causes on measurement of the melting temperature of the delta form.

<sup>29</sup> This group use the Roman numeral designations for the polymorphs adopted by Müller, however the form numbers of alpha and beta have apparently been reversed, so that; I is delta, II is beta and III is alpha.

The Proteus<sup>®</sup> analysis software for the Netzsch Jupiter<sup>®</sup> DSC enables the size of enthalpy changes associated with polymorph transitions to be assessed from transition endotherms in the same manner that heats of fusion are obtained from melting point endotherms. The values of the polymorph transition endotherms of the alpha and beta forms as well as those of melting events are shown in the following table together with literature values:

**Table 18 - Enthalpies of Melting & Transition of Phenylbutazone's Polymorphs**

Transition Endotherm (J/gram) \ Group	Present Investigation	Kaneniwa, Ichikawa, Matsumoto [27]	Beretzky, <i>et al.</i> [117]	Müller [18]	Burger, Ramberger [25]
Alpha to Delta	23.7				6.5 ± 1.6
Alpha (Delta) Melting	29.8	119.32		79.3	79.3
Beta to Delta	0.6				-1.6 ± 0.6
Beta (Delta) Melting	91.4	88.36		71.1	71.1
Delta Melting	90.9	93.41	107.96	72.3	72.3

A number of aspects of the data contained in this table deserve mention:

- There is wide variation between the values reported by different researchers.
- The value of the alpha melting endotherm recorded in-house is much smaller than the other two values reported in the literature.
- The size of the alpha-delta transition endotherm recorded in-house is much larger than that reported by Burger & Ramberger.
- Burger and Ramberger indicate the transition of the beta to the delta form is exothermic.

Müller provides the results of three DSC scans of the beta form at different heating gradients. These indicate that, for the beta polymorph at least, the rate of heating severely influences the size of the transition and melting enthalpies.

At the slowest ramp rate, 2K/min, the observed transition endotherm is very small, but the melting endotherm is apparently enlarged. Conversely, at the largest heating gradient, 20K/min, the transition endotherm is large, but the size of the melting endotherm is diminished.

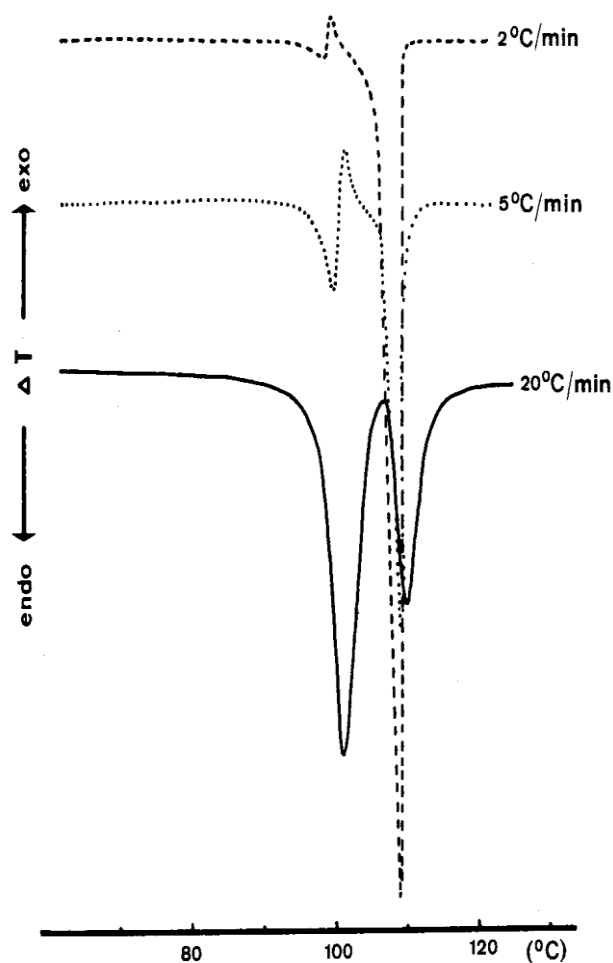


**Figure 62 - Beta Transition & Melting - Müller**

In a review of the transition behaviour of several APIs, the influence of a solid-state polymorphic transition in the vicinity of the melting point is examined by Giron, [42]. The period of heating near the transition temperature is shown to influence the size of the transition endotherm. This suggests that the polymorphic transition and nearby melting event are to some extent interrelated, and raises questions about the nature of the transition mechanism.

Possible variations in the kinetic parameters and methods to characterize their effect upon measured thermal properties of pharmaceutical compounds are discussed by Khawam and Flanagan, [110]. Exploring these methods is beyond the scope of the present investigation.

### 5.5.2 Solvates

Upon heating, those solvates containing solvents, whose boiling points are below the melting temperature of phenylbutazone, were observed to desolvate completely, leading to formation of the delta form before melting.

This contrasted with the thermal behaviour of at least one solvate with a high-boiling solvent, however the observed differences depended upon the heating programme employed. When submitted to swift temperature rise during *in situ* PXRD experiments and DSC scans, the solvate with cyclohexanone retained its solid/liquid lattice, until melting of the combined solvate occurred. Weight loss of the sample continued to occur for some time after the melting event, which is consistent with subsequent evaporation of solvent from the mixture of solvent and melted solute. By contrast, isothermal heating of the same solvate at 90°C; (i.e. well below the solvent's boiling point), over the course of two hours gave rise to formation of the delta polymorph. This indicates that evaporative solvent loss eventually leads to desolvation and formation of the delta form; a conclusion supported by the analogous behaviour under isothermal heating at 90°C of another solvate with a high-boiling solvent, the solvate with propylene carbonate. This solvate was not examined by DSC or by *in situ* X-ray diffraction to confirm that it too retains its solvate lattice, when subjected to a rapid temperature increase, however this result is anticipated.

No desolvation events were observed upon extended room-temperature storage of the solvates with high-boiling solvents that were tested. Desolvation transitions of a number of solvates with low boiling points did take place upon extended room temperature storage; the time period up to transition was observed to be variable. Conditions that triggered the onset of desolvation did not become clear during the experiments that were conducted.

## Conclusions

During this investigation, in which only pre-prepared phenylbutazone was used as starting material, a fully reliable solution crystallization technique for the formation of the pure delta polymorph was not identified. This difficulty seems counter-intuitive, in light of the fact that the alpha and beta polymorphs transform to the delta form in the solid state. One researcher, Tuladhar, has documented a solution crystallization method that resulted in formation of pure delta form, but this result could not be reproduced.

The delta polymorph displays no tendency to change to the other crystal forms in the solid state, which suggests that the delta form is the most stable polymorph. Neither comparison of the calculated densities of the alpha and delta forms, nor invocation of Ostwald's Rule of Stages provides a decisive indicator of the relative stability of the alpha/delta pair, however. The Rule of Stages does support the hypothesis that the beta polymorph is less stable than the alpha or delta forms.

The preferential solubility model of polymorph formation does not appear to be a useful guide to predicting the formation of particular phenylbutazone polymorphs during solution crystallization, even though differences in the solubilities of individual polymorphs have been measured, and have been demonstrated to persist over time.

Solvent choice does have a reproducible impact on polymorph composition in certain cases, and it is presumed that the progress of crystallization is subject to a kinetic rather than a thermodynamic control mechanism in many, if not all, instances.

The ability to produce pure delta form completely reproducibly from the alpha and beta polymorphs, by isothermal heating above the temperature of transition, makes this technique

the most reliable method to prepare pure delta form. This method was not observed to result in the formation of a liquid phase; the identified transitions occur entirely in the solid state. Based upon DSC-derived conversion values, the kinetic function for the alpha-delta transition appears to adhere to an Avrami-Erofeev model, and this is consistent with the findings of a previous study.

The results of DSC experiments on the established polymorphs present a conundrum; large variations exist in the enthalpies of fusion and of polymorphic transition measured by different research groups. From the limited amount of DSC data that has been collected during this investigation, the supposition is made that the proximity of the transition temperatures of the alpha and beta form to the temperature of the melting event means that the two events should not be considered as being entirely independent. This would explain the measurement of a high value for the transition enthalpy of the alpha-delta transformation and the depressed value of the measured enthalpy of the subsequent melting endotherm. Variability in the kinetic parameters of the transitions is also put forward as a possible explanation of these results. *In situ* synchrotron PXRD experiments on phenylbutazone's polymorphs would very likely provide valuable, supplementary information about the speed and conversion path of these transitions.

In the case of phenylbutazone, the comments of Borcka & Haleblian, concerning the superiority of PXRD as a means of polymorph identification, appear to be borne out. Indeed it is not unlikely that attempts to identify polymorphic forms by differential scanning calorimetry may have contributed to confusion in the identification of certain polymorphs during past investigations of this molecule.

The other crystal forms of phenylbutazone mentioned in the literature, most notably the gamma, epsilon and zeta forms, were not positively identified during solvent crystallizations



carried out during this investigation. However preliminary grinding experiments confirmed that changes occur in relative intensities of diffraction peaks of the known crystal forms. Only one researcher, Tuladhar, has reported that crystals of any of these novel forms can be prepared by conventional crystallization methods, which would constitute a reasonable basis for optimism that crystal specimens suitable for single crystal X-ray diffraction may be isolated. In view of the difficulty in growing high quality single crystals of even the established polymorphic forms of phenylbutazone, it seems unlikely that complete structural information for novel form(s) and/or their modifications can be obtained from classical, single crystal X-ray diffraction experiments.

This investigation identifies two new solvates, those formed with methyl-tertiary-butylether and with propylene carbonate, whose structures are determined to be monoclinic with space-group  $C2/c$ , thereby confirming the finding of Hosokawa *et al.* that phenylbutazone forms several solvates that are isostructural with one another. In addition, two cyclic ketone solvents are also found to form solvates with phenylbutazone, and, based upon PXRD pattern matching, these solvates appear to have crystal lattices that are identical with one another. Although the full structures of these newly discovered solvates with cyclohexanone and with cyclopentanone could not be confirmed, it is likely that they are also isostructural with the seven other solvates with space-group,  $C2/c$ .

Distinguishing discrete solvate structures by chemical formula units, there is as yet no clear indication that more than one solvate is formed between phenylbutazone and a given solvent. As evidenced by the low temperature PXRD pattern of the solvate with tetrahydrofuran, there is, however, good reason to believe that this solvate adopts more than one packing arrangement.

The ability to calculate theoretical powder diffraction patterns from structural models of the crystal lattice represents a powerful means of validating structure solutions of individual crystal forms, but the implications of disparities, such as those that have come to light during investigation of phenylbutazone's solvates, are not fully clear. The many reports of unconfirmed crystal forms of this and other important industrial materials serve to underscore the importance of full structure determination; be it via single crystal X-ray diffraction or via alternative methods.

Uncertainty continues to surround the nature and the crystal structures of many of the polymorphs of phenylbutazone. Thanks to synchrotron PXRD experiments, progress has been made in determining the unit cell of phenylbutazone's delta form. A plausible structural model for this polymorph is surely only a small distance away.

## References

1. Bernstein, J., *Polymorphism in Molecular Crystals*. 1 ed. IUC Monographs on Crystallography, ed. I.U.o. Crystallography. 2002, Oxford: Oxford University Press. 410.
2. Sharma, B.D., *Crystal Systems & General Chemistry*. Journal of Chemical Education, 1982. **59**.
3. Sharma, B.D., *Allotropes & Polymorphs*. Journal of Chemical Education, 1987. **64**.
4. Byrn, S., et al., *Pharmaceutical Solids: A Strategic Approach to Regulatory Considerations*. Pharmaceutical Research, 1995. **12**(7): p. 945.
5. Yu, L.X., et al., *Scientific Considerations of Pharmaceutical Solid Polymorphism in Abbreviated New Drug Applications*. Pharmaceutical Research, 2003. **20**(4).
6. Bauer, J., et al., *Ritonavir: An Extraordinary Example of Conformational Polymorphism*. Pharmaceutical Research, 2001. **18**(6).
7. Yang, W., et al., *Evaluation of phenylbutazone and poly(amidoamine) dendrimers interactions by a combination of solubility, 2D-NOESY NMR, and isothermal titration calorimetry studies*. Journal of Pharmaceutical Sciences, 2009. **98**(3): p. 1075-1085.
8. Price, S.L., *The Computational Prediction of Pharmaceutical Crystal Structures and Polymorphism*. Advanced Drug Delivery Reviews, 2004. **56**: p. 301-319.
9. Gavezzotti, A., *Are Crystal Structures Predictable?* Accounts of Chemical Research, 1994. **27**: p. 309-314.
10. Gavezzotti, A. and G. Filippini, *Polymorphic Forms of Organic Crystals at Room Conditions: Thermodynamic and Structural Implications*. Journal of The American Chemical Society, 1995. **117**: p. 12299-12305.
11. Gilmore, C.J., K. Shankland, and W. Dong, *A Maximum Entropy Approach to Structure Solution*, in *Structure Determination from Powder Diffraction Data*, W.I.F. David, et al., Editors. 2002, Oxford University Press: New York. p. 337.
12. Forney, B. *Phenylbutazone for Veterinary Use*. 2004 [cited; Available from: <http://www.wedgewoodpharmacy.com/monographs/phenylbutazone.asp>].
13. Hosokawa, T., et al., *Isostructurality among Five Solvates of Phenylbutazone*. Crystal Growth & Design, 2004. **4**(6): p. 1195-1201.
14. Ali, S.L., *Phenylbutazone*, in *Analytical profiles of drug substances*, K. Florey, Editor. 1991, Academic Press: San Diego, London. p. 483-521.
15. Hosokawa, T., et al., *Relationships between crystal structures and thermodynamic properties of phenylbutazone solvates*. Crystengcomm, 2004. **6**: p. 243-249.
16. Ibrahim, H.G., F. Pisano, and A. Bruno, *Polymorphism of phenylbutazone: Properties and compressional behavior of crystals*. Journal of Pharmaceutical Sciences, 1977. **66**(5): p. 669-673.
17. Matsunaga, J., N. Nambu, and T. Nagai, *Physicochemical Approach to Biopharmaceutical Phenomena .30. Polymorphism of Phenylbutazone*. Chemical & Pharmaceutical Bulletin, 1976. **24**(6): p. 1169-1172.
18. Mueller, B.W., *Polymorphism of Non-Steroidal Anti-Inflammatory Drugs .1. Polymorphism and Pseudo-Polymorphism of Phenylbutazone*. Pharmaceutica Acta Helvetiae, 1978. **53**(12): p. 333-340.
19. Tuladhar, M.D., *Effects of polymorphism and particle size on the dissolution of phenylbutazone tablets*, PhD Thesis, 1982, University of London: London.
20. Matsumoto, T., et al., *Effect of Environmental-Temperature on the Polymorphic Transformation of Phenylbutazone during Grinding*. Chemical & Pharmaceutical Bulletin, 1988. **36**(3): p. 1074-1085.

21. Matsuda, Y., et al., *Polymorphism of phenylbutazone by a spray drying method*. J Pharm Pharmacol, 1980. **32**(8): p. 579-80.
22. Al-Meshal, M.A.S. and P. York, *Effect of Crystallization Rate on the Polymorphism and Dissolution of Spray-Dried Phenylbutazone*. Journal of Pharmacy and Pharmacology, 1983. **35** II.
23. Matsuda, Y., et al., *Physicochemical characterization of spray-dried phenylbutazone polymorphs*. J Pharm Sci, 1982. **73**(2): p. 173-9.
24. Matsuda, Y., et al., *Kinetic Study of the Polymorphic Transformations of Phenylbutazone*. Journal of Pharmaceutical Sciences, 1984. **73**(10): p. 1453-1461.
25. Burger, A. and R. Ramberger, *On the Polymorphism of Pharmaceuticals and Other Molecular Crystals. II*. Mikrochimica Acta, 1979(2): p. 273-316.
26. Kaneniwa, N., J. Ichikawa, and K. Hayashi, *Dissolution Behavior of Phenylbutazone Polymorphs*. Yakugaku Zasshi-Journal of the Pharmaceutical Society of Japan, 1987. **107**(12): p. 1005-1007.
27. Kaneniwa, N., J. Ichikawa, and T. Matsumoto, *Preparation of Phenylbutazone Polymorphs and Their Transformation in Solution*. Chemical & Pharmaceutical Bulletin, 1988. **36**(3): p. 1063-1073.
28. Tuladhar, M.D., J.E. Carless, and M.P. Summers, *Thermal behaviour and dissolution properties of phenylbutazone polymorphs*. J Pharm Pharmacol, 1983. **35**(4): p. 208-14.
29. Rey-Mermet, C., et al., *Significance of Partial and Total Cohesion Parameters of Pharmaceutical Solids Determined from Dissolution Calorimetric Measurements*. Pharmaceutical Research, 1991. **8**(5): p. 636-642.
30. Hildebrand, J.H., J.M. Prausnitz, and R.L. Scott, *Regular & Related Solutions, The Solubility of Gases, Liquids and Solids*. 1970, New York: Van Nostrand Reinhold. 228.
31. Hildebrand, J.H. and R.L. Scott, *The solubility of nonelectrolytes*. 3rd ed ed. Monograph series / American Chemical Society ; no.17. 1951: Reinhold; Chapman & Hall. 488p., ill.,24cm.
32. Hancock, B.C., P. York, and R.C. Rowe, *The use of solubility parameters in pharmaceutical dosage form design*. International Journal of Pharmaceutics, 1997. **148**(1): p. 1-21.
33. Streng, W.H., *Characterization of compounds in solution : theory and practice*. 2001, New York ; London: Kluwer Academic/Plenum Publishers. xv, 273 p.
34. Tuladhar, M.D., J.E. Carless, and M.P. Summers, *The effects of polymorphism, particle size and compression pressure on the dissolution rate of phenylbutazone tablets*. J Pharm Pharmacol, 1983. **35**(5): p. 269-74.
35. Al-Meshal, M.A.S., *Physicochemical and tableting properties of crystallised and spray-dried phenylbutazone containing polymeric additives*. 1985, University of Bradford.
36. Stella, V.J., *Nonclassical Phase Transfer Behavior of Phenylbutazone*. Journal of Pharmaceutical Sciences, 1975. **64**(4): p. 706-708.
37. Stella, V.J. and J.D. Pipkin, *Phenylbutazone Ionization Kinetics*. Journal of Pharmaceutical Sciences, 1976. **65**(8): p. 1161-1165.
38. Singh, T.P. and M. Vijayan, *Structural Studies of Analgesics and Their Interactions .4. Crystal-Structures of Phenylbutazone and a 2-1 Complex between Phenylbutazone and Piperazine*. Journal of the Chemical Society-Perkin Transactions 2, 1977(5): p. 693-699.
39. Paradies, H.H., *Structure of Phenylbutazone and Mofebutazone in the Crystalline State and in Solution*. Journal of Pharmaceutical Sciences, 1987. **76**(12): p. 920-929.
40. Chauvet, A. and J. Masse, *Du Comportement Thermique de la Phenylbutazone*. Travaux de la Société de Pharmacie de Montpellier, 1978. **38**(1): p. 31-42.
41. Borka, L. and J.K. Haleblan, *Crystal Polymorphism of Pharmaceuticals*. Acta Pharmaceutica Jugoslavica, 1990. **40**(1-2): p. 71-94.
42. Giron, D., *Thermal Analysis in Pharmaceutical Routine Analysis*. Acta Pharmaceutica Jugoslavica, 1990. **40**: p. 95-157.

43. Giron, D., *Applications of thermal analysis and coupled techniques in pharmaceutical industry*. Journal of Thermal Analysis and Calorimetry, 2002. **68**(2): p. 335-357.
44. Giron, D., *Investigations of Polymorphism and Pseudo-Polymorphism in Pharmaceuticals by Combined Thermoanalytical Techniques*. Journal of Thermal Analysis & Calorimetry, 2001. **64**: p. 37-60.
45. Giron, D., *Thermal analysis and calorimetric methods in the characterisation of polymorphs and solvates*. Thermochemica Acta, 1995. **248**: p. 1-59.
46. Diamond. *I11 Powder Diffraction*. 2009 [cited; Available from: <http://www.diamond.ac.uk/Beamlines/Beamlineplan/I11/Index.htm>].
47. Gottlieb, H.E., V. Kotlyar, and A. Nudelman, *NMR Chemical Shifts of Common Laboratory Solvents as Trace Impurities*. J. Org. Chem., 1997. **62**(21): p. 7512-7515.
48. Tanaka, M., et al., *Binding Position of Phenylbutazone with Bovine Serum Albumin Determined by Measuring Nuclear Magnetic Resonance Relaxation Time*. Chemical & Pharmaceutical Bulletin, 1989. **37**(12): p. 3177-3180.
49. Simpson, J., *Organic Structure Determination Using 2D NMR Spectroscopy*. 2009, Oxford: Academic Press.
50. Ladd, M. and R. Palmer, *Structure Determination by X-ray Crystallography*. 4 ed. 2003, New York: Kluwer Academic/Plenum Publishers. 819.
51. Pecharsky, V.K. and P.Y. Zavalij, *Fundamentals of Powder Diffraction and Structural Characterization of Materials*. 1 ed. 2005, New York: Springer. 713.
52. Dinnebier, R.E. and S.J.L. Billinge, *Powder Diffraction. Theory and Practice*. 1 ed. 2008, Cambridge: Royal Society of Chemistry. 582.
53. Werner, P., *Autoindexing*, in *Structure Determination from Powder Diffraction Data*, W.I.F. David, et al., Editors. 2002, Oxford University Press: New York. p. 337.
54. *Powder and Small Molecule Single Crystal Diffraction*. Collaborative Computer Projects 14 1994 [cited; Available from: [www.ccp14.ac.uk](http://www.ccp14.ac.uk)].
55. Kohlbeck, F. and E.M. Hoerl, *Indexing program for powder patterns especially suitable for triclinic, monoclinic and orthorhombic lattices*. Journal of Applied Crystallography, 1976. **9**: p. 28-33.
56. Kohlbeck, F. and E.M. Hoerl, *Trial and error indexing program for powder patterns of monoclinic substances*. Journal of Applied Crystallography, 1978. **11**: p. 60-61.
57. Datta, S. and D.J.W. Grant, *Crystal structures of drugs: Advances in determination, prediction and engineering*. Nature Reviews Drug Discovery, 2004. **3**(1): p. 42-57.
58. Cockcroft, J.K., *Dragon, Version 5.01*. 2003: London.
59. Altomare, A., et al., *Expo User's Manual*, in *SIRWARE*, I.d. Cristallografia, Editor: Bari. p. A package for full pattern decomposition and for solving crystal structures by direct methods.
60. **IUCr**, *Space Group Symmetry*. International Tables for Crystallography, ed. T. Hahn. Vol. A. 1995, Dordrecht: Kluwer.
61. Massa, W. and R.O. Gould, *Crystal structure determination*. 2nd ed. 2004, Berlin: Springer. xi,210p.
62. Young, R.A., *Rietveld method*. New ed. International Union of Crystallography Monographs on Crystallography. 1995, Oxford: Oxford University Press. [308]p.
63. Giacovazzo, C., *Direct Phasing in Crystallography*. 1 ed. IUCr Monographs on Crystallography, ed. P. Coppens. 1998, New York: Oxford University Press. 767.
64. Bruno, I.J., et al., *New software for searching the Cambridge Structural Database and visualising crystal structures*. Acta Crystallographica Section B, 2002. **58**: p. 389-397.
65. Kraus, W. and G. Nolze, *Powdercell*, Bundesanstalt fuer Materialforschung und Pruefung: Berlin. p. powder pattern calculation from single crystal data and refinement of experimental curves.

66. Giacobazzo, C., et al., *Direct methods in powder diffraction - applications*, in *Structure Determination from Powder Diffraction Data*, W.I.F. David, et al., Editors. 2002, Oxford University Press: New York. p. 337.
67. Favre-Nicolin, V. and R. Cerny, *FOX, Free Objects for Xtallography*. p. "a free, open-source program for the ab initio structure determination from powder diffraction data".
68. Palatinus, L. and G. Chapuis, *SUPERFLIP - a computer program for the solution of crystal structures by charge flipping in arbitrary dimensions*. *Journal of Applied Crystallography*, 2007. **40**: p. 786-790.
69. Clegg, W., *Crystal Structure Analysis*. Texts on Crystallography, ed. IUCr. 2001, Oxford: Oxford University Press.
70. Keats, C.J., *Crystallization and Polymorphism of Putative Drugs, PhD Thesis*, 2001, Oxford University: Oxford.
71. Cockcroft, J.K., *Extinguishing of Single Crystals under Polarized Light*, J.J. Targett, Editor. 2007: London.
72. Burla, M.C., et al., *SIR2004: an improved tool for crystal structure determination and refinement*. *Journal of Applied Crystallography*, 2005. **38**(381-388).
73. Petricek, V., M. Dusek, and L. Palatinus, *Jana2006. The crystallographic computing system*. 2006, Institute of Physics: Prague.
74. Shmueli, U., *Theories & Techniques of Crystal Structure Determination*. 1 ed. IUCr Texts on Crystallography, ed. H. Schenk. 2007, New York: Oxford University Press. 269.
75. Wilson, A.J.C. and E. Prince, *International Tables for Crystallography*. Vol. C. 1999, Dordrecht, London: Published for the International Union of Crystallography by Kluwer Academic Publishers. 992p.
76. Betteridge, P.W., et al., *CRYSTALS, version 12: software for guided crystal structure analysis*. *Journal of Applied Crystallography*, 2003. **36**.
77. Trueblood, K.N., et al., *Atomic Displacement Parameter Nomenclature. Report of a Subcommittee on Atomic Displacement Parameter Nomenclature*. *Acta Crystallographica Section A*, 1996. **52**(5): p. 770-781.
78. Mueller, P., *Crystal structure refinement : a crystallographers guide to SHELXL*. IUCr texts on crystallography. 2006, Oxford: Oxford University Press. xvii, 213 p.
79. Mullin, J.W., *Crystallization*. 3rd ed. 1997, Oxford: Butterworth-Heinemann.
80. Kitamura, M., *Polymorphism in the Crystallization of L-Glutamic Acid*. *Journal of Crystal Growth*, 1989. **96**(3): p. 541-546.
81. Kitamura, M., *Crystallization Behaviour and Transformation Kinetics of l-Histidine Polymorphs*. *Journal of Chemical Engineering of Japan*, 1993. **26**(3): p. 303-307.
82. Kitamura, M., *Controlling factors and mechanism of polymorphic crystallization*. *Crystal Growth & Design*, 2004. **4**(6): p. 1153-1159.
83. Kitamura, M. and K. Nakamura, *Effects of solvent composition and temperature on polymorphism and crystallization behavior of thiazole-derivative*. *Journal of Crystal Growth*, 2002. **236**(4): p. 676-686.
84. Kitamura, M. and K. Onuma, *In situ observation of growth process of alpha-L-glutamic acid with atomic force microscopy*. *Journal of Colloid and Interface Science*, 2000. **224**(2): p. 311-316.
85. Jacques, S.D.M., et al., *An In-Situ Synchrotron X-ray Diffraction Tomography Study of Crystallization and Preferred Crystal Orientation in a Stirred Reactor*. *Crystal Growth & Design*, 2005. **5**(2): p. 395-397.
86. Grant, D.J.W. and T. Higuchi, *Solubility Behaviour of Organic Compounds*. *Techniques of Chemistry*, ed. A. Weissberger and W.J. Saunders. 1990, New York: Wiley. 600.
87. Shinoda, K., *Principles of solution and solubility*. *Undergraduate chemistry ; v. 5*. 1978, New York: M. Dekker. x, 222 p.

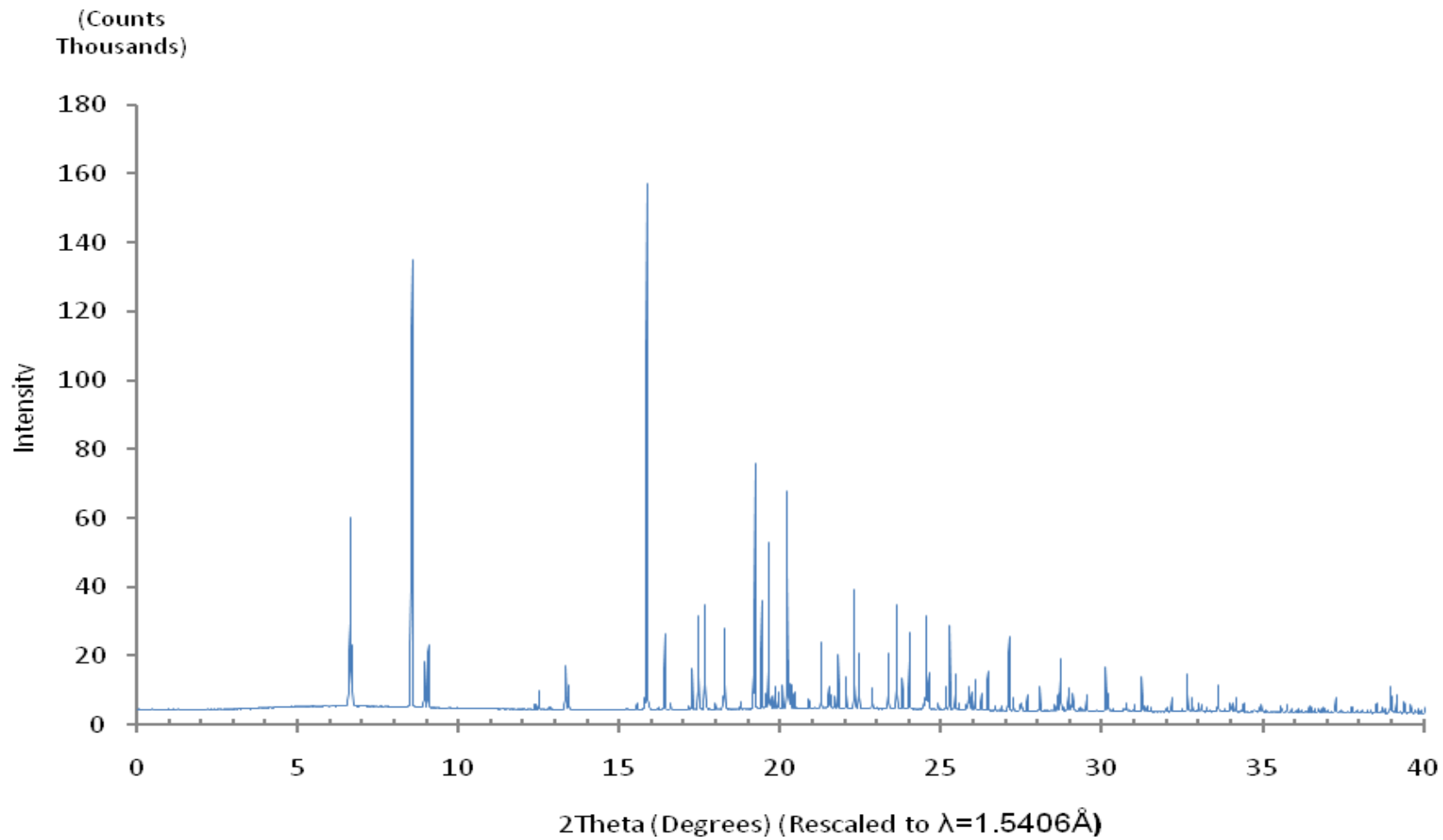
88. Barton, A.F.M., *CRC handbook of solubility parameters and other cohesion parameters*. 1983, Boca Raton, Fla.: CRC Press. [vii],594p.
89. Reuteler-Faoro, D., et al., *A New Equation for Calculating Partial Cohesion Parameters of Solid Substances from Solubilities*. *Journal of Physical Chemistry*, 1988. **92**(21): p. 6144-6148.
90. Carstensen, J.T., *Advanced Pharmaceutical Solids*. *Drugs and the Pharmaceutical Sciences*. 2001, New York: Marcel Dekker.
91. Pudipeddi, M. and A.T.M. Serajuddin, *Trends in solubility of polymorphs*. *Journal of Pharmaceutical Sciences*, 2005. **94**(5): p. 929-939.
92. Datta, S. and D.J.W. Grant, *Computing the relative nucleation rate of phenylbutazone and sulfamerazine in various solvents*. *Crystal Growth & Design*, 2005. **5**(4): p. 1351-1357.
93. Lewis, T.C., et al., *A computational and experimental search for polymorphs of parabanic acid - a salutary tale leading to the crystal structure of oxo-ureido-acetic acid methyl ester*. *Crystengcomm*, 2003: p. 3-9.
94. Gu, C.H., V. Young, and D.J.W. Grant, *Polymorph screening: Influence of solvents on the rate of solvent-mediated polymorphic transformation*. *Journal of Pharmaceutical Sciences*, 2001. **90**(11): p. 1878-1890.
95. Blagden, N. and R.J. Davey, *Polymorph Selection: Challenges for the Future?* *Crystal Growth & Design*, 2003. **3**(6): p. 873-885.
96. Threlfall, T., *Crystallisation of Polymorphs: Thermodynamic Insight into the Role of Solvent*. *Organic Process Research & Development*, 2000(4): p. 384-390.
97. Bernstein, J., R.J. Davey, and J.O. Henck, *Concomitant polymorphs*. *Angewandte Chemie-International Edition*, 1999. **38**(23): p. 3441-3461.
98. Datta, S. and D.J.W. Grant, *Effect of supersaturation on the crystallization of phenylbutazone polymorphs*. *Crystal Research and Technology*, 2005. **40**(3): p. 233-242.
99. Aguiar, A.J., et al., *Effect of polymorphism on the absorption of chloramphenicol from chloramphenicol palmitate*. *J Pharm Sci*, 1967. **56**(7): p. 847-53.
100. Burger, A. and R. Ramberger, *On the Polymorphism of Pharmaceuticals and Other Molecular Crystals. I*. *Mikrochimica Acta*, 1979(2): p. 259-271.
101. Gu, C.H. and D.J.W. Grant, *Estimating the relative stability of polymorphs and hydrates from heats of solution and solubility data*. *Journal of Pharmaceutical Sciences*, 2001. **90**(9): p. 1277-1287.
102. Urakami, K., et al., *A novel method for estimation of transition temperature for polymorphic pairs in pharmaceuticals using heat of solution and solubility data*. *Chemical & Pharmaceutical Bulletin*, 2002. **50**(2): p. 263-267.
103. Brown, M.E., *Reaction Kinetics from Thermal Analysis*, in *Introduction to Thermal Analysis*. 2001, Kluwer: Dordrecht. p. 181-214.
104. Jenkins, R., R.W. Gould, and D. Gedcke, *Quantitative X-ray spectrometry*. 2nd ed. *Practical spectroscopy series ; vol. 20*. 1995, New York, N.Y.: Dekker. xi,484p.
105. Klug, H.P., L. Alexander, and E. Kummer, *Quantitative Analysis with the X-Ray Spectrometer - Accuracy and Reproducibility*. *Analytical Chemistry*, 1948. **20**(7): p. 607-609.
106. Zevin, L.S., G. Kimmel, and I. Mureinik, *Quantitative X-ray Diffractometry*. 1995, New York ; London: Springer. xvii, 372 p.
107. Wong, E.R., et al., *Scrip - Fortran-IV Software for Quantitative XRD*. *Advances in X-Ray Analysis*, 1983. **26**: p. 157-162.
108. Walton, R.I., et al., *An in situ energy-dispersive X-ray diffraction study of the hydrothermal crystallization of zeolite A. 1. Influence of reaction conditions and transformation into sodalite*. *Journal of Physical Chemistry B*, 2001. **105**(1): p. 83-90.
109. Turrillas, X., et al., *Synchrotron-related studies on the dynamic and structural aspects of zirconia synthesis for ceramic and catalytic applications*. *Radiation Physics and Chemistry*, 1995. **45**(3): p. 491-508.

110. Khawam, A. and D.R. Flanagan, *Basics and applications of solid-state kinetics: A pharmaceutical perspective*. Journal of pharmaceutical sciences, 2006. **95**(3): p. 472-498.
111. Criado, J.M., A. Ortega, and F. Gotor, *Correlation between the shape of controlled-rate thermal analysis curves and the kinetics of solid-state reactions*. Thermochimica Acta, 1990. **157**(1): p. 171-179.
112. Brown, M.E., ed. *Handbook of Thermal Analysis and Calorimetry*. ed. P.K. Gallagher. Vol. 1. 1998, Elsevier: Amsterdam.
113. Galwey, A.K. and M.E. Brown, *Thermal decomposition of ionic solids*. Studies in physical and theoretical chemistry. 1999, Amsterdam ; New York: Elsevier. xxvi, 597 p.
114. Freeman, E.S. and B. Carroll, *The Application of Thermoanalytical Techniques to Reaction Kinetics: The Thermogravimetric Evaluation of the Kinetics of the Decomposition of Calcium Oxalate Monohydrate*. The Journal of Physical Chemistry, 1958. **62**(4): p. 394-397.
115. Freeman, E.S. and B. Carroll, *Interpretation of the kinetics of thermogravimetric analysis*. The Journal of Physical Chemistry, 1969. **73**(3): p. 751-752.
116. Forni, F., et al., *Thermal behaviour of melt crystallized phenylbutazone*. Journal of Thermal Analysis and Calorimetry, 1990. **36**(1): p. 35-44.
117. Beretzky, A., et al., *Pelletization of needle-shaped phenylbutazone crystals*. Journal of Thermal Analysis and Calorimetry, 2002. **69**(2): p. 529-539.
118. Gedcke, D. (2005) *How Counting Statistics Controls Detection Limits and Peak Precision*. Application Note, Ortec Incorporated **Volume**, 8



## Appendix 1 – Reference PXRD Patterns of Phenylbutazone’s Polymorphs

### Alpha Form (Synchrotron Data)



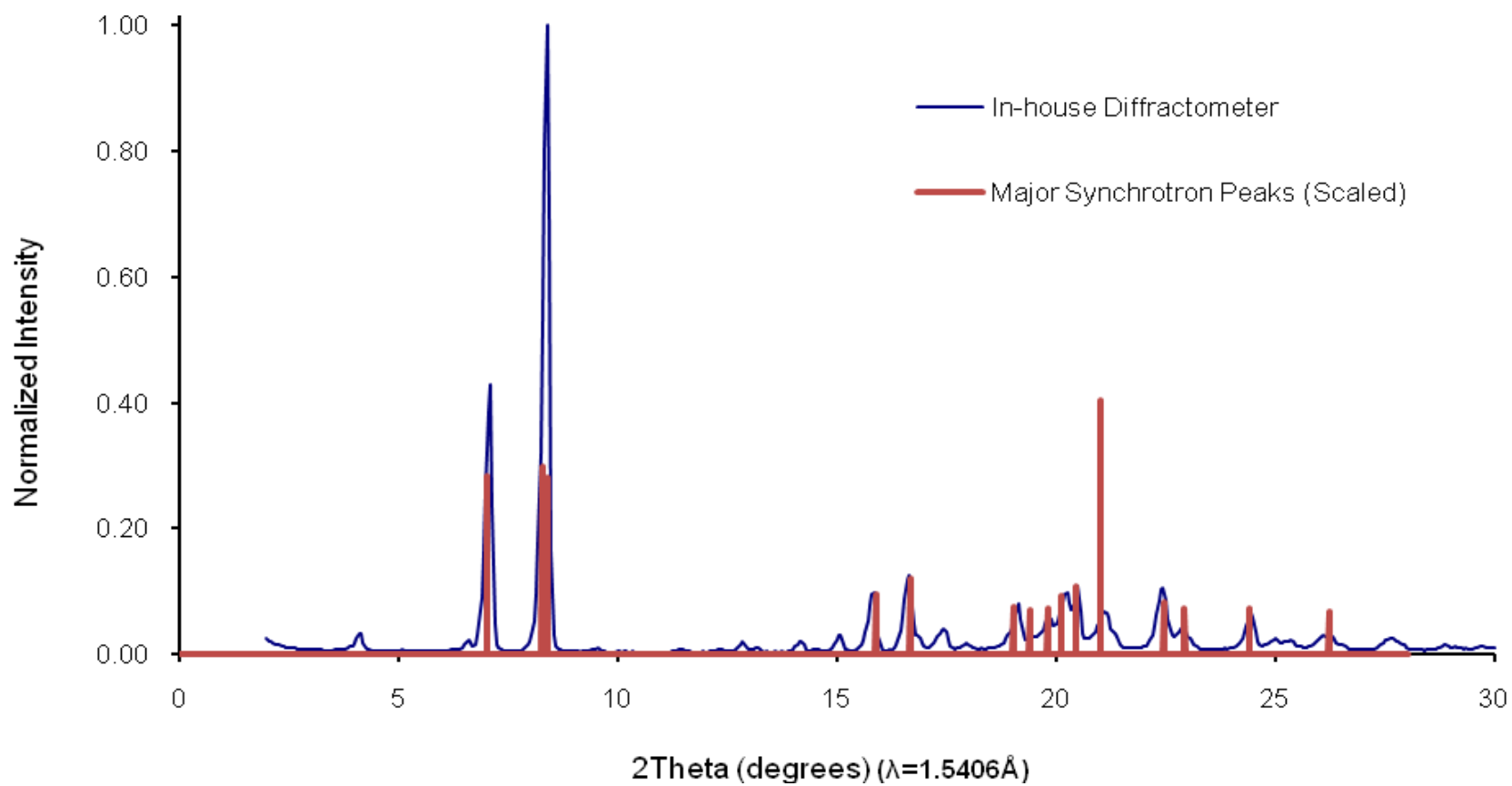
### Index Positions of Phenylbutazone Alpha in P2(1)/c

(a = 21.415Å, b = 5.729Å, c = 27.782Å, alpha = gamma = 90°, beta = 108.068°) (CuKα radiation)

H	K	L	D	2-theta	H	K	L	D	2-theta	H	K	L	D	2-theta
1	0	0	20.359	4.337	-2	1	3	4.658	19.039	4	1	0	3.805	23.3591
0	0	2	13.206	6.688	-1	0	6	4.608	19.2461	-3	1	5	3.7605	23.6398
-1	0	2	13.086	6.749	-2	0	6	4.593	19.3112	2	1	4	3.7195	23.9041
2	0	0	10.180	8.679	1	1	3	4.506	19.6838	-4	1	4	3.6873	24.1157
1	0	2	9.781	9.034	-3	1	1	4.465	19.867	1	1	5	3.6641	24.2711
-2	0	2	9.636	9.170	2	1	2	4.451	19.9294	2	0	6	3.6491	24.3723
2	0	2	7.071	12.507	-3	1	2	4.428	20.0344	4	1	1	3.6486	24.3754
-3	0	2	6.980	12.672	-1	1	4	4.419	20.0756	3	1	3	3.6402	24.4326
-1	0	4	6.945	12.736	0	0	6	4.402	20.1554	-5	0	6	3.5964	24.7349
3	0	0	6.786	13.035	3	1	0	4.378	20.2687	-1	1	6	3.5906	24.7755
0	0	4	6.603	13.398	-3	0	6	4.362	20.342	5	0	2	3.5901	24.7787
-2	0	4	6.543	13.522	0	1	4	4.327	20.5073	-2	1	6	3.5833	24.8268
1	0	4	5.777	15.325	4	0	2	4.321	20.5384	-6	0	2	3.5636	24.9663
-3	0	4	5.697	15.540	-2	1	4	4.310	20.589	4	0	4	3.5357	25.1668
0	1	1	5.599	15.816	-5	0	2	4.283	20.7216	-2	0	8	3.4724	25.6333
1	1	0	5.515	16.058	-3	1	3	4.276	20.7575	-3	1	6	3.4706	25.6468
-1	1	1	5.492	16.127	3	1	1	4.186	21.2084	4	1	2	3.4497	25.8048
3	0	2	5.394	16.420	3	0	4	4.135	21.4731	-1	0	8	3.4314	25.9444
-4	0	2	5.337	16.597	2	1	3	4.085	21.7406	-5	1	2	3.4303	25.9527
1	1	1	5.310	16.682	-5	0	4	4.076	21.7845	-3	0	8	3.4145	26.0752
0	1	2	5.256	16.855	5	0	0	4.072	21.8092	-5	1	3	3.4024	26.1693
-1	1	2	5.248	16.880	1	1	4	4.068	21.8303	-5	1	1	3.4011	26.1797
4	0	0	5.090	17.409	1	0	6	4.051	21.9232	6	0	0	3.3932	26.2421
-2	1	1	5.048	17.555	-3	1	4	4.040	21.9841	2	1	5	3.3808	26.3399
2	1	0	4.993	17.751	-4	0	6	3.999	22.2096	3	1	4	3.3528	26.5641
1	1	2	4.943	17.929	-1	1	5	3.986	22.2864	-5	1	4	3.3214	26.8196
-2	1	2	4.924	17.999	-2	1	5	3.940	22.5485	5	1	0	3.3189	26.84
2	0	4	4.890	18.125	3	1	2	3.927	22.6223	1	1	6	3.3076	26.9339
-1	1	3	4.861	18.235	-4	1	2	3.905	22.7525	0	0	8	3.3015	26.9843
-4	0	4	4.818	18.400	-4	1	1	3.896	22.8075	-4	1	6	3.2793	27.1704

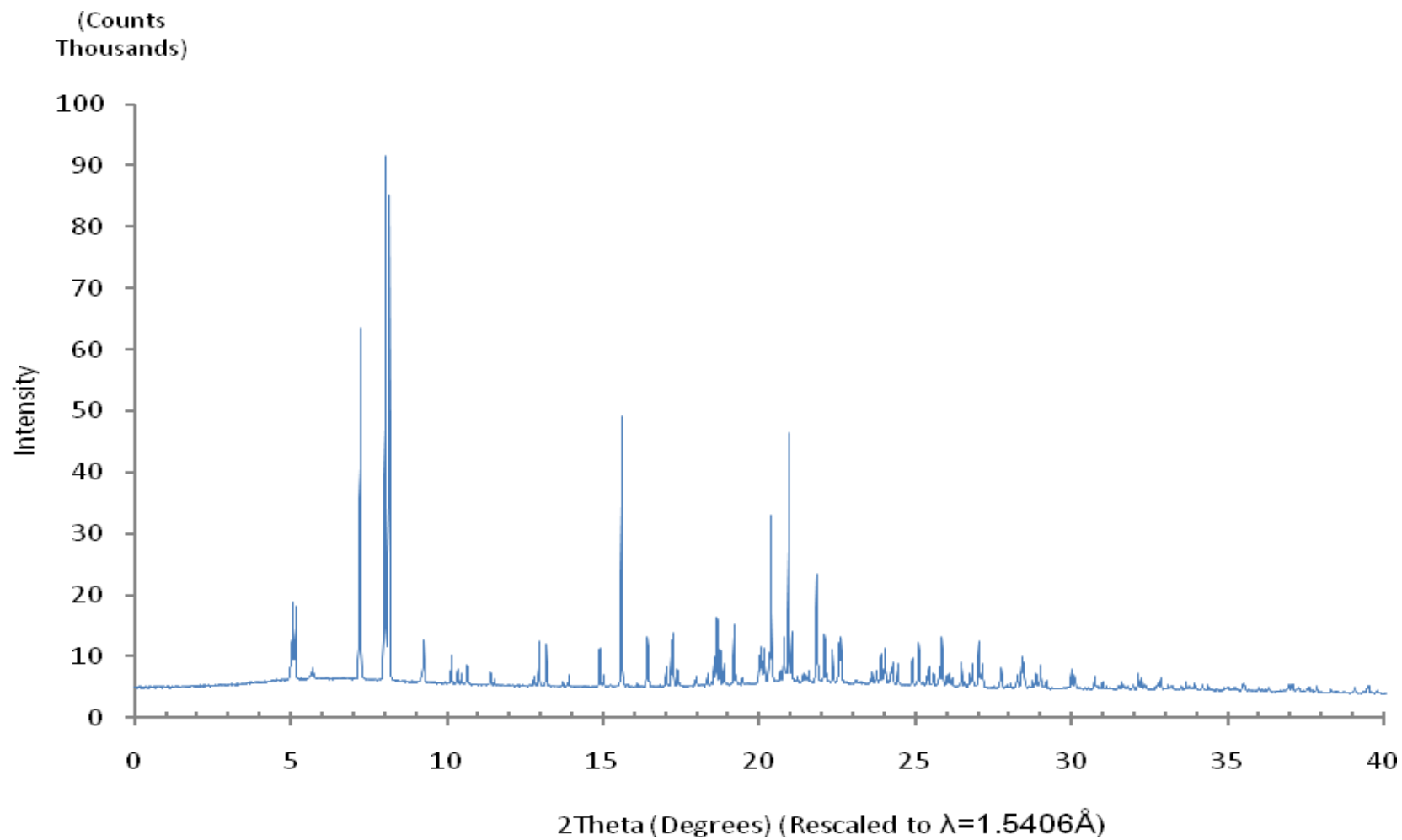
## Appendix 1 – Reference PXRD Patterns of Phenylbutazone’s Polymorphs

### Beta Form (Synchrotron & In-house Data)



## Appendix 1 – Reference PXRD Patterns of Phenylbutazone’s Polymorphs

### Delta Form (Synchrotron Data)



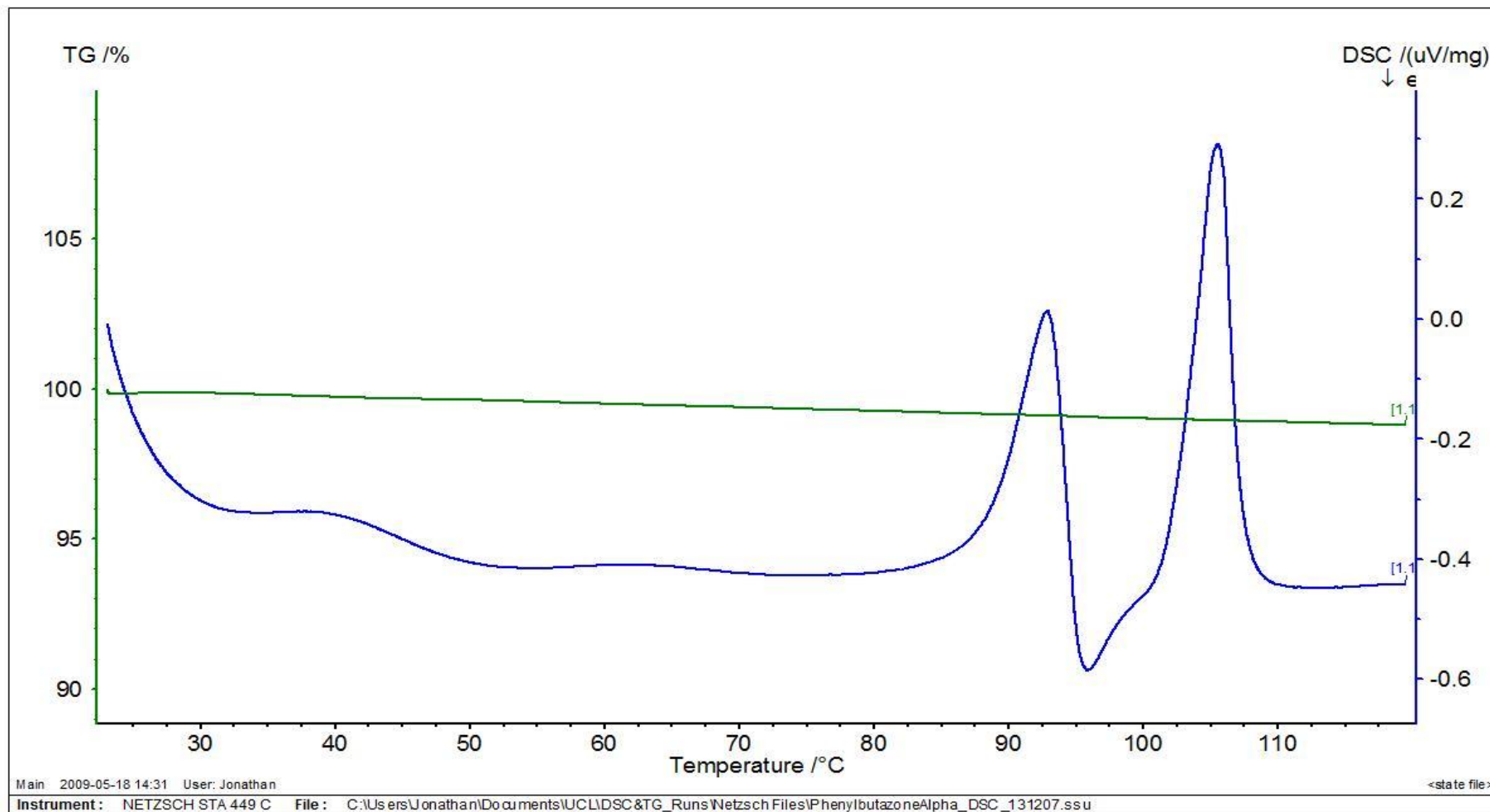
### Index Positions of Phenylbutazone Delta in Pnnm (or Pnn2)

(a = 34.147Å, b = 34.816Å, c = 5.7506Å, alpha = beta = gamma = 90) (CuKα radiation)

H	K	L	D	2-theta		H	K	L	D	2-theta		H	K	L	D	2-theta
1	1	0	24.379	3.621		6	1	0	5.617	15.765		0	5	1	4.434	20.008
0	2	0	17.408	5.072		1	1	1	5.597	15.821		5	6	0	4.422	20.063
2	0	0	17.073	5.172		2	6	0	5.494	16.119		3	4	1	4.421	20.067
1	2	0	15.509	5.694		6	2	0	5.409	16.373		4	3	1	4.411	20.112
2	1	0	15.329	5.761		4	5	0	5.396	16.415		6	5	0	4.407	20.134
2	2	0	12.189	7.246		1	2	1	5.392	16.427		5	0	1	4.399	20.170
1	3	0	10.988	8.040		2	1	1	5.384	16.450		1	5	1	4.397	20.178
3	1	0	10.819	8.166		5	4	0	5.373	16.485		5	1	1	4.364	20.332
2	3	0	9.598	9.206		2	2	1	5.201	17.034		0	8	0	4.352	20.389
3	2	0	9.527	9.276		3	6	0	5.170	17.138		1	8	0	4.317	20.556
0	4	0	8.704	10.154		0	3	1	5.153	17.195		4	7	0	4.298	20.651
4	0	0	8.537	10.354		3	0	1	5.133	17.262		2	5	1	4.292	20.679
1	4	0	8.434	10.480		6	3	0	5.110	17.340		8	0	0	4.268	20.794
4	1	0	8.291	10.662		1	3	1	5.095	17.391		5	2	1	4.265	20.811
3	3	0	8.126	10.878		3	1	1	5.078	17.450		7	4	0	4.255	20.858
2	4	0	7.755	11.402		2	3	1	4.933	17.967		8	1	0	4.237	20.951
4	2	0	7.665	11.536		3	2	1	4.923	18.003		2	8	0	4.217	21.049
3	4	0	6.914	12.793		1	7	0	4.922	18.008		4	4	1	4.183	21.225
4	3	0	6.877	12.863		5	5	0	4.876	18.180		8	2	0	4.146	21.417
1	5	0	6.823	12.965		7	1	0	4.831	18.350		3	5	1	4.132	21.490
5	1	0	6.702	13.200		4	6	0	4.799	18.473		5	3	1	4.113	21.587
2	5	0	6.448	13.723		2	7	0	4.775	18.565		3	8	0	4.065	21.846
5	2	0	6.358	13.918		6	4	0	4.763	18.613		6	6	0	4.063	21.856
4	4	0	6.095	14.522		1	4	1	4.751	18.660		1	6	1	4.056	21.897
3	5	0	5.940	14.902		4	1	1	4.725	18.764		5	7	0	4.021	22.091
5	3	0	5.886	15.040		7	2	0	4.697	18.877		6	1	1	4.018	22.105
0	6	0	5.803	15.256		3	3	1	4.694	18.889		8	3	0	4.006	22.172
1	6	0	5.721	15.477		2	4	1	4.619	19.199		7	5	0	3.995	22.232
6	0	0	5.691	15.558		4	2	1	4.600	19.280		2	6	1	3.973	22.361
0	1	1	5.674	15.605		3	7	0	4.558	19.460		6	2	1	3.940	22.548
1	0	1	5.671	15.614		7	3	0	4.497	19.725		4	5	1	3.935	22.578

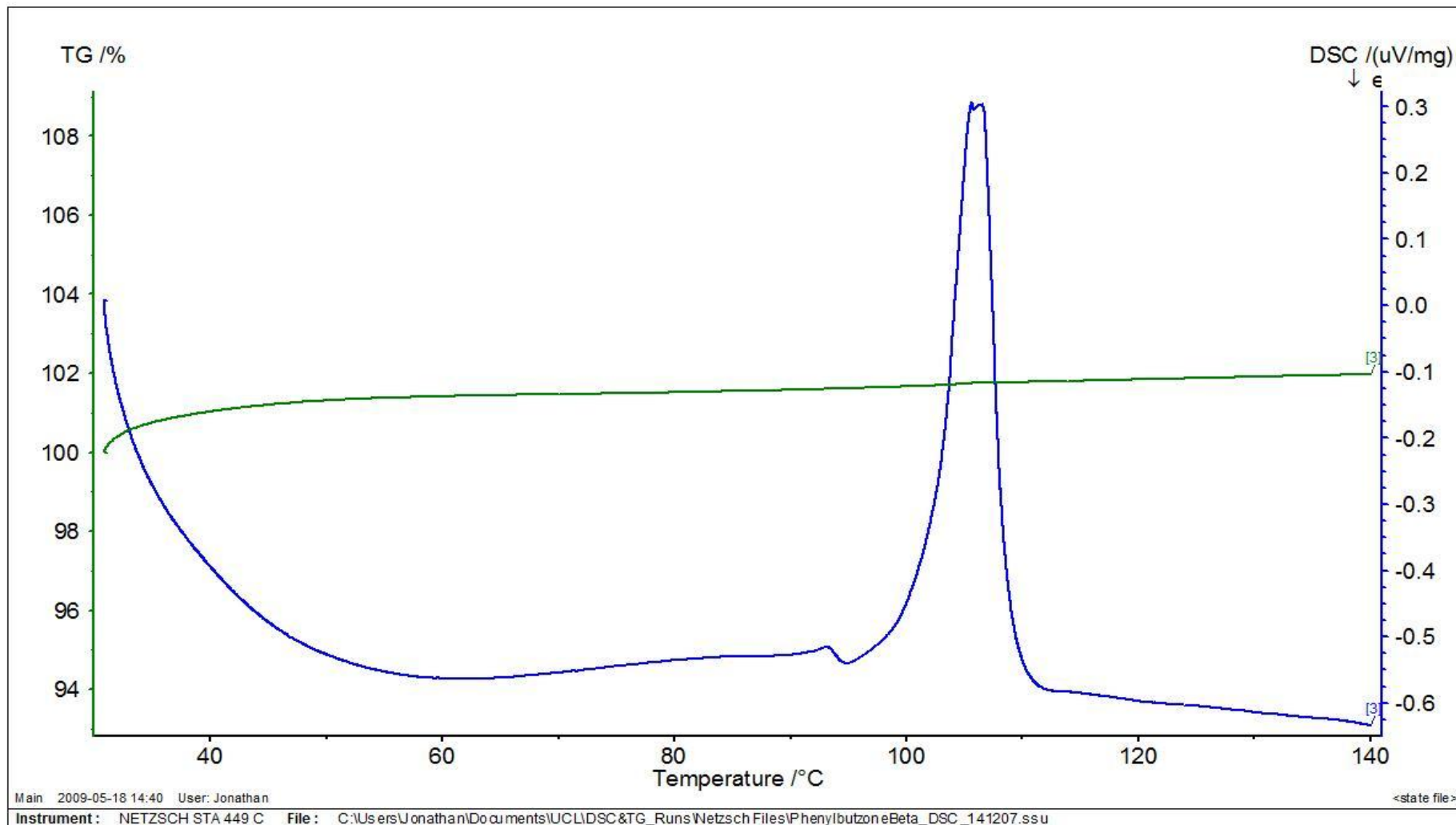
## Appendix 2 – DSC/TGA Scans of Phenylbutazone's Polymorphs

Alpha Form – Temperature Ramp Rate 10K/minute



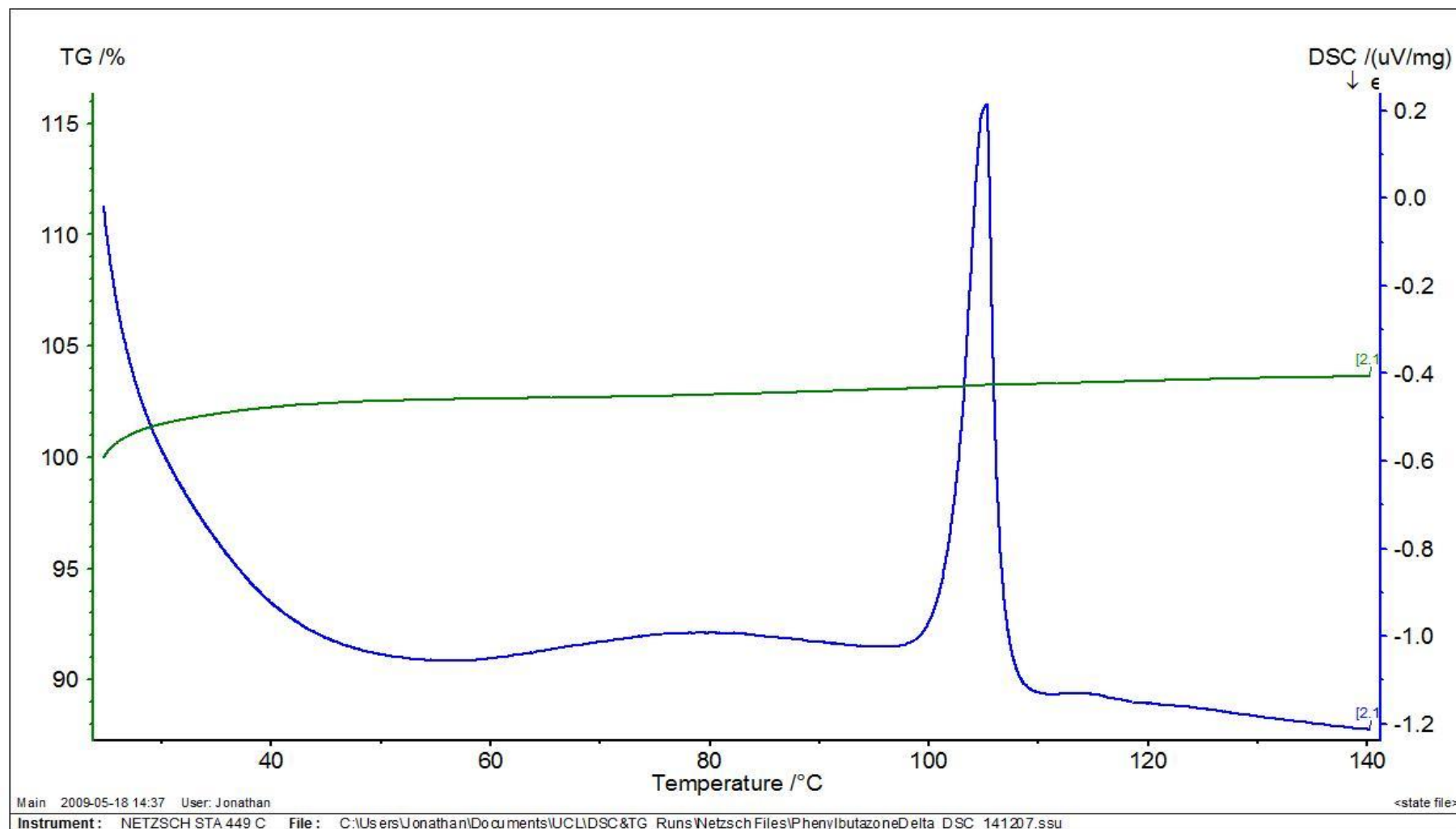
## Appendix 2 – DSC/TGA Scans of Phenylbutazone's Polymorphs

Beta Form – Temperature Ramp Rate 5K/minute



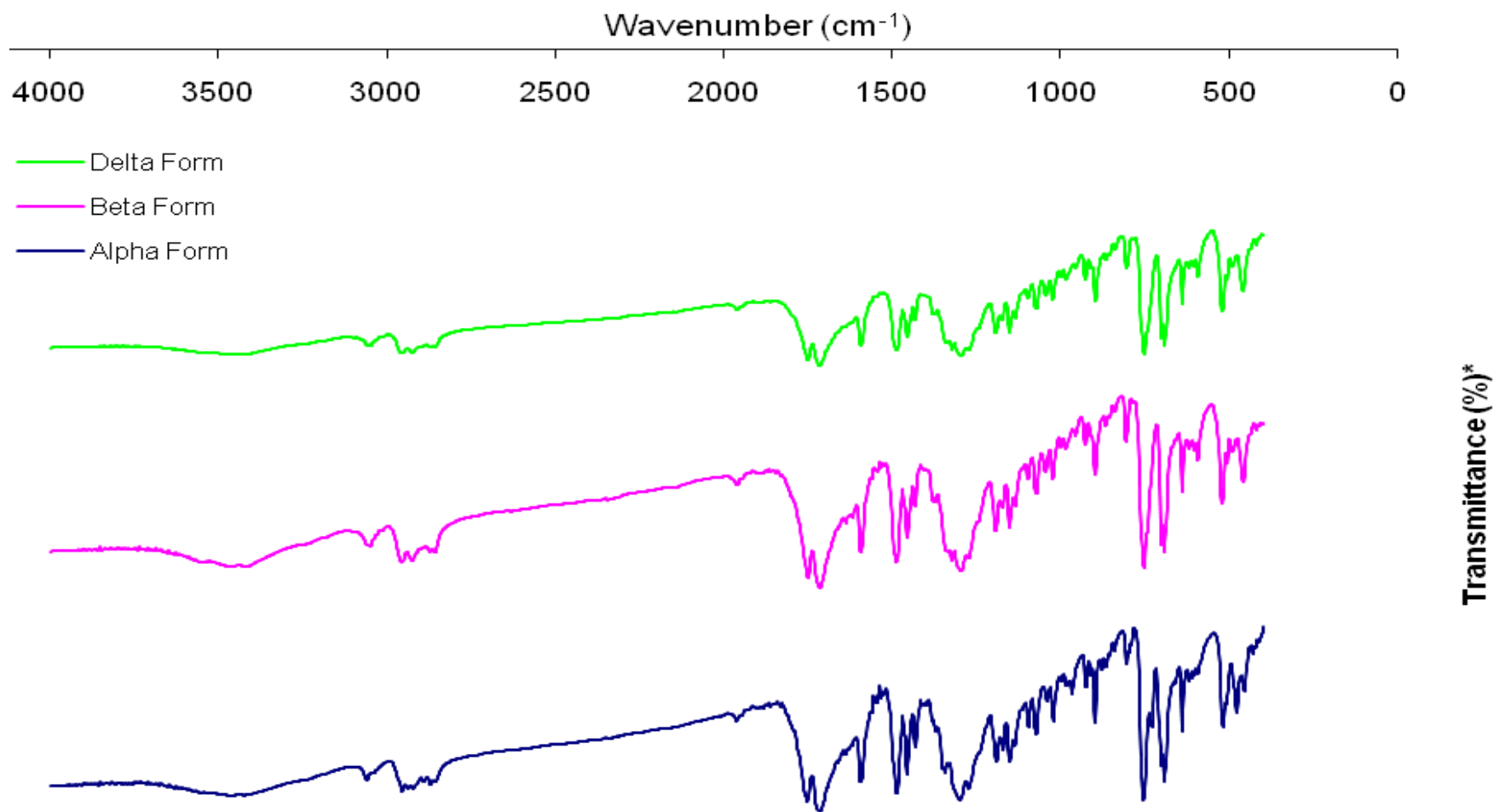
## Appendix 2 – DSC/TGA Scans of Phenylbutazone's Polymorphs

Delta Form – Temperature Ramp Rate 5K/minute





### Appendix 3 – IR Spectra of Phenylbutazone's Polymorphs



\*N.B. Series are offset; i.e. absolute transmittance numbers are relative only to other values in the same series

## Appendix 4 – <sup>1</sup>H NMR Spectrum of Phenylbutazone in CDCl<sub>3</sub>

Group Number	Predicted Chemical Shift by Group (ppm)	Observed Chemical Shift by Group (ppm)	Peak Magnitude
(Tanaka <i>et al.</i> & Yang <i>et al.</i> )	(Tanaka <i>et al.</i> )		T = Trace, W = weak M = Medium, S = Strong
		0.61286	T
		0.77865	T
<b>1</b>	0.900	0.8909	S
<b>CH3</b>		0.90545	S
		92009	S
<b>2</b>	1.356	1.34957	W
<b>CH2</b>		1.36424	W
		1.37906	W
		1.39371	W
<b>3</b>	1.479	1.4463	W
<b>CH2</b>		1.47342	W
		1.47903	W
		1.48591	W
		1.49384	W
		1.50041	W
		1.50629	W
		1.5109	W
<b>H2O</b>	1.56	1.57882	W
<b>4</b>	2.084	2.06789	W
<b>CH2</b>		2.07956	W
		2.0844	W
		2.08904	W
		2.09598	W
		2.10042	W
		2.11189	W
<b>?</b>		2.30353	T
<b>5</b>	3.384	3.25404	M
<b>CH</b>		3.37803	M
		3.38953	M
		3.40106	M
		3.42906	M
		3.44087	M
		3.50962	M
		3.52157	M
		4.2875	T
		4.31284	T
		5.2689	T
		5.62753	T
		7.02237	T

<b>6</b> <b>Phenyl</b> <b>para</b>	7.170	7.15373	M
		7.16145	M
		7.16962	M
		7.17876	M
		7.1875	M
		7.19616	M
		7.20487	M
<b>Solvent Residual</b>	7.25	7.2581	S
<b>7</b> <b>Phenyl</b> <b>meta</b> <b>ortho</b>	7.314	7.27994	S
		7.29433	S
		7.30023	S
		7.30983	S
		7.31853	S
		7.33623	S
		7.34911	S
		7.3582	S
	7.47459	T	

## Appendix 5 – Treatment of Background Counts

The approach recommended by a number of manufacturers of X-ray diffraction equipment, and adopted by a number of texts on X-ray diffraction in order to characterise the incidence of background counts in X-ray diffraction experiments is to consider the arrival of individual X-ray photons at the detector. Gedcke, [118], describes the arrival times at the detector in terms of a queuing phenomenon in which the time for an individual photon to be registered by the detector is infinitesimally small. These arrivals may therefore be regarded as discrete events which, when occurring in large enough numbers at a particular detection step, display a good approximation to the Poisson distribution. The applicability of the poissonian queuing approximation is supported by the postulate that individual X-ray photons travel along different path lengths en route to the detector, both in PXRD and SCXRD experiments.

The practicalities of constructing detectors with infinitesimally short counting times and low or no dead times between counting events, does not, in the opinion of Jenkins *et al.*, [104], jeopardize the integrity of such an approximation. Having established the poissonian nature of the counting events, the treatment of errors then follows directly.

### Equation 40 - Probability Density Function of the Poisson Distribution

$$\text{Prob}(N) = \frac{\mu^N e^{-\mu}}{N!}$$

Where:

$N$  = Number of events in a finite time interval of duration,  $t$

$\mu$  = Average count number of events in time interval,  $t$

In the case of X-ray photons reaching a point detector, the event is a single count at a detector. For the Poisson probability distribution, the standard deviation of the occurrence of count number,  $N$ , is defined as follows:

$$\sigma_N = \sqrt{\mu}$$

In single crystal diffractometry the quantity above is frequently referred to as the standard error in the raw count statistic; this is calculated prior to data reduction.

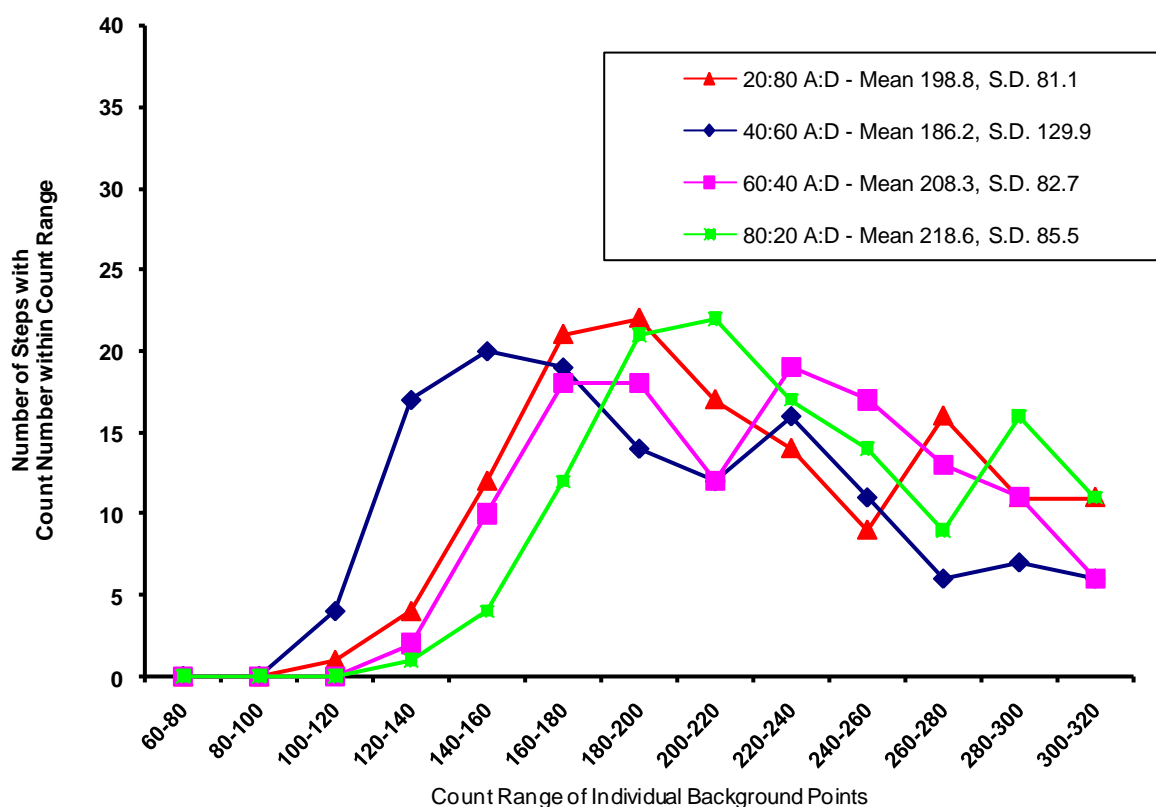
Where the measurement time at a particular measurement angle is repeated several times, Gedke makes the further approximation that the average number of counts,  $N$ , in the reference counting period,  $t$ , will approach the mean value,  $\mu$ . He states as an assumption that counting events are uniformly and randomly distributed over the sampling intervals. This simplification is also made by Massa, [61]. Presumably such an approach may also encompass the use of extended count times, which are sufficiently long such that the count time may be considered as an aggregate of a number of time intervals,  $t$ .

Treatment of the background is handled simply by many crystallographic software programs that include a background subtraction algorithm; for example many of the software programs designed to carry out LeBail extractions of intensities. Typically the background is assumed to be constant, and a line is drawn under the peak representing the level of the background in the region of interest were that region not to contain a diffraction peak. In cases where the baseline is non-linear, programs often allow a sloped, linear background line to be applied beneath the peak; the user is usually able to set his or her own choice of reference background points that delimit the region of interest. This graphical approach allows the analyst to cope with the non-linear baselines that are frequently encountered in diffraction experiments. For quantitative X-ray analysis, a mathematical approach based upon a gaussian

approximation to the Poisson probability density function is outlined by Gedcke, however it is not reproduced here.

During this investigation an analysis of background counts was performed. PXRD patterns were collected on prepared mixtures of the alpha and delta forms using high counting times to obtain a large population of background counts for each measurement step of  $0.05^\circ$  2theta. A maximum background count number was estimated, and subsequently used to filter background from non-background steps. A histogram of counts per background measurement step is shown below.

**Figure 63 - Background Count Distribution of PXRD Patterns - Flat Plate Diffractometer**



The distribution displays a count range with a maximum number of 2theta step observations followed by a clear drop off thereafter. In these experiments the drop-off is observed to occur in the range of 280-320 counts.

Indexing assumptions enable the crystallographer to build an informed opinion about the location of peak information, with which previous background assumptions can be checked and modified. Although this iterative process is laborious when compared with the simplicity of auto-background subtraction algorithms, it provides a clearer understanding of the baseline assumptions, and is likelier to draw attention to errors in indexing or space-group assignment.

## List of Abbreviations

Below is a listing of abbreviations used in the text:

API	Active Pharmaceutical Ingredient
CIF	Crystallographic Information File
CSD	Cambridge Structural Database
DSC	Differential Scanning Calorimetry
FOM	Figure of Merit
IR	InfraRed (Spectrometry)
IUCr	International Union of Crystallography
NMR	Nuclear Magnetic Resonance
PDF	Powder Diffraction File, or Probability Density Function
PPM	Parts per Million
PXRD	Powder X-ray Diffraction
SCXRD	Single Crystal X-ray Diffraction
SD	Standard Deviation
TGA	Thermogravimetric Analysis